Hao-Chen Huang

Experimental study on creep of frozen marine fine-grained soil in Longyearbyen, Svalbard

NTNU
Norwegian University of
Science and Technology

DTU   UNIS
The University Centre in Svalbard

Hao-Chen Huang

Experimental study on creep of frozen marine fine-grained soil in Longyearbyen, Svalbard

NTNU

Norwegian University of
Science and Technology

Preface

This master's thesis in geotechnical engineering is the final part of my MSc study in the Nordic joint program in Cold Climate Engineering. The experimental work with the thesis was done in the summer of 2020 at the University Centre in Svalbard (UNIS) and the thesis was finalized in October 2020. The thesis is performed within the Department of Civil and Environmental Engineering in NTNU, in cooperation with the Technical University of Denmark (DTU) and UNIS.

The main supervisor at NTNU was Professor Gudmund Reidar Eiksund. DTU supervisor was Professor Thomas Ingeman-Nielsen at the Department of Civil and Environmental Engineering. Arne Aalberg was the supervisor at UNIS. The experimental tests carried in UNIS Cold lab were done with the great help from Professor Aleksey Shestov.

Hao-Chen Huang

Abstract

In recent years, new challenges have arisen due to problems related to warming ground temperatures associated with permafrost degradation. The frozen soil creep is one of the main sources of the degradation. Creep has given rise to many foundation failures in cold regions. In Longyearbyen, the marine sediment composition of permafrost has led to greater creep. The creep behavior of frozen soils depends on several numbers of factors and is complex. Stress and temperature histories as well as the actual composition of the frozen soil are only some aspects that have to be considered when analyzing the mechanical response. Considering the complexity of the creep behavior, experimental studies are necessary to be able to address the permafrost degradation behavior produced by creep.

This study studies the rheological properties of the saline frozen fine-grained soil from a Nunataryuk project test site located within the previous NGTS project site called UNIS East in Longyearbyen by doing creep and strength laboratory tests. Focus on studying the creep properties that will lead to settlements of the foundations. A series of unconfined constant stress creep tests at low stresses were carried out for the soil in question to obtain the relationship between strain rate and stress. With the results from the soil tests, the calibration of the creep parameters in the creep model can be obtained. These parameters of the frozen soil are intended to be applicable to the Nunataryuk pile campaign of deep circular footings and screw anchors embedded in saline permafrost soils.

The design parameters obtained from this experimental study can give us better idea for future foundation design under the consideration of limiting long-term creep settlements to tolerable levels.

Contents

List of figures

List of tables

Chapter 1 Introduction

The definition of frozen ground is soil or rock with a temperature below 0℃. Frozen soil is then categorized as a kind of frozen ground, related to the state that the soil particle is bonded by ice that leads to the increase of the soil combined strength and make the soil impervious to water seepage.

The 0℃ in the definition of frozen ground is because the freezing point of pure water is 0℃. However, many different soil conditions, especially salinity, can lead to an unfrozen ground at 0℃ or even lower. As we know, salinity exerts a major influence on the rheologic and strength properties of the soils owing to the higher unfrozen water contents in the pore phase. This kind of marine deposits is vulnerable to thawing and makes the infrastructure built upon highly susceptible to climate warming. Hence the analysis of the soil thermal properties is important. In this global climate change time, thermal properties can also be applied when predicting the warming effect to the frozen ground. Things need to be noted are that warming is amplified in the Arctic region, the amplification of global warming in the Arctic region can be due to feedback mechanisms from loss of sea ice or changes in atmospheric and oceanic circulation. (Førland, Benestad, Hanssen-Bauer, Haugen, & Skaugen, 2011) The proposed increase in temperatures will influence permafrost temperatures and active layer depth. These changes demand for adjustments in foundation design.

Beside thermal properties, mechanical properties are essential for any geotechnical work for frozen soil. The mechanical properties of frozen soil are complex and depend on interrelated functions of the soil structure, moisture and ice content, saturation, temperature, stress and loading rate. The most important characteristic by which frozen soil differs from other materials is that its matrix changes continuously with varying temperature and applied stress (Andersland

& Ladanyi, 2004) All of these requires more investigations into soil conditions. When it comes to establishing an engineering work on frozen ground, geotechnical investigations are mandatory. These include classification of the soils, measurement of water content, pore water salinity, and wet and dry densities. These investigations vary from site to site and should be done locally. These investigations can then be used as influencing factors for the foundation design in the frozen soil. Design capacities in permafrost is typically based on limiting facility movements, such as creep, heave and thaw settlements. These movements are in general caused by freeze-thaw cycle in the active layer and creep in permafrost.

To limit the displacement, the foundation design in frozen ground area is generally carrying the load to the permafrost region to reach the stability. However, the permafrost will still undergo some displacement under load due to creep after a long-time span. The displacement from creep is highly depend on the temperature, stress, and salinity of the soil. Every of the soil condition can continuously change the soil behaviour for the foundation.

1.1 Frozen ground

Frozen ground is separated to two parts: the perennial frozen part called the permafrost and the seasonally frozen part called active layer. Permafrost is defined as soil or rock with temperatures below 0℃ over at least two consecutive winters and the intervening summer (Andersland & Ladanyi, 2004). The active layer is defined as the soil layer where the temperature fluctuates above and under 0℃ isotherm and is where all the frost activity takes place. Figure 1-1 explains the layers of the ground and the temperature profile the ground experiences through the year. Thickness of the frozen ground is determined by the mean annual surface temperature (T_m) and heat flow from the earth's interior corresponding to the local geothermal gradient. (Andersland & Ladanyi, 2004)
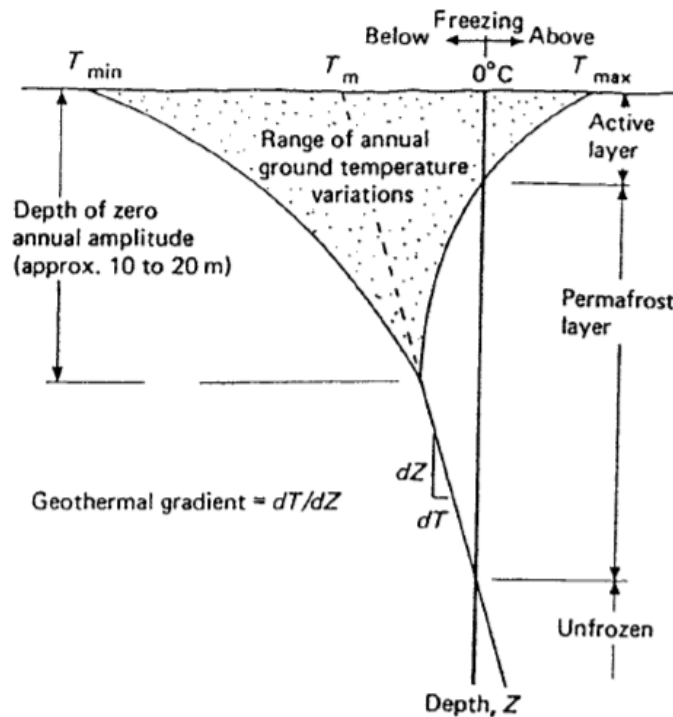
Figure 1-1Temperature profile in permafrost(Andersland & Ladanyi, 2004)

Ground temperatures are dependent on air and ground surface temperatures, heat flow from the interior of the earth, and soil thermal properties. (Andersland & Ladanyi, 2004)

It is necessary to establish a ground thermal regime for frozen ground. The thermal regime in the ground can be theoretically presented by a set of equations. They are here given as presented by Andersland & Ladanyi (2004)

The ground surface temperature ($T_{s,t}$) can be simply estimated as a sinusoidal fluctuation as shown in Figure 1-2 that repeats itself daily and annually, Equation(1.1) gives the estimation of ground surface temperature based on the observation data of the mean annual ground temperature, T_m and the subsurface amplitude, A_s

$$T_{s,t} = T_m + A_s \sin \frac{2\pi t}{P} \qquad (1.1)$$

where t is time, hours or days and P is the period, 24 hours or 365.25 days. T_m is the mean annual temperature and A_s is the surface temperature amplitude.
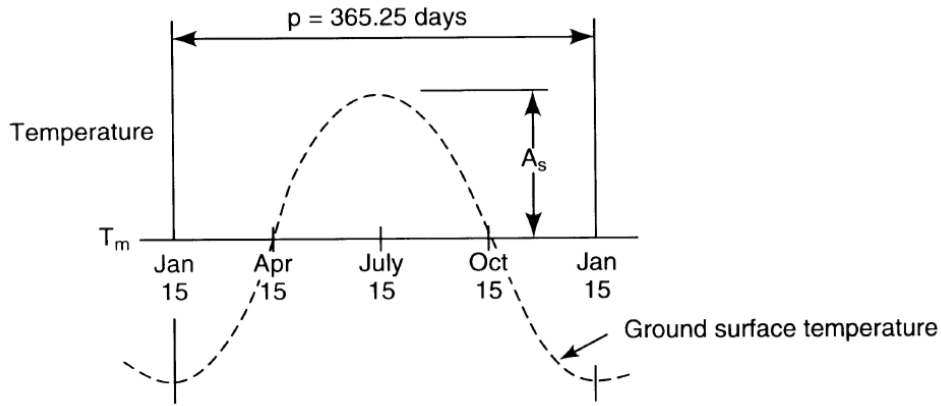
Figure 1-2 The variation of ground surface temperature during a year . (Andersland & Ladanyi, 2004)

Generally, temperature changes at the surface and at soil depth z are not in phase. A shift to the left or lag will occur as seen from Figure 1-3. For example, if the first week of January is found to be the coldest time of the year, this minimum temperature will occur later in deeper layers of the soil. This is recognized as lag time, and can be understood as the time required for the minimum temperature to diffuse from the ground surface downward to the soil depth z. Hence in a homogeneous soil with no change of state, the temperature at a given depth and time $(T_{z,t})$ can be calculated as Equation(1.2)

$$T_{z,t} = T_m + A_s \cdot \exp\left(-z \cdot \sqrt{\frac{\pi}{\alpha_u p}}\right) \cdot \sin\left(\frac{2\pi t}{p} - z \cdot \sqrt{\frac{\pi}{\alpha_u p}}\right) \qquad (1.2)$$

Where α_u is the soil thermal diffusivity. Thermal diffusivity is depended on the thermal conductivity, heat capacity and bulk density of the soil mass. It is the value which establish the

4

rate of heat transfer and how the heat will be used to increase the temperature of the soil mass. And where heat flow from the interior of the Earth is assumed to be negligible.
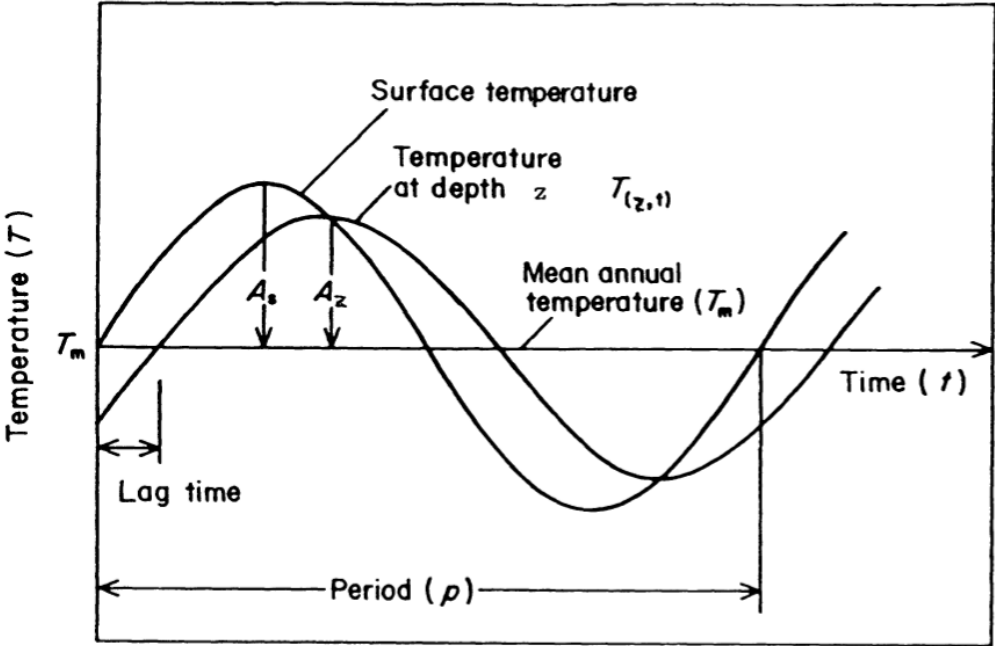
Figure 1-3 Surface and ground temperatures under homogeneous conditions.Sinusoidal fluctuation.

(Andersland & Ladanyi, 2004)

However, Equation(1.2) is simplified equation indicating the trends found in the ground. They can be modified significantly by the effects of soil latent heat, differences in frozen and thawed soil thermal properties (conductivity&diffusivity), nonhomogeneous soils, and nonsymmetrical surface temperatures because of seasonal snow cover, vegetation, and other local climatic influences. (Andersland & Ladanyi, 2004)

In general, the temperature at a given depth will fluctuate between an upper and a lower limit that will have a trumpet shape as Figure 1-4 shows. The amplitude of the attenuation with depth (A_Z) is given by Equation(1.3)

$$A_z = A_s \cdot \exp\left(-z \cdot \sqrt{\frac{\pi}{\alpha_u p}}\right) \qquad (1.3)$$

The range in temperatures or limits of the temperature swings (T_z), are given by equation (1.4).

It gives the maximum and minimum ground temperature for any point below ground surface, z.

$$T_z = T_m \pm A_s \cdot \exp\left(-z \cdot \sqrt{\frac{\pi}{\alpha_u p}}\right) \qquad (1.4)$$
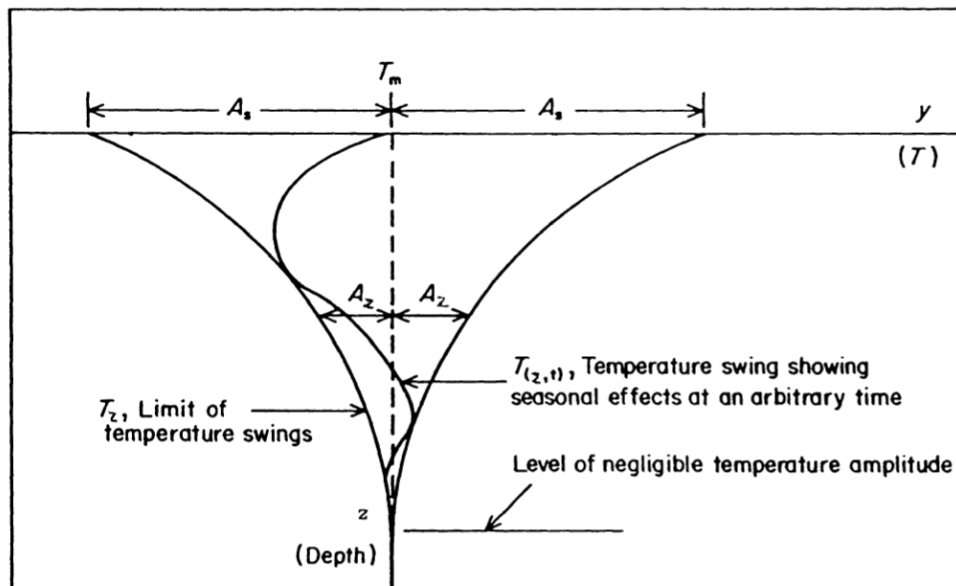
Figure 1-4 Temperature attenuation with depth(Andersland & Ladanyi, 2004)

1.2 Longyearbyen, Svalbard

The Svalbard archipelago located in the Arctic Ocean stretches over 63000 km^2 where 60% of the total area is covered by glaciers, leaving 40% to periglacial environment and permafrost. (Humlum, Instanes, & Sollid, 2003) Grey area in Figure 1-5 indicates permafrost areas.

Longyearbyen is the administrative centre on the archipelago and is situated in a valley. The Longyear Valley is cut out in easily weathered sedimentary rocks and on the valley bottom a

braided river system is created from drainage of two glaciers. (Humlum, Instanes, & Sollid, 2003)

Figure 1-5 Map of Svalbard Archipelago(Humlum, Instanes, & Sollid, 2003)

The mean annual air temperature in Svalbard has increased between 3℃ and 5℃ during the last 40 to 50 years. (Gilbertt, Instanes, Sinitsyn, & Aalberg, 2019) Research has shown that the rate of warming in Svalbard is more than twice the Arctic average and about seven times the global average for the last three decades period. (Nordli, et al., 2020) The continuous warming trend observed in Svalbard during the last 30 years has raised concerns about the stability and durability of existing infrastructure on permafrost. The envisaged rise in temperatures would thaw the frozen ground underpinning many buildings, roads and airports, cause more avalanches, and landslides. As well increasing the uncertainties related to the design of new structures and infrastructure in the region. (Gilbertt, Instanes, Sinitsyn, & Aalberg, 2019) Future design for buildings in Svalbard will have to increase investment to relocate buildings from avalanche paths and drill deeper infrastructure foundations as permafrost thaws.

1.3 Thesis outline

1.3.1 Problem definition

The Norwegian GeoTest Sites(NGTS) infrastructure project launched five test sites in different soils located in Norway and Svalbard in 2016. One of the test sites is located near the University Centre at Svalbard and is called UNIS East site. Many master's studies have been investigated on the soil extracted from the UNIS East site. However, they all put focus on the study of thermal properties of the soil. (Nybo, 2017) (Bratlie, 2018) (Eiken, 2019) Few laboratory tests have been carried out to study the mechanical properties of the soil at the site. However, I was intrigued to know more about how the mechanical behaviour of the soil is.

In Spring 2020, the Nunataryuk project installed a pile test within the UNIS East site to monitor the pile settlement under load in a long time span in the saline permafrost. This gave me the opportunity to study the soil at the site. Therefore, this thesis aims to study the soil properties especially the creep behaviour in order to predict the creep settlement at the site. As well give the question to see if the prediction corresponds to the recording from the field.

1.3.2 Scope and Objectives

The main scope of this thesis is to find the soil creep parameters by doing a series of laboratory uniaxial compression tests and to bring these parameters into creep model in order to predict the creep settlements of the soil for the saline permafrost site at UNIS East.

The following objectives are important to achieve this:
- Laboratory investigations will be performed to identify geotechnical parameters for the saline permafrost site at Longyearbyen, Svalbard.

- Choose the most adapted creep model for the further consideration of creep design.

- To investigate methods for analyzing the creep settlement for foundation design in frozen ground.

- To present the prediction of the creep settlement from the laboratory tests for the test site at UNIS East in Longyearbyen, Svalbard.

1.3.3 Limitations

Loads are assigned in the static mode and dynamic and cyclic are not considered in the analysis. Besides, only unconfined uniaxial compression tests were performed. Shear strength was only assumed by the Mohr-Coulomb failure criterion. Lateral stress was not considered in this thesis.

Experiments to determine the soil thermal properties and unfrozen water content were not performed in this study.

Samples were chosen to be tested for strength at only one specific temperature, no temperature variation was studied for the strength properties of the soil in this thesis.

Design approach in this study only focused on limiting creep settlement, other criteria to fulfil a satisfying foundation design was not addressed here.

1.3.4 Approach

The first procedure of this master thesis is literature review on the basic soil classification methods, the creep theory and some creep models in the function of strain/strain rate versus stress developed over time. To be continue, the thesis presents some simple wide-used

approached for analysing the creep settlement under stress of two typical foundations in the frozen ground areas.

The experimental study part of this master thesis is all laboratory works. Soil samples from a site at Longyearbyen, Svalbard were carried to perform a series of soil classification tests such as water content, densities, cohesive properties, salinity, etc. Soils also being remoulded into cylindrical samples for uniaxial compression tests.

With the experimental test results, combining with the literature studying theory, the creep settlement can be predicted at the site.

1.3.5 Structure of the report

The report is structured as follows:

- **Chapter 1 Introduction**

  The first chapter introduces the background information regarding the frozen ground and the basic information on Longyearbyen, Svalbard. The outline of the thesis is also presented here.

- **Chapter 2 Soil Classification**

  In this chapter, the methods to analysis the soil components and weight-volume parameters and the way to classify them are introduced.

- **Chapter 3 Creep**

  This chapter is focused on how the creep developed within the frozen soil influenced by different factors. The creep models to be used for establishing the relationship between the strain or strain rate with stress are presented.

- **Chapter 4 Creep considerations for foundation design**

Two foundation design are discussed here: pile foundation and shallow foundation. The theories presented here are design principle that has been used for a long time in the permafrost regions.

- **Chapter 5 Experimental Investigations**

  This chapter combines all the testing results obtained from the laboratories. It also briefly introduced the site condition from some literature survey and geo thermistor data installed in the borehole. The case study is put in the last in this chapter to illustrate how the soil tests can used in practical engineering design.

- **Chapter 6 Conclusions and recommendations for further work**

  The final chapter includes conclusions of the study and suggestions for further work to be done to advance in this research field.

Chapter 2 Soil Classification

Soil is an aggregation of particles that may range very widely in size. It is the by-product of mechanical and chemical weathering of rock. Soil, being a mass of irregular-shaped particles of varying sizes, will consist of the particles (or solids), voids (pores or spaces) between particles, water in some of the voids, and air taking up the remaining void space. At temperatures below freezing the pore water may freeze, with resulting particle separation (volume increase). When the ice melts particles close up (volume decrease). If the ice is permanent, the ice-soil mixture is termed permafrost. The term permafrost is being described in Section1.1.

Unlike other engineering material such as concrete that the properties can be controlled during manufacture. Soil as a naturally occurring material, the properties can never be certain without tests. Since the variety of soils is very wide, and no two sites have identical soil conditions. It is therefore necessary to evaluate the soil properties present at every site by doing soil classification tests.

2.1 Soil Analysis

Soil analysis can be done by experiment, and the analysis enables the soil properties to be used to predict their likely behaviour under defined working conditions.

Before the laboratory tests, soil can be simply identified at the site by doing some visual or tactile inspections. For example, it is easy to differentiate gravel and sand by visual inspection. And there are two ways to differentiate silt and clay, firstly, clay lumps are more difficult to crush using the fingers than silt. The second way is by moistening a spot on the soil lump and rub your finger across it. If it is smooth it is clay; if marginally streaked it is clay with silt; if

rough it is silt. After these at site procedures are done, the soil then need to be carried to the laboratory for further analysis as described in the following sections.

2.1.1 Phase relationships

Frozen soils are a four-phase system consisting of solid particles, ice, unfrozen water, and gas or air. In unfrozen state, the system become three-phase as the ice disappearing and becoming water. Figure 2-1 reveals the phase relationships of frozen and unfrozen soil. Soil parameters that in connection with phase relationships like water content, densities, etc, are defined in Appendix A.
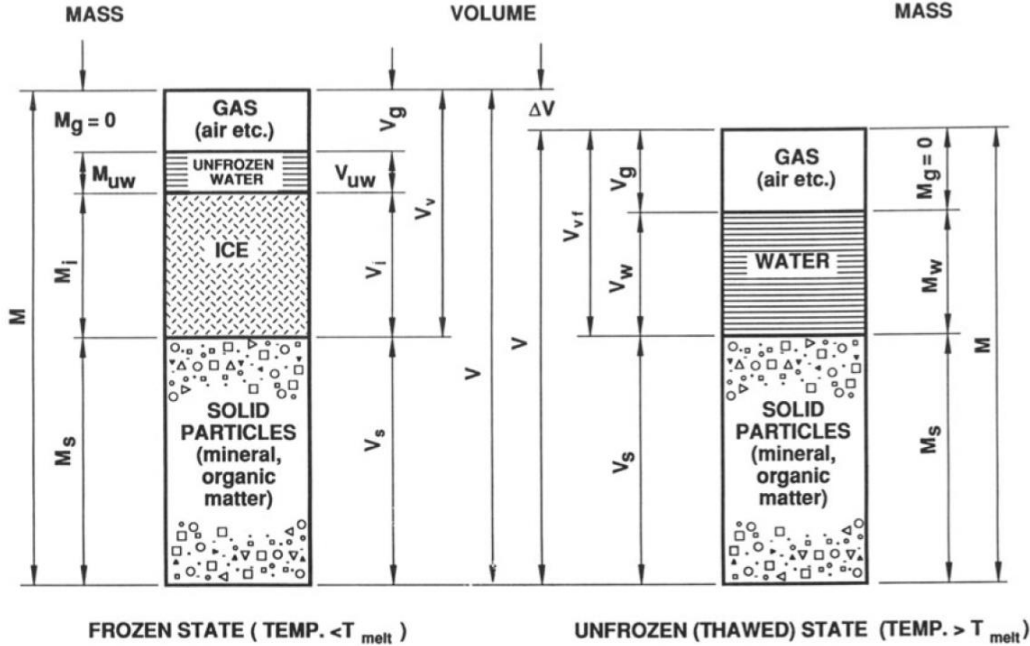
Figure 2-1 Mass-volume relationships for frozen and unfrozen soil(Andersland & Ladanyi, 2004)

2.1.2 Salinity

Salinity is the amount of water dissolved in a body of water. In other words, as the ratio of mass of salt to the mass of water.

In frozen soil, salinity is one of the undesirable properties for engineers. Frozen saline soil is known to reduce the soil mechanical strength and rise the creep rate due to the consequence of higher unfrozen water contents in the pore phase (Nixon & Lem, 1984), as illustrated in Figure

2-2. The salinity levels are of great importance for soil characteristics and hence the choice of foundation principle.
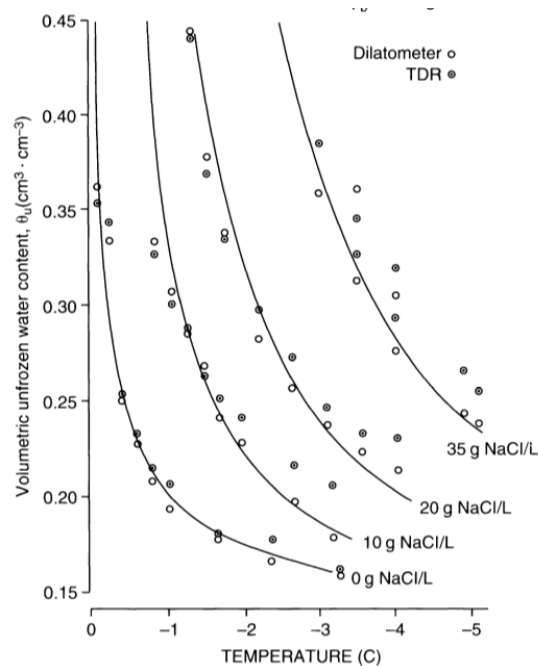
Figure 2-2 Relationship between volumetric unfrozen water content, temperature and salinity (Patterson & Smith, 1985)

Freezing point depression

Due to the presence of pore-water solutes, Solutes present in pore water in frozen soil leads to the depression of the freezing point, such called freezing point depression. The freezing point of water may be depressed several degrees below 0°C. As shown as ΔT in Figure 2-3. Freezing point depression makes more ice to thaw at the same temperature. Therefore, part of the ice will thaw and leads to the increase of unfrozen water content.

The ice is a bonding agent, fusing together adjacent soil particles or blocks of rock to increase their combined strength and make them impervious to water seepage. The lost of ice will decrease the strength of the soil. Increased pore water salinity depresses the soil freezing point.
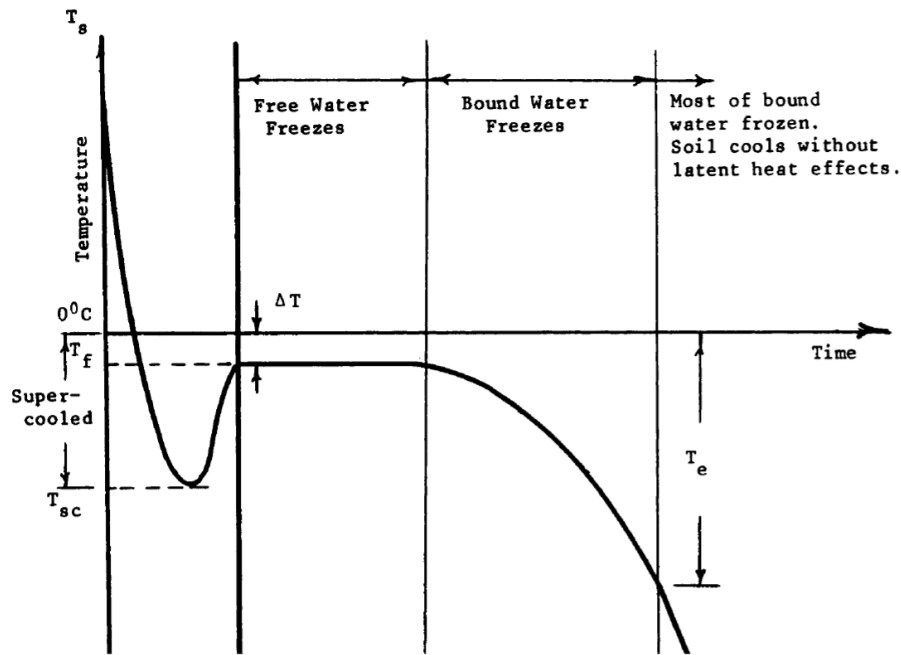
Figure 2-3 Cooling curve for soil, water and ice(Andersland & Ladanyi, 2004) (After (Lunardini, 1981))

Figure 2-3 shows how cooling of a soil-water system develop. First, if the water is absolutely pure, the water will be super cooled to a temperature, T_{sc}. This supercooling is a metastable equilibrium state, this state will last until an abrupt of nucleation centers. These nuclei can be aggregations of water molecules or soil particles. Secondly, when ice is formed, latent heat is released which cause a rise in temperature to the freezing point, T_f . T_f is close to 0°C for coarse grained soil and can be depressed down to –5°C for fine grained soil (Andersland & Ladanyi, 2004). When T_f is reached, free water in the soil pores will continue to freeze at this temperature. The freezing point depression, ΔT, in a soil depends on the size of soil pores, water content and solute content.

An important characteristic of frozen natural soil is that even though it exists below the freezing point of pure bulk water, not all of the water is necessarily frozen. Unfrozen pore water in the soil exists as a thin liquid-like layer on the mineral particles, where the high intermolecular forces suppress the freezing (disordering the structure of the water molecules), while the rest of

15

the water pore is weakly bound and can be frozen more easily.

Investigations have shown that the amount of unfrozen water depends on the specific surface area of the mineral particles, where presence of unfrozen water films on particles in a frozen clay has been observed down to a temperature of -110 ⁰C.

A two-component system of water and salt (NaCl) is illustrated in Figure 2-4, the temperature needed to change the phase from liquid to ice decreases with the increasing of salt content.
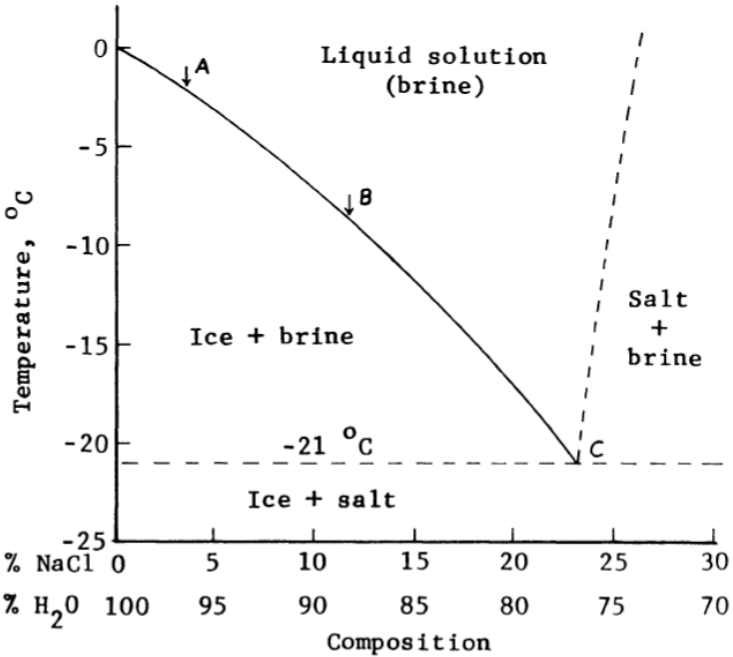
Figure 2-4 Solubility of ice in NaCl brine(Pounder , 1965)

An empirical equation developed by Velli & Grishin(1983) established the relationship between freezing point depression and salinity as shown in equation (2.1)

$$\Delta T = T_k \left[\frac{S_n}{1000 + S_n} \right] \qquad (2.1)$$

T_k is a reference temperature, is 57°C for sea salt, 62°C for NaCl; S_n is salinity in g/l (or ppt)

2.1.3 Atterberg limits

The Atterberg limits comprise three consistency limits: liquid limit, plastic limit, and shrinkage limit. Fine soil is being selected for these tests as the aim of the tests is to measure the plasticity of the soil. Which states the ability of a soil to undergo changes of shape without rupture or a change in volume. And this is normally only existing in cohesive soils namely the fine-grained size soil. The determination of liquid limit (w_L) and plastic limit (w_P) can classify the soil with the chart in Figure 2-5. These Atterberg parameters are described in Appendix A.
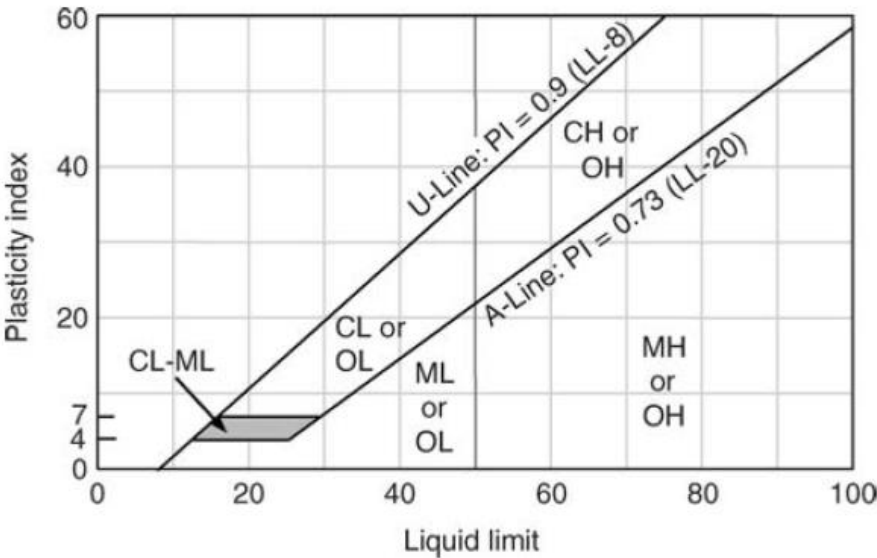
Figure 2-5 Casagrande's PI-LL chart(Das, 2011)   (After (Department of the Navy, 1982))

2.1.4 Particle size distribution

When examining the soil gathered from the site, it is important to investigate the variation and distribution of particle sizes to gather an understanding of the general type of soil that is present in the area. This is done to correctly classify the soil, as the distribution of particle size affects the general strength and load capacity of the soil and thus is an important parameter for understanding the local soil. It is also important as the amount of unfrozen water present in

frozen soil at a given temperature can be related to the specific surface area of the mineral particles. (Andersland & Ladanyi, 2004) Figure 2-6 shows the typical particle size distribution curve for different soils.
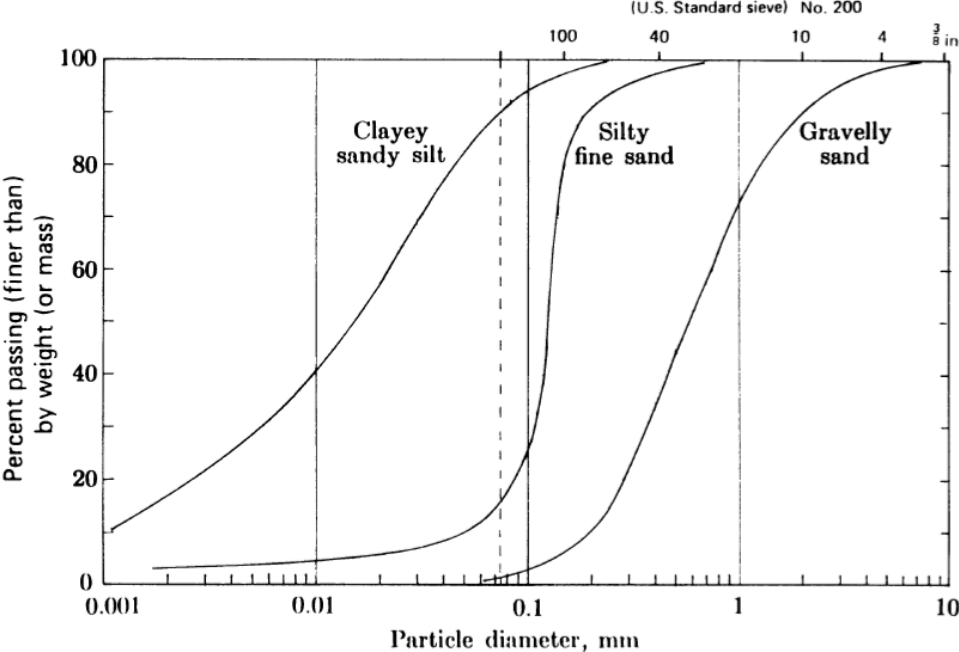
Figure 2-6 Typical grain-size distribution curvesfor several soils (Andersland & Ladanyi, 2004)

Depending on the size, soil particles can be divided to four categories: gravel-size particles range from 20mm to 4.75mm, sand-size particles range from 4.75mm to 0.075mm, silt-size particles range from 0.075mm to 0.002mm and clay-size particles is less than 0.002mm. Gravels and sands are called coarse-grained soils, while silts and clays are called fine-grained soils. For course-grained soils, the method of determining the particle size distribution is by sieving. On the other hand, fine soil particles in the dry state tend to cohere or form lumps that are unsuitable for sieve analysis. Therefore, the sedimentation method is then applied.

The sedimentation method is based on Stoke's Law. Stokes's law relates the diameter of a sphere to its fall velocity in a liquid, see equation (2.2)

$$v = \left(\frac{\gamma_s - \gamma_f}{18\mu}\right) D^2 \qquad\qquad (2.2)$$

where v is the fall velocity of the sphere, γ_s is the unit weight of the sphere, γ_f is the unit weight of the fluid (soil plus water), μ is the viscosity of the liquid, and D is the sphere diameter.

With the particle size analysis result, a ternary diagram Figure 2-7 can be used to classify the soil if the soil only composed of sand, silt and clay. With the percentage of 100% in total, the soil will be represented as a dot in the diagram.
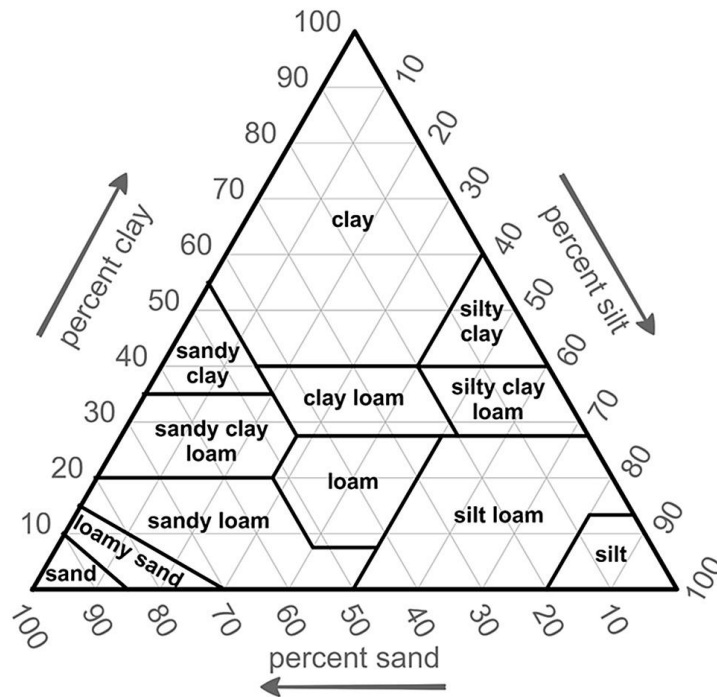
Figure 2-7 Triangular classification chart(Groenendyk, Ferré, Thorp, & Rice, 2015)

The homogeneous of soil particle is very important when it comes to analysis of the soil bearing capacity and settlement. The coefficient of uniformity (C_u) and coefficient of curvature (C_c) represent how a soil is graded as defined in Equation (2.3)&(2.4)

$$C_u = \frac{D_{60}}{D_{10}} \qquad\qquad (2.3)$$

$$C_c = \frac{(D_{30})^2}{(D_{10})(D_{60})} \qquad\qquad (2.4)$$

D_{60} is the grain diameter (in mm) corresponding to 60% passing, D_{10} is the grain diameter (in mm) corresponding to 10% passing, D_{30} is the grain diameter (in mm) corresponding to 30% passing.

A well-graded soil may have a C_u of 15 or more. A C_c value between 1 and 3 is typical for a well-graded soil. (Andersland & Ladanyi, 2004)

Chapter 3 Creep

When a frozen soil specimen is subjected to a constant stress, it will respond with an instantaneous deformation and a time-dependent deformation. The studies herein put focus on the time-dependent deformation, namely the creep. Creep of frozen soils is one of the most important topics in engineering activities when frozen soils are involved. It is the progressive time-dependent inelastic deformation under constant load and temperature.

Theories of creep have been developed to two viewpoints: the macroanalytical or engineering direction and the micromechanistic or physical direction. The engineering theory of creep is a collection of laws that are found, by experience, to describe the observed manifestations of creep. It aims to describes a number of different creep manifestations in simple mathematical terms. The form established by engineering theory of creep to express the stress dependence of creep rate will be in power form. On the other hand, the physical theory of creep is to establish a set of laws that would be able to describe the observed phenomena of creep in terms of previously established quantities and laws of physics. The expression of physical theory of creep uses either a hyperbolic sine or an exponential form. (Ladanyi, 1972)

The following sections will be the illustration of different creep models. Some of them are in power form, the others are in exponential form. The equations in power form are more widely used for further design application as they lead to relatively simple mathematical expression.

3.1 Creep curves for frozen soils
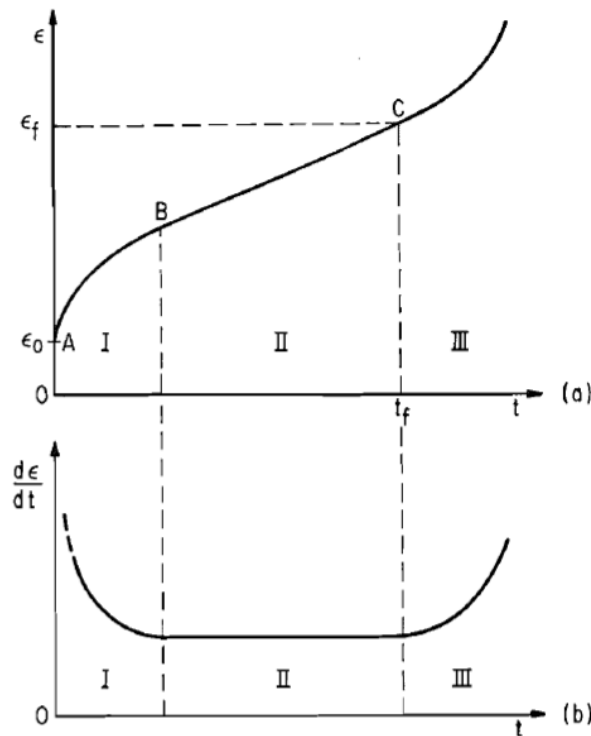
Figure 3-1 Strain(a) and strain rate(b) versus time in constant stress creep test(Ladanyi B. , 1972)

Creep curve is a graph between strain versus time. It can be divided to several sections, which represent the various stages of the deformation. The first section is the one corresponds to an almost instantaneous deformation, ε_0, that arises immediately upon application of the load. This deformation can be either elastic or elasto-plastic depending upon the value of the load, at small loads the plastic portion may be absent. After the instantaneous deformation, creep curve is developed into three periods as shown in Figure 3-1.

Three periods of time are observed during which the creep rate is in order (I) decreasing, (II) remaining essentially constant, and (III) increasing. These are often called the periods of primary, secondary and tertiary creep.

The shape of creep curve for frozen soils is influenced not only by temperature but also by the

22

magnitude of applied stress, soil type, and its density. As a result, it may not behaves as shown in Figure 3-1, as sometimes the second and tertiary creep may not develop if the applied stress is really low. Also the transition time of each stage of creep may vary, for example if the stress applied is really high, the primary or secondary creep stage will develop only for a pretty short time. The shape of creep curves for frozen soils is influenced not only by the soil type, its density, ice saturation and temperature, but also by the applied stress-and strain history.
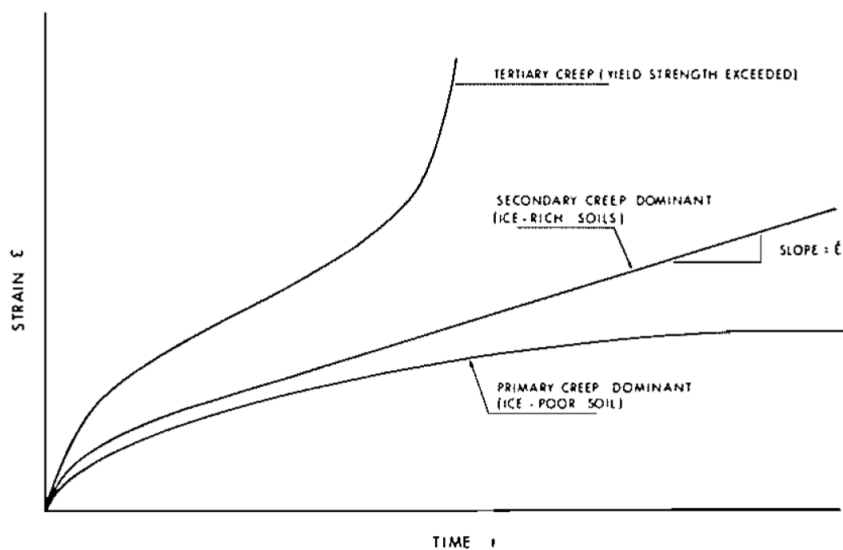
Figure 3-2 Creep curve variations(Nixon & McRoberts, 1976)

As shown in Figure 3-2, ice-rich and ice-poor soil are dominated by different kinds of creep. In general, the behavior of ice poor soils at low stresses appear to be dominated by primary creep. On the other hand, ice-rich soils exhibit a creep behavior similar to ice. It is apparent that if the soil particles or groups of particles are separated by ice, then the behavior of the ice phase will dominate the load-deformation behavior. In the creep data for ice reviewed here, the deformation behavior may be characterized typically by a short period of primary creep, followed by continuous secondary creep.

In practice one is mainly concerned with the prediction of displacements is the secondary or steady-state creep stage. This is so because the tertiary stage is usually considered to be beyond

the point of creep failure, while the primary stage represents, for long time intervals, only a small portion of the total time. (Johnston & Ladanyi, 1972)

3.2 Factors influencing creep of frozen soils

The creep of frozen soil depends on two external variables of stress and temperature and some internal variables of structure and components. Many studies have made in order to ascertain how stress, temperature, salinity, structure, etc., might affect the creep strain rate of frozen soil.

It is worth to keep in mind that these factors can not be well separated. They have the connection with other at certain level. For example, the moisture content is the key factor that influences the strength of the frozen soil. Among the moisture content, the ice is the one that provides the strength to the frozen soil. And the strength of ice depends on many factors, the most important of which are temperature, pressure and strain rate, as well as the size, structure and orientation of grains. Hence in the following sections, many factors that influence the strength behavior, or precisely, the creep behavior, will be described. But these factors are not all of the effects that influence the creep behavior as there are too many to list.

3.2.1 Stress

It is intuitive to link the stress factor that influences the magnitude of creep. The higher the stress applied, the more the soil deformed. For frozen soils under various constant stresses, the growth of deformations with time shows typical creep curves. (Figure 3-3). Which represent the relationship between relative deformation, ε, and time, t, each curve corresponds to a given stress $\sigma=$ const.
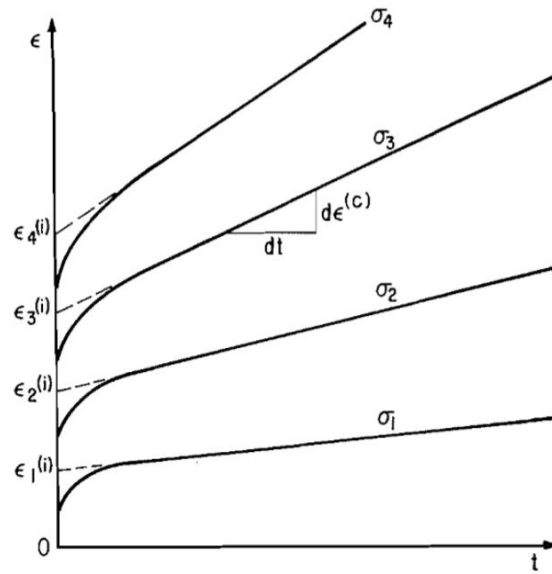
Figure 3-3 Creep curves with different stress applied $\sigma_1 < \sigma_2 < \sigma_3 < \sigma_4$ (Ladanyi B. , 1972)

Depending upon the amount of the load, the time of transition from one stage into another will vary. Figure 3-4 shows the creep curves that developed three stages of creep. It is clear to see that the larger the stress, the quicker the creep proceed to the next stage. For very large loads, like $\sigma_1 - \sigma_3$ in Figure 3-4, the tertiary creep set in almost immediately when the load is applied. This states that the frozen soil under high load will lead to the failure without experiencing the time-dependent deformation.
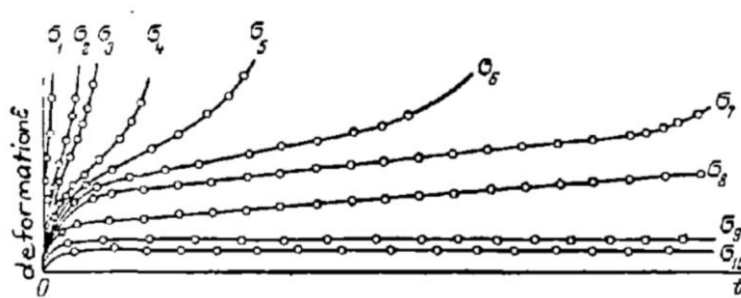
Figure 3-4 Creep curve under various stress $\sigma_1 > \sigma_2 > \sigma_3 > \cdots > \sigma_{10}$ (Vialov, et al., 1962)

3.2.2 Temperature

The behavior of frozen soils is very sensitive to temperature change and therefore temperature becomes an important parameter in design. Because of its direct influence on the strength of intergranular ice, and on the amount of unfrozen water in a frozen soil, the temperature has a marked effect on all aspects of the mechanical behavior of frozen soils. Rising temperatures could significantly affect the stability of soil containing a lot of water, big volume inclusions like ice lenses or wedges. Decreasing temperature results in an increase in strength of frozen soil, but at the same time it increases its brittleness.

The duration of each stage of creep increases as the temperature is lowered.
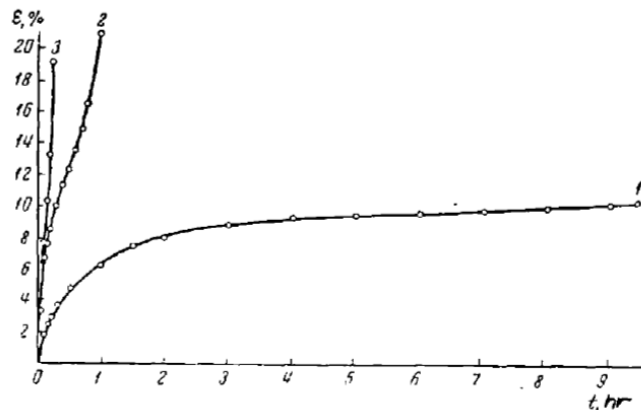
Figure 3-5 Creep curves for Calloivan sandy loamat temperature of -20C(1), -10C(2), and -5C(3)

(Vialov, et al., 1962)

3.2.3 Solutes

Salinity accelerates the creep rate of a frozen soil under load and reduces its shear strength owing to the higher unfrozen water contents in the pore phase. (Nixon & Lem, 1984)

The higher solute content, the larger axial strain under a certain stress level.

A clear understanding of the strength and deformation characteristics of saline permafrost is required for the design of foundations in coastal and offshore arctic regions.
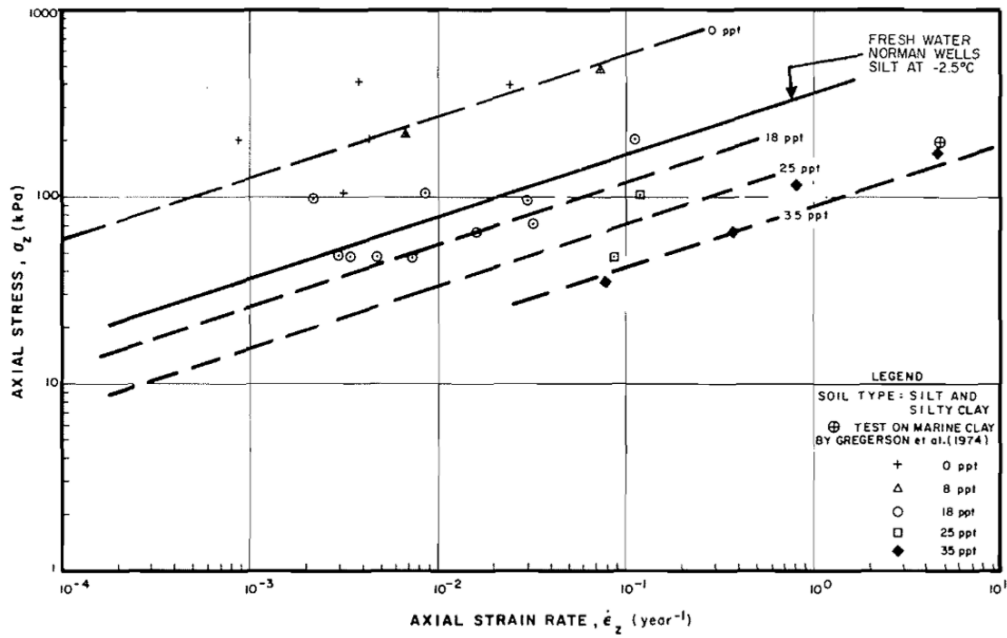
Figure 3-6 Effect of salinity on creep of frozen soils at -5°C (Nixon & Lem, 1984).
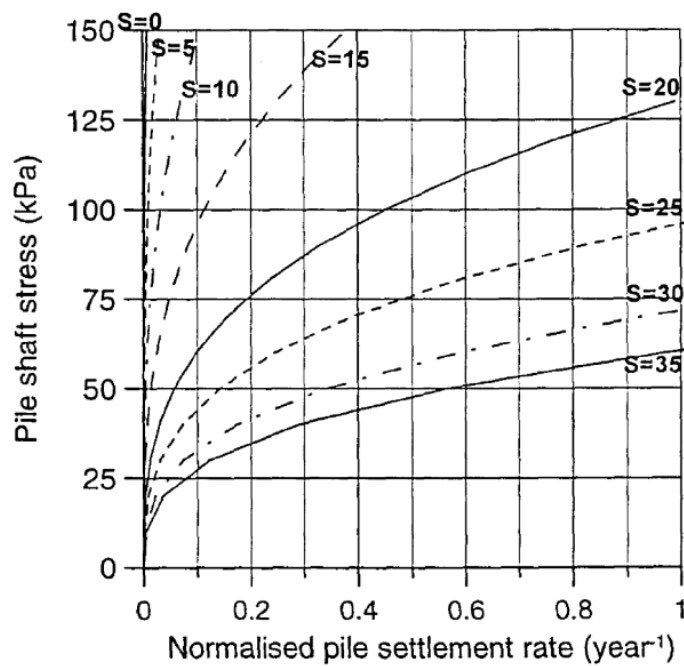
Figure 3-7 Normalized pile settlement rate for various salinities at -5°C (S in ppt) (Instanes & Instanes, 1999)

3.2.4 Moisture content

Many studies have been conducted to investigate the relationship between water content and the strength properties of frozen soil. Studies have shown a general relationship between strength of frozen soil and water content. It states that under complete saturated situation, the unconfined compression strength decreases with increasing water content initially until the strength of the soil falls below the strength of ice to a minimum value. With increasing water content the strength then increases from this minimum value until the strength of ice is reached again. (Shusherina & Bobkov, 1969)

In frozen soil, the water content includes the unfrozen water and ice content. The unfrozen water within the frozen soil has a significant influence on the strength and creep behavior of frozen soils. Water can be present as an adsorbed water film around fine particle surfaces or as free water in the pores. The smaller the particles, the higher the unfrozen water content.

It is important to consider the water content in two terms as the unfrozen water and ice bring totally different mechanical behavior of frozen soil. In general, ice fractures at strains below 0.05 (Mellor, 1972) but most frozen soils usually do not attain a maximum stress until much larger strains are reached. In some instances, maximum stress does not occur even at strains as large as 0.30. The fracture of ice, the strongest bonding component of most frozen soils, generally does not occur at the same strain as that at which the frictional resistance reaches a maximum. (Sayles, 1973) Therefore, in considering the strength of frozen soil as a function of water content, the fracture of the ice should be considered the initial onset of failure of the frozen soil. In the study conducted by Sayles and Carbee (1981), it is shown that the initial fracture strength of saturated frozen silt increases with an increase in ice volume. The result is shown in Figure 3-8.
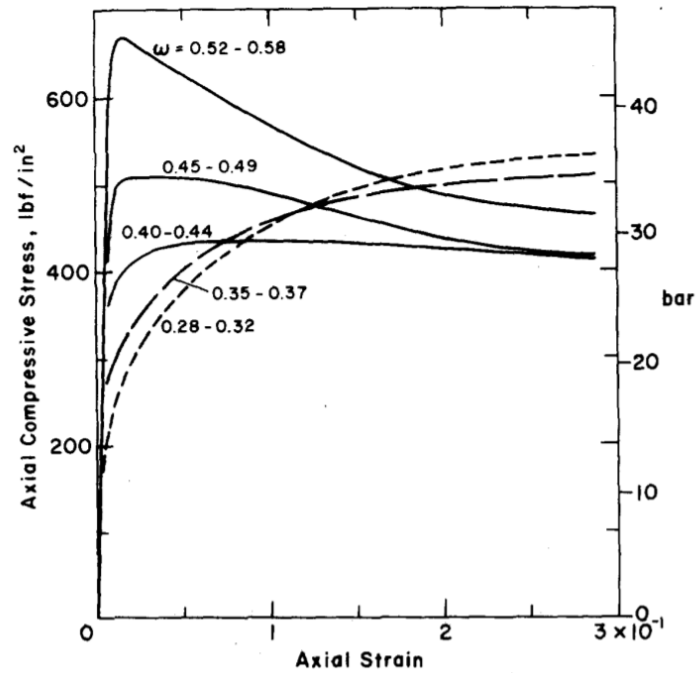
Figure 3-8 Average stress-strain curves for five different total water content ranges(Sayles & Carbee, 1981)

In spite of the presence of unfrozen water, when ice fills most of the pore space, the mechanical behavior of a frozen soil will reflect closely that of the ice.

3.2.5 Dry density

Dry density plays an important role for the secondary creep rate while the stress applied is low. For example, Zhu and Carbee (1987) found that the secondary creep rate decreases by three orders as the dry density increases from 1.07 to 1.40 g/cm^3 at a stress level of 10 kg/cm^2. But when the applied stress is 20 kg/cm^2, there is not much difference in creep rate for each density.
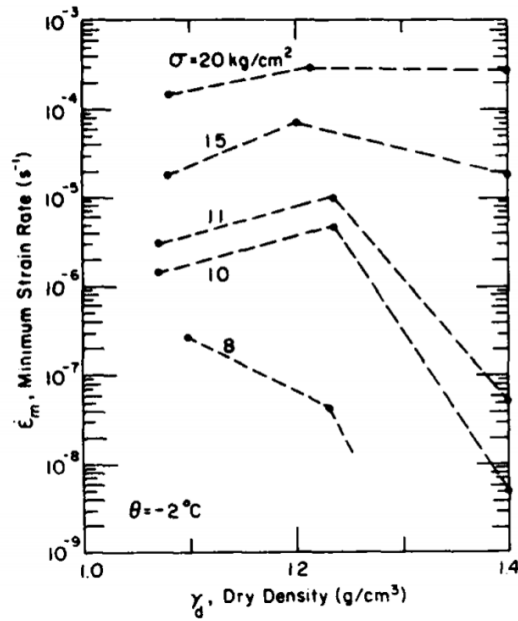
Figure 3-9 Minimum creep rate as a function of dry density for various stress at T=-2℃ (Zhu & Carbee, 1987)

Studies have shown that for soil whose density less than 1.5 g/cm^3, the creep rate generally becomes lower as the density increases since the soil particle impedes the movement of dislocation within the ice crystals. However, at very low density, i.e. density<0.95 g/cm^3, the introduction of soil particles into the ice matrix reduces the average grain size of the ice crystals, thereby giving rise to higher creep rates than pure ice. For dense soils, whose densities are higher than 1.5 g/cm^3, the long-term creep characteristics are ill-defined. The creep mechanism in dense, fine-grained frozen soils is further complicated by the presence of interconnecting network of unfrozen water. For such dense soils, time-dependent consolidation will occur, resulting in increased effective strength and, therefore, a strengthening of the soil matrix. Further, the presence of unfrozen water reduces the average ice crystal size and also assist grain-boundary sliding, thus facilitating plastic flow of the ice matrix. (Hooke, Dahlin, & Kauper, 1972)

The change in creep behavior due to the variation of density is attributed to the change in

deformation mechanism. The stress resistance of frozen soil is relied on the bonding force and frictional resistance between the soil particles combined with that of the fractured ice crystals.

3.3 Creep models

There are many creep models developed during the past few decades. The creep characteristics of frozen soil has significant influences on infrastructure stability in cold regions. It is important for frozen ground engineering to describe the creep properties of frozen soil with accurate models.

Various equations have been suggested to describe and predict the creep behavior for ice, ice-rich frozen soil and ice-poor frozen soil. Ice-rich frozen soil has been reported to have similar mechanical properties as ice, hence the models for ice can also be applied to ice-rich soils. Besides the ice content, soil type also plays the important role when analyzing the parameters related to the creep properties.

3.3.1 Glen Creep Law (1955)

One of the most common ways of describing the creep deformation of frozen soil is the relation introduced by Glen in 1955 for the secondary creep rates of polycrystalline ice as shown in equation(3.1). It has been used widely since then in various forms to describe the creep rate of frozen materials at constant temperatures.

$$\dot{\varepsilon} = B\sigma^n \quad\quad\quad (3.1)$$

where $\dot{\varepsilon}$ is the steady state creep rate; σ is the applied stress.

B and n are material parameters, depend on temperature, salinity, density, composition, and microstructure of the material and also to some extent on the applied stress level. An important point to note is that the value of B and n are dependent on the unit of the stress and strain rate. They don't hold constant for the same soil if the testing units have been changed. It is worth to notice that n is much independent on temperature. Since the wide variety of these properties from soil to soil, the B and n parameters are usually determined from a number of constant stress creep tests for different soils where the strain has been recorded as a function of time.

This relation is used for the secondary creep period, i.e. the part of the creep curve where the strain rate remains the same and at minimum rate. See Figure 3-1.

This creep model can also be valid if the applied stress come from triaxial direction.

Equation (3.1) can be rewritten as equation(3.2).

$$\dot{\varepsilon}_e = B\sigma_e{}^n \tag{3.2}$$

$\dot{\varepsilon}_e$ is the equivalent strain rate; σ_e is equivalent stress. They are defined in Eq.(3.3) and **Error! Reference source not found.**(3.4) (Johnston & Ladanyi, 1972)

$$\dot{\varepsilon}_e{}^2 = \frac{2}{9}[(\dot{\varepsilon}_1 - \dot{\varepsilon}_2)^2 + (\dot{\varepsilon}_2 - \dot{\varepsilon}_3)^2 + (\dot{\varepsilon}_3 - \dot{\varepsilon}_1)^2] \tag{3.3}$$

$$\sigma_e{}^2 = \frac{1}{2}[(\sigma_1 - \sigma_2)^2 + (\sigma_2 - \sigma_3)^2 + (\sigma_3 - \sigma_1)^2] \tag{3.4}$$

Studies have been developed to investigate the parameters of this model. And they are listed in

Table 3-1 and Table 3-2

	B ($kPa^{-n} \times year^{-1}$)	n
−1℃	4.5×10^{-8}	3.0
−2℃	2.0×10^{-8}	3.0
−5℃	1.0×10^{-8}	3.0
−10℃	5.6×10^{-9}	3.0

Table 3-1 Tentative creep constants for ice-rich soil under different temperatures(Morgenstern , Roggensack, & Weaver , 1979)

Salinity (ppt)	B ($kPa^{-n} \times year^{-1}$)	n
0	5×10^{-10}	3.0
5	2.0×10^{-9}	3.0
10	7.0×10^{-9}	3.0
15	2.5×10^{-8}	3.0
20	1.0×10^{-7}	3.0
25	2.5×10^{-7}	3.0
30	6.0×10^{-7}	3.0
35	1.0×10^{-6}	3.0

Table 3-2 Creep constants for ice-rich soils with different salinityat temperature=-5C (Nixon & Lem, 1984)

3.3.2 Vialov Creep Model (1962)

Vialov(1962) suggest probably the oldest form of creep equation for frozen soil in Equation(3.5)

$$\varepsilon = \left[\frac{1}{\omega(\theta + 1)^k}\right]^c \sigma^c t^b \qquad\qquad (3.5)$$

σ is applied constant stress (MPa) , t is the time elapsed after the application of the load(hr), θ is the temperature below the freezing point of water. c, b, ω, k are constants depend on the soil properties as listed in Table 3-3

Table 3-3 Constants for different soils for primary creep estimation(Weaver & Morgenstern, 1981)

Soil	c	b	ω $(MPa \cdot h^{\frac{b}{c}}/°C^k)$	k	Sources
Suffield clay	2.38	0.333	0.73	1.2	(Sayles & Haynes, Creep of frozensilt and clay, 1974)
Bat-Baioss clay	2.50	0.450	1.25	0.97	(Vialov, et al., 1962)
Hanover silt	2.04	0.151	4.58	0.87	(Sayles & Haynes, Creep of frozensilt and clay, 1974)
Callovian sandy loam	3.70	0.370	0.88	0.89	(Vialov, et al., 1962)
Ottawa sand (1)	1.28	0.449	44.7	1.0	(Sayles, 1968)
Ottawa sand (2)	1.32	0.263	21.0	1.0	(Weaver & Morgenstern, 1981)
Manchester fine sand	2.63	0.631	2.29	1.0	(Sayles, 1968)

This model is designed for predicting the creep for the whole period of creep, and mainly for soils that only develop the creep in primary stage. Hence it's for ice-poor soils. Figure 3-10 shows the analytical creep curve plotted based on this model for a ice-poor soil. This curve shows the develop process of the primary creep.
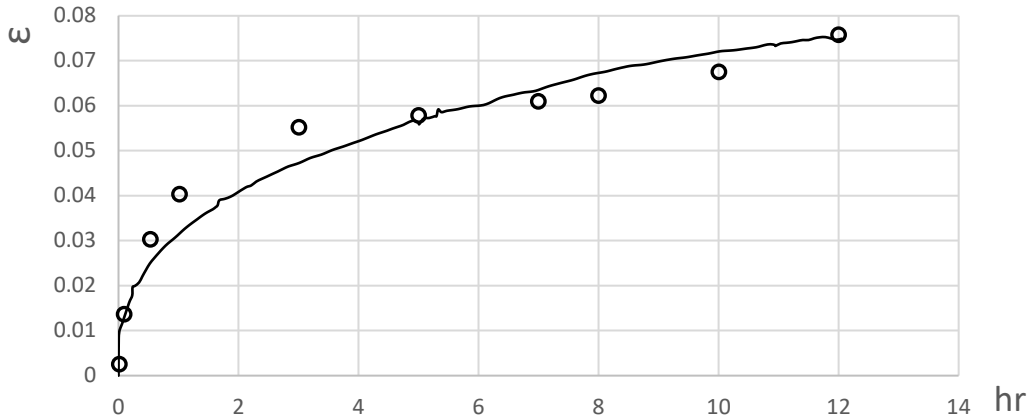
Figure 3-10 Analytical creep curveplotted according to Equation(3.5)and experimental points. Tested soil:

Callovian sandy loam with T=-10C; Stress=30kg/cm2 (Adapted from (Vialov, et al., 1962))

3.3.3 Ladanyi Creep Model (1972)&(1983)

The term Ladanyi used to predict the creep is by approximating the creep curve by straight line as indicated as $\varepsilon^{(i)}$-c in Figure 3-11. This method is aiming to establish a law that describes these straight lines rather than the actual creep curves. Though applying this method might lead to some error, but the error will keep decreasing during the continued creep. For frozen soils, according to Vialov (1959), for time intervals longer than about 24 hours, the amount of strain developed during the secondary creep period is large compared with the strain developed during primary creep, so that the proposed straight-line approximation seems acceptable for most practical long term problems.

The equation is then made to predict the strain at secondary creep period as shown in equation (3.6)

$$\varepsilon = \varepsilon^{(i)} + \varepsilon^{(c)} \tag{3.6}$$

$\varepsilon^{(i)}$ is the pseudo-instantaneous strain; $\varepsilon^{(c)}$ is the creep strain, also known as the time depend displacement. In here, the total strain is governed by constant stress and temperature. (Ladanyi

35

B. , 1972)
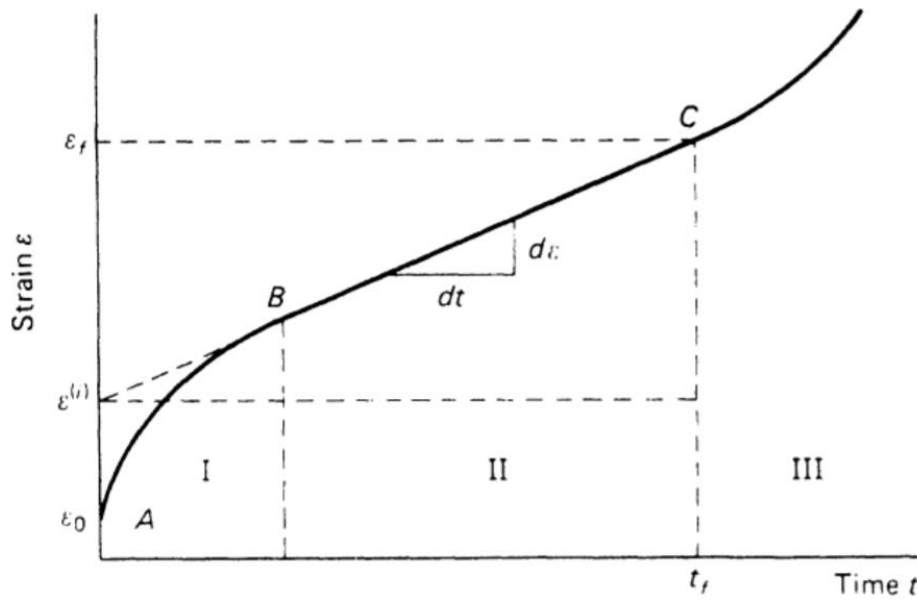
Figure 3-11 Basic creep curve with the definition of instantaneous strain(Andersland , Sayles, & Ladanyi, 1978)

The pseudo-instantaneous strain is composed of an elastic(reversible) portion, $\varepsilon^{(ie)}$, and a plastic(irreversible) portion, $\varepsilon^{(ip)}$. Hence it can be written as equation (3.7)

$$\varepsilon^{(i)} = \varepsilon^{(ie)} + \varepsilon^{(ip)} \tag{3.7}$$

The elastic portion of $\varepsilon^{(i)}$ can be written as equation(3.8)

$$\varepsilon^{(ie)} = \sigma/E(T) \tag{3.8}$$

where $E(T)$ is a fictitious Young's modulus, it also contains the delayed elasticity effect. The plastic portion may often be written as a pure power expression as equation(3.9)

$$\varepsilon^{(ip)} = \varepsilon_k \left[\frac{\sigma}{\sigma_k(T)}\right]^{k(T)} \tag{3.9}$$

$\sigma_k(T)$ plays the role of a temperature dependent deformation modulus, the exponent $k(T) > 1$ is usually little affected by the temperature, while ε_k, is an arbitrary small standard strain unit introduced only for convenience in calculation and plotting of data.

36

These instantaneous strains, however, is very little compared to the creep strain. According to experimental studies (Vialov, 1959), for time intervals greater than about 24 hours the two instantaneous strain terms together become less than 10% of the creep strain. Hence the creep strain is what need to focus on.

The creep strain can be calculated by giving the law of strain rate then multiplying the strain rate by time and the creep strain will be known. The strain rate, $\dot{\varepsilon}$, is therefore written in equation (3.10)

$$\dot{\varepsilon} = \frac{d\varepsilon}{dt} = \dot{\varepsilon}_c \left[\frac{\sigma}{\sigma_c(T)} \right]^{n(T)} \tag{3.10}$$

$\sigma_c(T)$ and $n(T)$ are creep parameters, both depending on the temperature, $n(T)$ parameter is much less depending on the temperature than $\sigma_c(T)$. $\dot{\varepsilon}_c$ is a small arbitrary standard strain rate, being introduced to put the equation into a normalized form. The $\sigma_c(T)$ parameter is the uniaxial stress that causes a constant creep rate equal to $\dot{\varepsilon}_c$. The magnitude of $\sigma_c(T)$ depends on the value chosen for $\dot{\varepsilon}_c$. For frozen soils, it may be convenient to take, e.g., $\dot{\varepsilon}_c = 10^{-5} min^{-1} = 1.44\%/day$

The creep model developed above is based on the assumption that the soil is under uniaxial unconfined compression test with the friction angle equal to 0. The author later then found the way of writing the creep and creep strength equations under triaxial compression conditions.

In the theory developed by Ladanyi(1983) for triaxial compression test, it divided the soils into two categories. The first one is for "cold" soil. According to U.S.S.R. (1976) Standards, the "cold" term here refers to temperature lower than -0.3℃ for silty sands, -0.6℃ for sandy loams,

37

-1.0°C for clay loams and -1.5°C for clay. It is assumed that this kind of soil contains very little unfrozen water, which do not consolidate under confining pressure but show an increasing brittleness with increasing strain rate. In this kind of soil, the friction angles vary with the strain rate as shown in Figure 3-12(a). The creep rate for cold hard frozen soil can be calculated as equation (3.11)

$$\dot{\varepsilon}_e = \dot{\varepsilon}_c \left[\frac{\sigma_e}{\sigma_c(1 - \sin\phi_c) + 3\sigma_m \sin\phi_c} \right]^{n(T)} \qquad (3.11)$$

$\dot{\varepsilon}_e$ and σ_e vary for different pressure conditions. They are defined in Eq.(3.3) &(3.4)

For most common condition, the axial symmetry, with $\sigma_2 = \sigma_3, \dot{\varepsilon}_2 = \dot{\varepsilon}_3$ then $\sigma_e = (\sigma_1 - \sigma_3), \dot{\varepsilon}_e = \dot{\varepsilon}_1$.

ϕ_c is the slope angle of a Coulomb envelop at $\dot{\varepsilon}_e = \dot{\varepsilon}_c$.

$$\sigma_m = \frac{\sigma_1 + \sigma_2 + \sigma_3}{3} \qquad (3.12)$$
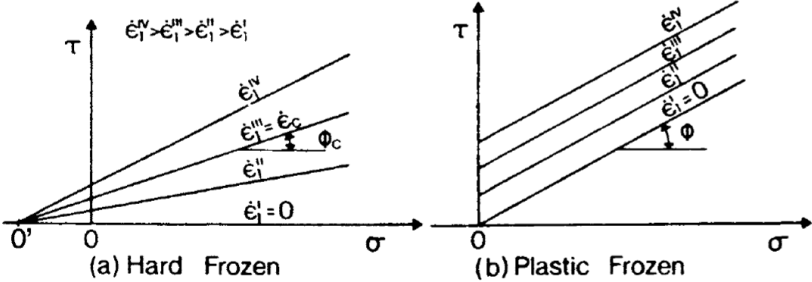
Figure 3-12 Simplified failure envelopes for (a)Hard Frozen(ice-rich), and (b)Plastic Frozen(ice-poor) frozen soils

(Ladanyi, 1983)

For warm soil, i.e. temperature for clay higher than -1.5°C, on the other hand, having a constant internal friction angle, ϕ, as shown in Figure 3-12(b). The "warm" soil contains large quantities

of unfrozen water, which consolidates under confining pressure. The creep rate can then be calculated as equation(3.13)

$$\dot{\varepsilon}_e = \dot{\varepsilon}_c \left[\frac{\sigma_e - 3\sigma_m \sin \phi}{\sigma_c (1 - \sin \phi)} \right]^{n(T)} \tag{3.13}$$

However, in practice, the effect of confining pressure on creep settlement of foundations is often neglected because it leads to safer design. (Linell & Lobacz, 1980) As a result, the general creep rate equation (3.10) is considered valid for most foundation design in permafrost areas.

3.3.4 Zhu & Carbee Creep Model (1987)

Zhu & Carbee (1987) performed a series of uniaxial constant stress compression test on frozen silt in Fairbanks, Alaska. These tests were conducted at seven temperatures ranging from -0.5°C to -10°C and three nominal densities refer to low, medium to high as 1.08, 1.20 and 1.40g/cm^3. The constant-stress creep tests were conducted at stress levels causing test durations from a few minutes to more than two months.

It pointed out that different deformation mechanisms are dominant within different ranges of strain rate hence the relationship of stress and strain rate can not be described by a single power law or exponential equation. As a result, it established two different equations based on distinguishing of two different strain rate ranges.

However, in Zhu and Carbee's study, the three stages of creep didn't behave as shown in Figure 3-1 with the flat zone developed by secondary creep stage. Their study, on the other hand, showed quick shift from primary creep to tertiary creep, leaved the secondary creep stage as a

point or relatively short period. As shown in Figure 3-13. This might be caused by the reason that the soil was remolded and the distilled water was added to the sample to make it water content of 12%. With this water content, the soil was still not ice-rich soil, hence the primary creep dominated the constant compression stress test until the failure happened and led to tertiary creep.
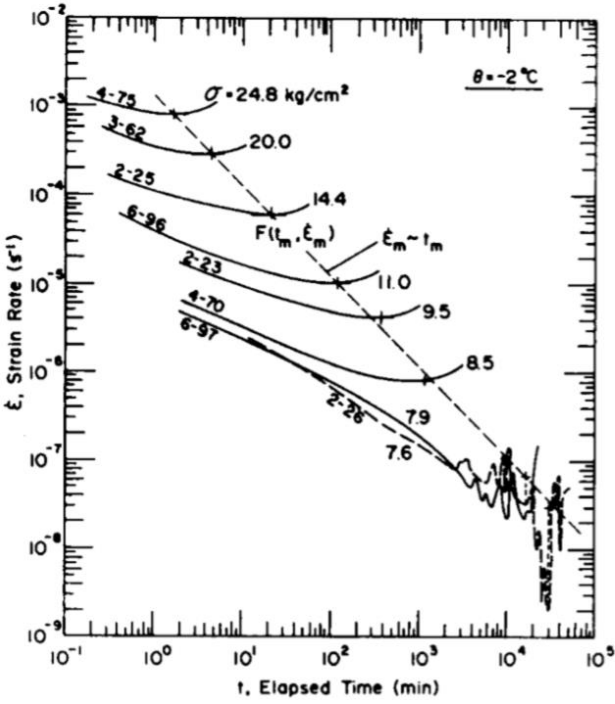
Figure 3-13 Creep curve in log-log scale under different stresses(Zhu & Carbee, 1987)

Therefore, the authors defined the minimum creep rate, $\dot{\varepsilon}_m$, namely the secondary creep rate, $\dot{\varepsilon}$, as the failure creep rate. Correspondingly, the time to the minimum strain rate, t_m, is the time to creep failure. As shown in Figure 3-14

Zhu & Carbee then developed the creep model for calculating the secondary creep rate for different creep type based on the creep rate, if the creep rate is larger than the critical creep rate, $\dot{\varepsilon}_{cr}$, then it's categorized as short-term creep, on the contrary, the creep rate less than the critical creep rate is long-term creep. These two creeps are considered to have different deformation

mechanisms. The constitutive equations for the frozen silt with medium density can be described by the following exponential equations. (Zhu & Carbee, 1987)
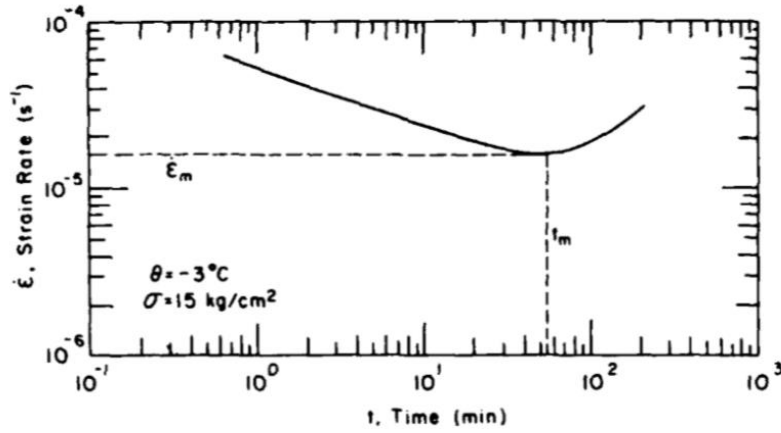
Figure 3-14 Typical creep curve of Zhu & Carbee's studyunder relatively high stress (Zhu & Carbee, 1987)

The test for short-term creep ($\dot{\varepsilon} > \dot{\varepsilon}_{cr}$) normally lasts less than 1 day. The secondary creep rate, $\dot{\varepsilon}$, for short-term creep can then be calculated as Eq.(3.14)

$$\dot{\varepsilon} = \dot{\varepsilon}_r \, exp\left[-K\left(\frac{1}{\sigma} - \frac{1}{\sigma_r}\right)\right]$$

(3.14)

$\dot{\varepsilon}_r$ and σ_r are reference values independent of temperature and are used for convenience in presenting this data. These two values should be obtained by linear regression analysis, Zhu and Carbee got: $\dot{\varepsilon}_r = 8.84 \times 10^{-3} \, s^{-1}$; $\sigma_r = 71.4 \, kg/cm^2$ for their tested frozen silt. K is a function of temperature and can be determined by equations (3.15)(3.16).

$$K = 53.1(\theta/\theta_0)^{0.72} \quad \text{for} \ -0.5°C \geq \theta \geq -2°C$$

(3.15)

$$K = 42.4(\theta/\theta_0)^{1.02} \quad \text{for} \ -2°C \geq \theta \geq -7°C$$

(3.16)

where θ is the test temperature in °C, and θ_0 is a reference temperature taken as -1°C.

41

For long-term creep ($\dot{\varepsilon} \leq \dot{\varepsilon}_{cr}$), the exponential equation is illustrated in Eq.(3.17)

$$\dot{\varepsilon} = \dot{\varepsilon}_{cr} \, exp\left[-K'\left(\frac{1}{\sigma} - \frac{1}{\sigma_{cr}}\right)\right] \tag{3.17}$$

$\dot{\varepsilon}_{cr}$ is the critical creep rate, equal to $10^{-6} \, s^{-1}$. σ_{cr} is the critical creep strength that correspond to the critical creep rate for various temperature (See Figure 3-15) and can be calculated as Eq. (3.18) and the unit is in kg/cm^2

$$\sigma_{cr} = 5.2(\theta/\theta_0)^{0.78} \tag{3.18}$$

The parameter K' in equation (3.17) is under a function of temperature can be calculated as

$$K' = 134(\theta/\theta_0)^{1.04} \tag{3.19}$$
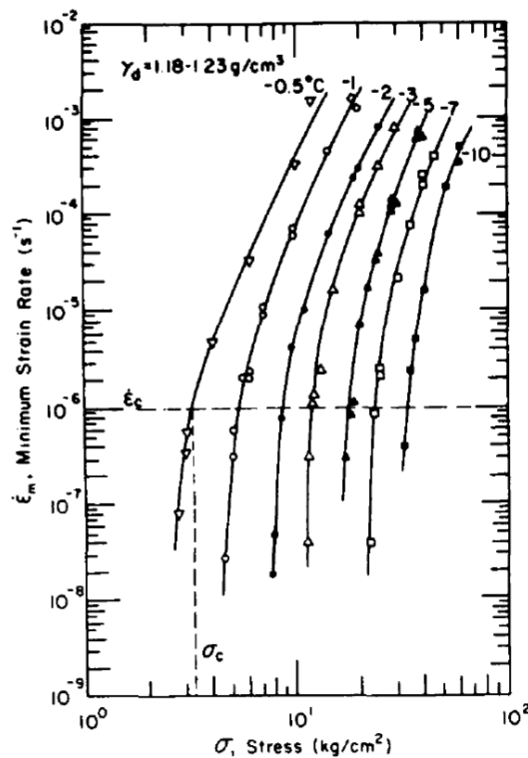
Figure 3-15 Minimum strain rate vs stressin log-log scale at various temperature (Zhu & Carbee, 1987)

42

Observing Figure 3-15, Zhu & Carbee assume the curves can be represented approximately as a set of bilinear curves, which deflect at the strain rate $\dot{\varepsilon}_{cr}$ of $10^{-6}\ s^{-1}$. The straight lines can be expressed by power equation(3.20)

$$\dot{\varepsilon} = \dot{\varepsilon}_{cr}\left(\frac{\sigma}{\sigma_{cr}}\right)^n \tag{3.20}$$

where the exponent n depends upon temperature. For short-term creep ($\dot{\varepsilon} > \dot{\varepsilon}_{cr}$), n can be evaluated by Eq.(3.21)

$$n = 5.59(\theta/\theta_0)^{0.223} \tag{3.21}$$

For long-term creep ($\dot{\varepsilon} \leq \dot{\varepsilon}_{cr}$), n can be evaluated by Eq.(3.22)

$$n = 27.36(\theta/\theta_0)^{0.233} \tag{3.22}$$

This power function is similar to the one proposed by Ladanyi (1972) in equation(3.10). The main difference is in Equation(3.10) the use of $\dot{\varepsilon}_c$ is to put the eqaution into the normalized form. But in Equation(3.20), the parameter $\dot{\varepsilon}_{cr}$ is defined to separate two different creep forms, the short-term creep and the long-term creep.

It is important to note that regression analysis used to obtained the creep parameters in this section are only for specific soil, frozen silt in Fairbanks. The critical creep rate will be varied under different conditions, thus equation (3.15) (3.16) (3.18) (3.19) (3.21) (3.22) can only be considered as an special formula for the frozen silt in Fairbanks.

3.4 Conclusion

The creep modeling is highly depended on extensive experimental work due to many factors such as solute content, water or ice content, dry density as well as especially temperature that influence the creep behaviors of frozen soils. Studies have been put focus on empirical models

which often precisely describe creep behaviors of frozen soils under certain conditions but with serious limitations for extension.

In this chapter, four creep laws are described. Among them, two are used for ice-rich soils, Norton-Bailey creep model and Ladanyi creep model. These ice-rich soils developed creep mainly under secondary creep stage. These models may give good results for long-term creep for ice-rich soil, where approximately constant strain rate dominates the creep behavior. However, the predictions overestimate the strain when the primary creep process dominates.

On the other hand, creep law developed by Vialov and Zhu & Carbee are based on the tests for ice-poor soils. Vialov's creep model can predict the strain developed over time, but this model can not be based upon strain rate as the strain rate can't hold constant for primary creep as developed for ice-poor soil. Zhu & Carbee, on the contrary, developed the model based on creep rate. Normally, the creep failure is defined as the point of the start of tertiary creep. But in their study, secondary creep only developed for a sudden period then continued with tertiary creep. Hence, they defined the secondary or the minimum creep rate as the failure creep rate and establish the creep law to predict this creep rate.

Four creep model were developed under different soil conditions at different sites. It's important to keep in mind that the mechanical behavior of a frozen soil is dynamic and complex. When formulating a relationship for the stress and deformation, it is essential to understand the characteristics of the soil being evaluated. This requires a range of laboratory investigations, which will then allow site specific soil parameters to be determined. After determining the characteristics of frozen soils, the creep tests then can be performed and the parameters in the creep models are therefore to be decided.

Chapter 4 Creep considerations for foundation design

Since frozen soils are relatively strong and have low permeability, they may be used successfully as materials for various types of engineering construction. In this chapter, the design under the consideration of creep of pile foundation and shallow foundation will be introduced. Since pile foundation is generally wide used in the cold regions, the investigations of pile foundation thus can be separated to two kinds: the friction pile and the end-bearing (pile tip) pile.

One of the most important considerations in foundation design is to ensure the functionality of the foundation and the structure above by minimizing the foundation movement and distortion. It is called the service limit state. The service limit state involves calculation of movements using deformation parameters. Satisfying the service limit state ensures that the foundation will meet a chosen degree of confidence against excessive movement or distortion of the structure. (Briaud, 2013)

In cold regions, when the design is being made for constructions on the frozen soils, it is necessary to take into consideration the specific properties of such soils. The strength and deformation properties of frozen soils depend essentially upon soil-temperature, soil-composition, and soil-texture (grain-size distribution, moisture content, ice content, salinity, etc.). In frozen fine-grained soils, the volume of ice may be greater than that of the soil solids. Thawing of this ice can change a perennially frozen soil from a firm bearing material into a slurry with no supporting capacity.

When it comes to design the stable structures under the consideration of creep as the

deformation resources, the creep equations introduced in the former chapter can then be used. The parameters in the creep equations have been obtained under various tests for the target soil. Hence these parameters include the deformation properties of the frozen soil and then can be used for further approximation of the creep behavior under the foundation load.

For foundation under long-term load on the frozen soil, the creep takes a big portion of the deformation. It is because creep is a behavior that will continue forever, it cannot be reduced to zero. If the soil for foundation design is not homogeneous, the creep may lead to crack in the buildings above the foundation. Calculations for deformation are necessary. Such calculations consist of determining the displacement of creep in a given time interval, does not exceed a certain permissible value. A criterion of allowable displacement is hence needed in order to determine the design load for the foundation.

4.1 Pile Foundations

Pile foundations are the part of structures used to carry or transfer the load from the structures. By how the load is being carried, there are two different types of piles. The first one is friction or cohesion pile, which resists the load from the adhesion or friction strength developed between the soil and the pile lateral surface. The other is end-bearing pile, which is built on solid stable base and can transmit a foundation load to a solid ground.

Pile constructions in permanently frozen ground are generally only embedded in frozen soils. Hence the pile derives the major portion of their load-bearing capacity from adfreeze bond developed between the soil or backfill (slurry) and the pile lateral surface, whereas only a small fraction of their capacity at service loads is due to their end bearing. The end bearing is normally counted only where the pile end attains an ice-free bedrock or dense thaw-stable granular

material. (Andersland & Ladanyi, 2004)

Figure 4-1 Building supported by concrete piles in Pyramiden, Svalbard, Norway
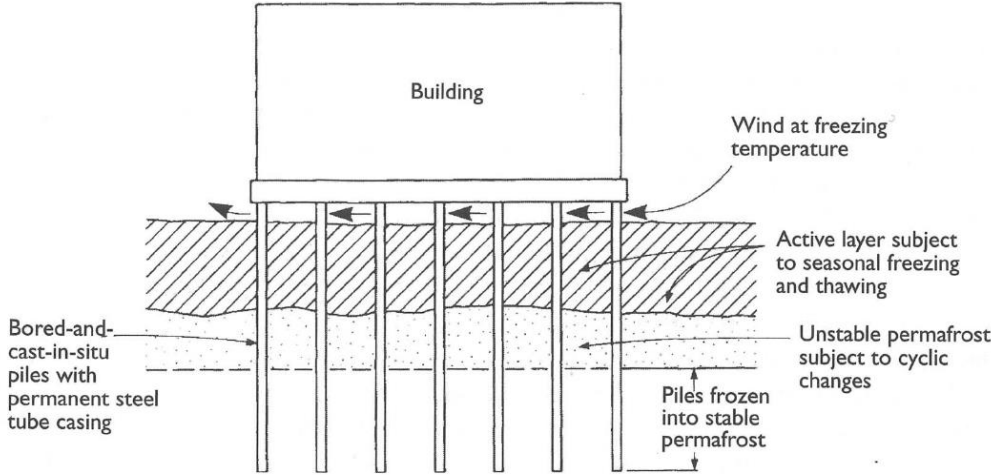
Figure 4-2 Schematic diagram of a pile foundation

4.1.1 Friction Pile

In this section, the study put focus on the discussion of the deformation of the soil along the

pile shaft. Figure 4-3 illustrates the cross section of the pile with the emplacement method of

placement into the oversize hole. Pile was put into a pre-bored or pre-thawing oversize hole and

the soil/water slurry was used as a backfill material. The interface between the pile and the backfill soil gives the adfreeze strength of the structure.
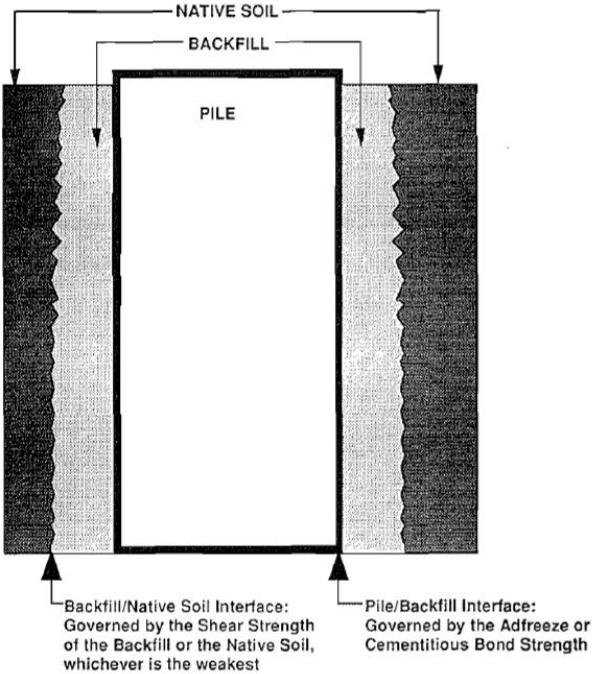
Figure 4-3Pile cross section showing location of interfaces(Biggar & Sego, 1992)

When it comes to the pile foundation, the soil offers the adfreeze strength to contribute to the main part of pile bearing capacity. Adfreeze bond of frozen soil against a structure depends essentially on the physical properties of the soil, the characteristics of the interface, the temperature, and the type and the rate of loading.

When it comes to pile bearing capacity, one of the most important characters to consider is the required depth of the embedment. Permafrost conditions at a site are often in a delicate state of thermal equilibrium, which renders permafrost a very difficult material on which to carry out construction without some thawing of the frozen soil. The situation is further aggravated by the impervious nature of the permafrost; rainfall and water from melting snow cannot drain into the ground, but instead forms pools and lakes. This induces a net increase of heat flux into the

permafrost, thereby lowering the permafrost table. This is particularly Important during the design life of a structure when a degrading thermal regime can reduce the effective pile embedment area and increase the downdrag loading on the piles. (Weaver J. S., 1979) Therefore, a pile embedment depth is determined which can support the imposed loads on the pile under the worst loading conditions, unless suitable end-bearing in a competent material can be obtained.

Pile failure can occur in the form of either gross disruption of the adfreeze bond or excessive settlement engendered by creep of the frozen soil. As a result, there are two criteria that must be satisfied for pile design in permafrost. First, there must be an adequate margin of safety against gross failure. Second, pile settlements must be held within specified acceptable limits over the design life of the structure. (Nixon & McRoberts, 1976) Generally, for ice-poor soil, the design consideration will put focus on the allowable adfreeze strength. On the other hand, as ice-rich soil displays non-attenuating creep characteristics, the design load is hence determined from consideration of tolerable creep settlements during the service life of the structure. In this study, the discussion put focus on the assessment of creep settlements to limit the distortion and deformation of the structure.

Pile creep in frozen soils has been predicted using a simple shear analytical model. The deformation of the soil around a pile shaft may be idealized as shearing of concentric cylinders as shown in Figure 4-4. τ is the average applied adfreeze stress or the pile shaft stress, P_S is the load carrying capacity of a friction pile. The analysis is needed which relates the steady pile settlement rate to the pile shaft stress and the constant ground temperature. The analysis here aims to calculate the allowable loading on a pile which will maintain the settlements within tolerable limits based on knowledge of the creep rate of the foundation soil. (Nixon & McRoberts, 1976)
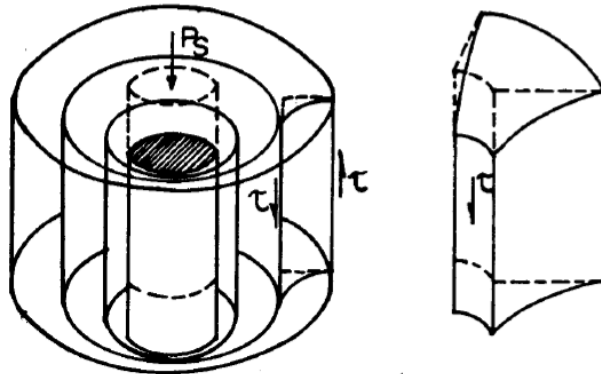
Figure 4-4Analytical Model for friction piles(Weaver J. S., 1979)

As we shall see, the problem of a cylindrical pile in frozen ground is formulated in terms of the shear stress, τ and the shear strain rate, $\dot{\gamma}$ induced in the frozen ground around the pile. It is therefore necessary to rederive the flow law established in section 3.3.1 and 3.3.2 in a form applicable to the problem at hand. (Nixon & McRoberts, 1976)

For the problem of a vertically loaded pile in frozen soil, the strains around the pile in the tangential (θ) direction are zero, and consequently each element of frozen soil deforms under plane strain conditions. The following analysis shows how the shear strain rate related to shear stress for a ice-rich frozen soil subjected to simple shear under plane strain conditions.

Plane strain for a material element in an axis system with orthogonal axes 1-3 is per definition (zero strain in direction 2) in Eq.(4.1)

$$[\dot{\varepsilon}_1, \quad \dot{\varepsilon}_2 = 0, \quad \dot{\varepsilon}_3 = -\dot{\varepsilon}_1] \tag{4.1}$$

Insert and derive from Eq.(3.3), the equivalent-strain rate for this case is then calculated in Eq.(4.2)

$$\dot{\varepsilon}_e = \sqrt{\frac{2}{9}\left[(\dot{\varepsilon}_1 - 0)^2 + \left(0 - (-\dot{\varepsilon}_1)\right)^2 + \left((-\dot{\varepsilon}_1) - \dot{\varepsilon}_1\right)^2\right]} = \frac{2}{\sqrt{3}}\dot{\varepsilon}_1 \qquad (4.2)$$

Further, by using Hookes law in 3D we write Equation(4.3)

$$\varepsilon_2 = \frac{1}{E}\left[\sigma_2 - \frac{1}{2}(\sigma_3 + \sigma_1)\right] \text{ or } 0 = \frac{1}{E}\left[\sigma_2 - \frac{1}{2}(\sigma_3 + \sigma_1)\right] \qquad (4.3)$$

which yields the stress state for the plane strain conditions as in Equation(4.4)

$$\left[\sigma_1, \ \sigma_2 = \frac{1}{2}(\sigma_1 + \sigma_3), \ \sigma_3\right] \qquad (4.4)$$

Equivalent stress from Eq.(3.4) then yields to Eq.

(4.5)

$$\sigma_e^2 = \frac{1}{2}\left\{\left[\sigma_1 - \left(\frac{1}{2}(\sigma_1 + \sigma_3)\right)\right]^2 + \left[\frac{1}{2}(\sigma_1 + \sigma_3) - \sigma_3\right]^2 + (\sigma_3 - \sigma_1)^2\right\}$$

(4.5)

$$\sigma_e = \frac{\sqrt{3}}{2}(\sigma_1 - \sigma_3)$$

Then, inserting the results of (4.2) and (4.5) into the generalized Norton-Bailey's steady-state creep rate equation(3.2) yields to equation (4.6)

$$\frac{2}{\sqrt{3}}\dot{\varepsilon}_1 = B\left[\frac{\sqrt{3}}{2}(\sigma_1 - \sigma_3)\right]^n$$

(4.6)

$$\dot{\varepsilon}_1 = \left(\frac{\sqrt{3}}{2}\right)^{n+1} B(\sigma_1 - \sigma_3)^n$$

For Ladanyi's steady-state creep equation (3.10), the model in plain strain condition can be developed to equation(4.7)

$$\frac{2}{\sqrt{3}}\dot{\varepsilon}_1 = \dot{\varepsilon}_c \left[\frac{\frac{\sqrt{3}}{2}(\sigma_1 - \sigma_3)}{\sigma_c(T)} \right]^{n(T)} \tag{4.7}$$

$$\dot{\varepsilon}_1 = \left(\frac{\sqrt{3}}{2}\right)^{n(T)+1} \dot{\varepsilon}_c \left(\frac{\sigma_1 - \sigma_3}{\sigma_c(T)}\right)^{n(T)}$$

In order to develop the steady-state creep equation into the shearing form, the concept of simple shear is then established. For a situation of simple shear strain ("simple shear"), or plane shear strain rate, the equations are developed in the same manner. The shear strain (shear distortion) in the coordinate system 1-3 is given by $\gamma_{1-3} = \gamma = \varepsilon_1 - \varepsilon_3$ (where due to the plane strain assumption $\varepsilon_3 = -\varepsilon_1$ as in Equation(4.1)). Correspondingly the shear strain rate (shear distortion rate) yields as shown in Eq.(4.8)

$$\dot{\gamma} = \dot{\varepsilon}_1 - \dot{\varepsilon}_3 = \dot{\varepsilon}_1 - (-\dot{\varepsilon}_1) = 2\dot{\varepsilon}_1 \tag{4.8}$$

The shear stress in the plane strain configuration relates to the principle stresses by:

$$\tau = \tau_{1-3} = \frac{1}{2}(\sigma_1 - \sigma_3) \tag{4.9}$$

Finally, when combining Eq.(4.8) and Eq.(4.9) into Eq.(4.6) we get for the pure shear strain rate as shown in equation(4.10)

$$\dot{\gamma} = 3^{\frac{n+1}{2}} B\tau^n \tag{4.10}$$

Similarly, Eq.(4.7) can be rewritten as Eq.(4.11)

$$\dot{\gamma} = 3^{\frac{n(T)+1}{2}} \dot{\varepsilon}_c \left(\frac{\tau}{\sigma_c(T)}\right)^{n(T)} \tag{4.11}$$

It is important to bring the analysis to be useful in the field. In the field, the practical method is to predict the soil creep deformation in the vertical direction as a source of pile settlements. Therefore, Figure 4-5 shows how the relationship between the shaft stress and its influence to the soil shear distortion and vertical displacement. The following analysis will be addressed for calculating pile vertical displacement in the term of shaft stress.
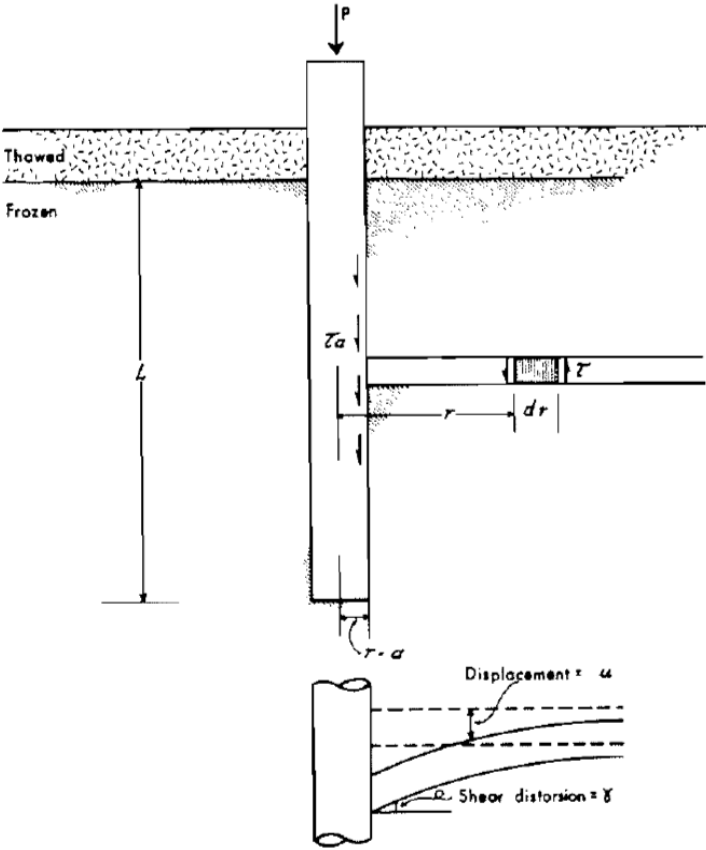
Figure 4-5 Pile in frozen soil, vertical displacement and definition(Nixon & McRoberts, 1976)

The upper part of Figure 4-5 shows the vertical shear stress, τ, at any radial distance from the pile surface (radius r), may be expressed by the shear shaft stress (τ_a) transferred from the pile to the soil (or to the grout) at the pile periphery (where r = a), by:

$$\tau = \tau(r) = \tau_a(a/r) \tag{4.12}$$

The bottom part of Figure 4-5 illustrate a given horizontal soil layer develops vertical

displacements u, with largest vertical displacement at the pile and decreasing displacement away from the pile. The displacement is a function of r, written $u(r)$. The shear distortion γ (also denoted shear strain or shear angle) within the soil layer in relation to the displacement u as:

$$\gamma = -\frac{du}{dr} \tag{4.13}$$

The minus sign in the equation is due to the definition of the positive direction of vertical soil displacement u, where $u(r)$ decreases for increasing distance (r) from the pile.

Correspondingly, the shear strain rate is $\dot{\gamma} = d\gamma/dt$, i.e., change in shear angle per time unit, and relates to the displacement rate, $\dot{u}$, by the following:

$$\dot{\gamma} = -\frac{d\dot{u}}{dr} \tag{4.14}$$

What we seek from these equations is the displacement rate of the soil in contact with the pile (at boundary $r = a$), which provides us with the displacement function and displacement rate function for the pile itself. The displacement rate of the pile is thus $\dot{u}_a = \dot{u}(r = a)$. The solution is determined by solving equation(4.14) for $d\dot{u}$ and integrating with respect to r, as shown in Eq.(4.15)

$$\dot{u}_a(r = a) = \int_{r=a}^{\infty} -\dot{\gamma}\,dr \tag{4.15}$$

Pile displacement rate is equal to the soil displacement rate at the surface of the pile, $r = a$, whereas soil displacement is zero at sufficient distance $r = \infty$ from the pile.

Deriving from Eq.(4.10), the displacement rate can be calculated as Eq. (4.16)
Note that this is integral of a function "below" the argument axis (the r-axis), which requires either taking the absolute value of the integral or multiplying with -1.

$$\dot{u}_a(r=a) = \int_{r=a}^{\infty} -\dot{r}\,dr = \int_{r=a}^{\infty} -\left[3^{\frac{(n+1)}{2}}B\tau^n\right]dr$$

$$= \int_{r=a}^{\infty}(-1) - \left[3^{\frac{(n+1)}{2}}B\tau_a\left(\frac{a}{r}\right)^n\right]dr$$

$$= 3^{\frac{(n+1)}{2}}Ba^n\tau_a{}^n \int_a^{\infty}\left(\frac{1}{r}\right)^n dr \tag{4.16}$$

$$= 3^{\frac{(n+1)}{2}}Ba^n\tau_a{}^n\left(\frac{1}{-n+1}\right)\left[\frac{1}{r^{n-1}}\right]_{r=a}^{r=\infty}$$

$$= 3^{\frac{(n+1)}{2}}Ba^n\tau_a{}^n\left(\frac{1}{1-n}\right)\left[\frac{1}{\infty^{n-1}} - \frac{1}{a^{n-1}}\right]$$

$$= 3^{\frac{(n+1)}{2}}Ba^n\tau_a{}^n\left(\frac{1}{n-1}\right)\left(\frac{1}{a^{n-1}}\right)$$

$$= \frac{3^{\frac{(n+1)}{2}}}{n-1}Ba\tau_a{}^n$$

Correspondingly, Equation(4.11) can be derived to Equation

$$\dot{u}_a = \frac{3^{\frac{(n(T)+1)}{2}}}{n(T)-1}a\dot{\varepsilon}_c\left(\frac{\tau_a}{\sigma_c(T)}\right)^{n(T)} \tag{4.17}$$

There are five assumptions to be followed to make the analysis valid: (1) The analysis is insensitive to change in normal stress on the lateral surface of the pile. (2) There is no slip at the pile-soil interface. (3) Gravity forces are negligible. (4) The soil is homogeneous and isotropic and the properties are uniform with depth. (5) The shear stress is uniformly distributed over the pile length embedded in frozen soil.

For assumption (1), it's because that almost available data were obtained from uniaxial tests, the data presented in the creep form shows that the long-term deformation behaviors of ice and

ice-rich frozen soils are independent of lateral stress. Assumption (2) is satisfied at low stress level since it is proved that the slip does not occur if the stress applied at the interface is less than the adfreeze bond strength. Assumption (4) is due to that geothermal gradients in permafrost are typically greater than 30 m/℃ and thus, in most long pile configurations the temperature distribution may be assumed uniform with depth. However, if a non-uniform temperature-depth profile can be justified, Nixon and McRoberts (1976) have shown how the analysis may be developed to account for depth-dependent soil properties. Similarly, radial inhomogenity may be incoperated into the analysis by considering the soil as concentric homogeneous cylinders and integrating the strains across each region. (Weaver J. S., 1979) Finally, the shear stress distribution along the pile varies with load level and time. It is triangular at low loads, with its maximum at the top of the embedded pile length, and becomes more uniform with increasing load level and load duration. The observed initial triangular stress distribution can be attributed to pile deformability, resulting in shear displacements having maximum values at the top and decreasing with depth eventually to zero at some level within the embedded pile length. On the other hand, in a uniform soil it can be expected that, for equal shear displacements or displacement rates, equal amounts of shear strength will be mobilized and the resulting stress distribution will be uniform. There are essentially three cases in which equal displacements along the pile, and therefore the uniform stress distribution assumed in (5), can be expected to occur in practice: (a) when the pile is much less deformable than the soil, (b) when, after a long time interval, initially nonuniform displacements at the pile-soil interface equalize because of relaxation of stresses in the soil, and (c) after slip has occurred. Case (c) can't be brought to practice as it disobeys assumption (2). (Johnston & Ladanyi, 1972)

The above synthesis justifies the use of this analysis for the prediction of stresses and strains around a friction pile in frozen soils.

In Nixon and McRoberts(1976)'s study, it's shown that the displacement rates are constant after

a relatively short period of time, and thereafter are predictable using the analysis developed previously. For example, the pile in ice-rich permafrost at 0 ℃ reached steady state displacement and stress conditions in less than 2 days as shown in Figure 4-6. Within 15 days, the pile at -2℃ had achieved steady state also as shown in Figure 4-7. This fulfills the criteria(b) for assumption(5) as described beforehand. Pile load tests carried out over a time less than that reqiured to achieve equilibrium would considerably over-estimate the displacement rate in the long term, unless of course the foregoing analysis was used to interpret the results. It is therefore important to carry out pile load tests for a sufficient time period if a steady displacement rate is desired. It is seen that uniform stress conditions were obtained in a short time period for the 'warmest' situation. This lends credence to a design method where the warmest permafrost temperatures would be used to obtain the pile displacements for half of the year and the pile settlements could be assumed negligible for the coldest half of the year. (Nixon & McRoberts, 1976)
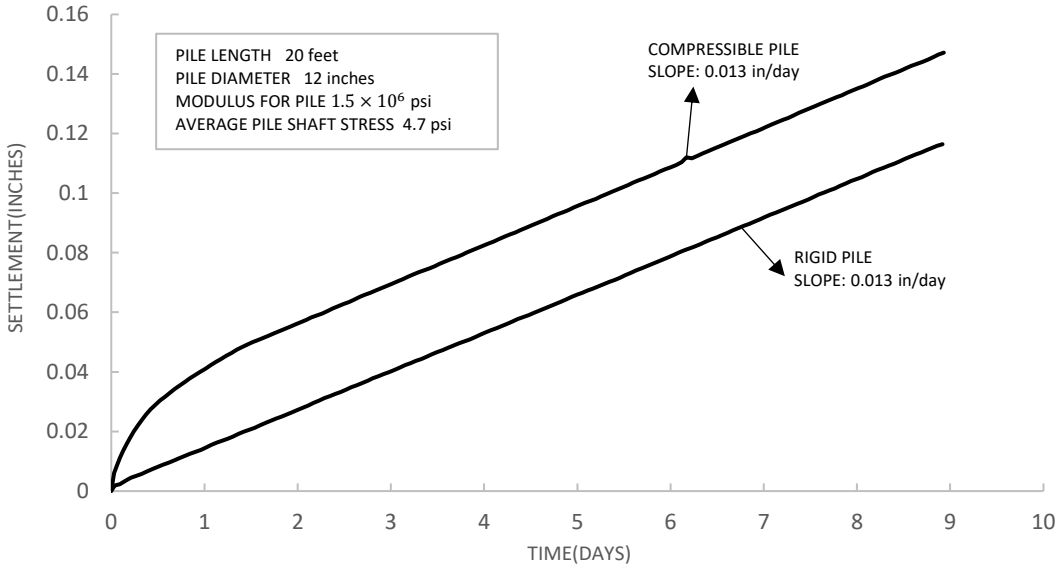
Figure 4-6 Settlement of a compressible pile in ice-rich permafrost T = 0℃(Nixon & McRoberts, 1976)
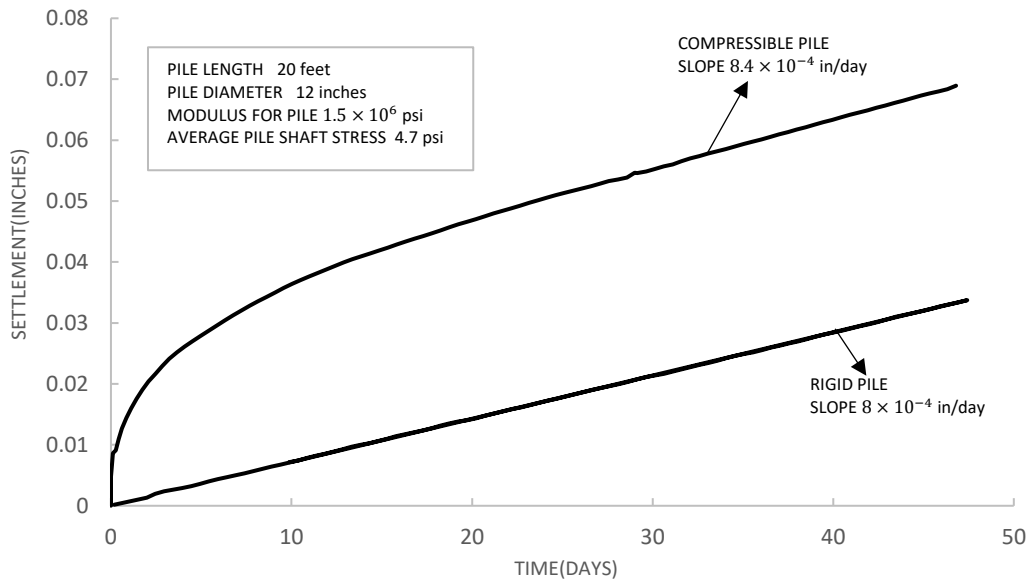
Figure 4-7 Settlement of a compressible pile in ice-rich permafrost T = -2°C(Nixon & McRoberts, 1976)

Considering the problem of a pile in frozen ground at constant temperature it is assumed for the present that the pile material is considerably more rigid in the long-term than the surrounding frozen soil and that the shear stress is distributed uniformly along the pile shaft. The load carrying capacity of a friction pile, P_s, under length L is therefore given by equation(4.18)

$$P_s = 2\pi a L \tau_a \tag{4.18}$$

Deriving from equation(4.16), the load carrying capacity of a friction pile can then be calculated in the term of pile displacement rate as in equation(4.19)

$$P_s = 2\pi a L \left(\frac{\dot{u}_a}{a}\right)^{\frac{1}{n}} \left(\frac{n-1}{3^{\frac{n+1}{2}}}\right)^{\frac{1}{n}} \left(\frac{1}{B}\right)^{\frac{1}{n}} \tag{4.19}$$

If the soil has multiple layers, equation(4.19) will be extended to equation(4.20)

$$P_s = \sum_{i,k} \left[2\pi a \left(\frac{\dot{u}_a}{a}\right)^{\frac{1}{n_i}} L_i \left(\frac{n_i - 1}{3^{\frac{n_i+1}{2}}}\right)^{\frac{1}{n_i}} \left(\frac{1}{B_i}\right)^{\frac{1}{n_i}} \right] \tag{4.20}$$

Where k is the number of soil layers.

Similarly, for equation(4.17), the load carrying capacity can be calculated as in Eq.(4.21)

$$P_s = 2\pi a L \times \sigma_c(T) \left(\frac{\dot{u}_a}{a}\right)^{\frac{1}{n(T)}} \left(\frac{n(T) - 1}{3^{\frac{n(T)+1}{2}}}\right)^{\frac{1}{n(T)}} \left(\frac{1}{\dot{\varepsilon}_c}\right)^{\frac{1}{n(T)}} \tag{4.21}$$

Increases in allowable pile loads suggested by this analysis may be accomplished in a number of ways: (a) increase in depth of embedment, as pile load is directly proportional to embedment for a constant ground temperature situation; (b) increase in pile diameter, although this may be less effective than generally supposed; (c) lowering of ground temperatures, this will provide a striking reduction in creep displacement rates; and (d) designing the structural support to tolerate larger settlements over the expected life of the structure. (Nixon & McRoberts, 1976)

There does not appear to be much evidence for frozen soil creeping faster than ice, and in most cases the analysis for ice provides an upper (conservative) estimate of pile settlement. Therefore, studies have been put focus on analyzing the settlement in ice-rich soils based on the test for ice. Nonetheless, the similar analysis can also bring up to be used for ice-poor soils from the constitutive equation of Eq,(3.5) by Vialov.

Deriving from Eq.(3.5), the foregoing analysis can then be used for ice-poor soils as described as follows. Firstly, it's essential to develop the strain-stress equation into the form of shear strain

versus shear stress as the same way of deriving equation(4.10). In this condition, equation(3.5) can be rewritten as equation(4.22)

$$\gamma = 3^{\frac{c+1}{2}} \left[\frac{1}{\omega(\theta + 1)^k} \right]^c \tau^c t^b \tag{4.22}$$

Where γ and τ are shear strain and shear stress respectively. c, ω, θ, k and b are defined in section 3.3.2. t is time.

Equation(4.22) is analogous to equation(3.5) and so the friction pile displacement may be related to the applied shaft stress accordingly as in equation(4.23)

$$\frac{u_a}{at^b} = \frac{3^{\frac{c+1}{2}}}{c-1} \left[\frac{1}{\omega(\theta + 1)^k} \right]^c \tau_a^c \tag{4.23}$$

The load carrying capacity of a friction pile in an ice-poor frozen soil is thus given by equation(4.24)

$$P_s = 2\pi a L \left(\frac{u_a}{at^b} \right)^{\frac{1}{c}} \left(\frac{c-1}{3^{\frac{c+1}{2}}} \right)^{\frac{1}{c}} \omega(\theta + 1)^k \tag{4.24}$$

Studies have shown that the analysis above gives a rather conservative calculation compare to the real data from the fields. This makes the analysis valuable as conservative design leads to safer foundations. However, more rational design approach is still worth to pursue, hence the simplified analysis has been developed further to address some conditions like the effect of lateral normal pressure. In this study, it aims to give a general concept of how the first procedure of the design established to consider the creep for friction piles in permafrost.

4.1.2 End-bearing pile

The behavior of a pile tip in permafrost is considered similar to a circular footing on a viscous

half space. Ladanyi and Johnston (1974) develop a method for predicting the creep settlement of frozen soil under deep circular loads. It uses experimentally determined frozen soil parameters to calculate the time and temperature dependent settlement and rupture of deep circular footings as well as circular plate and screw anchors embedded deeply in frozen soils. The method proposed is based on the theory of cavity expansion. The cavity expansion theory used on the soil under deep load is proposed as shown in Figure 4-8. It is assumed that during the penetration of the punch a rigid cone (or wedge) of soil is formed at the base of the punch, the lateral surface of which is acted upon by a uniformly distributed soil pressure whose normal component is equal to the cavity expansion pressure, P_i. (Ladanyi & Johnston, 1974)
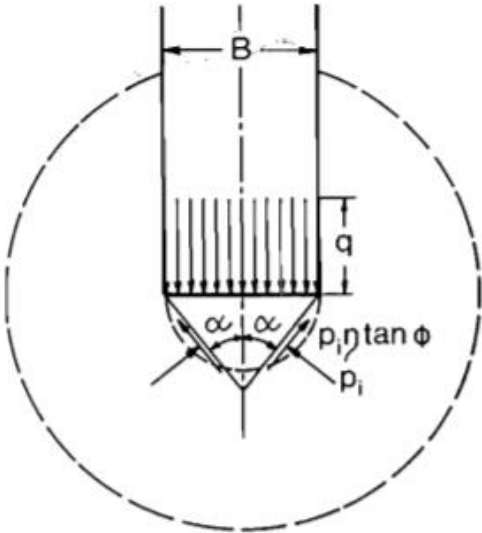
Figure 4-8 Cavity expansion sketch(Ladanyi & Johnston, 1974)

A simplified solution is available at present that can be applied to solving a cavity expansion problem in materials with time dependent properties such as frozen soils. The procedure consists in expressing the deformation and strength properties of frozen soil as functions of time and temperature. This solution is based upon isochronous stress-strain curves, the resulting load displacement relationship will also be of an isochronous type. Consequently, such a solution can be used directly only for finding the amount of creep settlement of a deep footing under a

step-load and at a given freezing temperature.

In order to facilitate the use of the theory in the design, the theory has been developed step by step as introduced in the following. First, the stresses and displacements in each separate region around the cavity have been found. Then, by satisfying the continuity and the boundary conditions, the relationship between the pressure P_i in the cavity and the corresponding radial displacements or displacement rate of the cavity wall has been determined.

To start with, the volume change is the first thing to consider with in the cavity expansion theory. For a settlement u_a in a frozen soil from a circular punch, it will result in a volume displacement of V_s

$$V_s = \pi a^2 u_a \tag{4.25}$$

where $a = B/2$, is the radius of the punch.

The original volume of the hemisphere to be expanded by the punch penetration is V_{io}

$$V_{io} = \frac{2}{3}\pi a^3 \tag{4.26}$$

After the punch penetration, the volume is expected to expand to V_i

$$V_i = V_{io} + V_s \tag{4.27}$$

From Eq.(4.27), the ratio of the before and after volume of the cavity can be expressed in Eq.(4.28).

$$\frac{V_i}{V_{io}} = 1 + \frac{3}{2}\left(\frac{u_a}{a}\right) \tag{4.28}$$

From the geometry of Figure 4-9, by equating the volumes of the failure zone before and after the displacement u_i, of the inner boundary, and after neglecting certain small magnitudes of higher order, the following expression can be deduced as shown in Eq.(4.29) (Ladanyi & Johnston, 1974)

$$\frac{V_i}{V_{io}} \cong \left(1 - \frac{u_i}{r_i}\right)^{-3} \tag{4.29}$$

where u_i is the radial displacement of the cavity wall, r_i is the corresponding radius as shown in Figure 4-9.
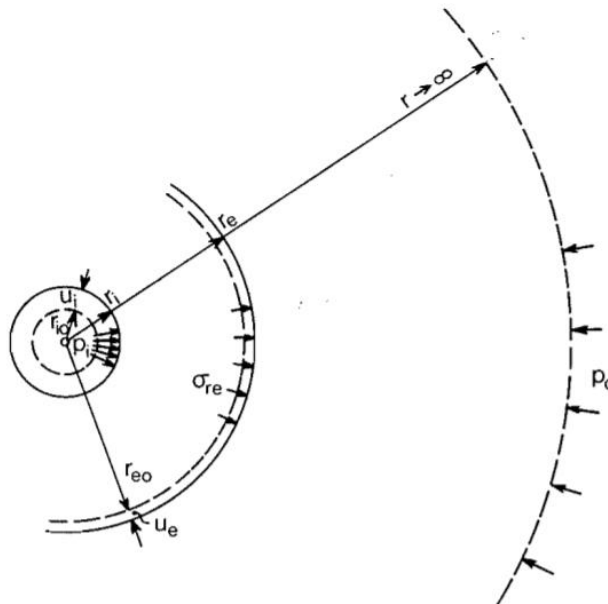
Figure 4-9 Notation in cavity expansion theory(Ladanyi & Johnston , 1974)

Hence from Eq.(4.28) and Eq.(4.29), the radius dependent pile settlement relation can be express as in Eq.(4.30)

$$\frac{u_a}{a} = \frac{2}{3}\left[\left(1 - \frac{u_i}{r_i}\right)^{-3} - 1\right] \tag{4.30}$$

The normalized pile tip displacement can also be transferred to indicate the pile settlement rate for creep at a steady state condition, therfore Eq.(4.30) is rewritten as Eq.(4.31)

$$\frac{\dot{u}_a}{a} = \frac{2}{3}\left[\left(1 - \frac{\dot{u}_i}{r_i}\right)^{-3} - 1\right] \tag{4.31}$$

For ice-rich soil, Ladanyi & Johnston (1974) defined the corresponding displacement field as in Eq.(4.32)

$$\frac{\dot{u}}{r} = \frac{B}{2}\left(\frac{3}{2n}\sigma_E\right)^n \left(\frac{r_e}{r}\right)^3 \tag{4.32}$$

σ_E is the applied end-bearing pressure.

From Eq.(4.31) and Eq.(4.32), and $r_e = r = r_i$, the normalized pile velocity can be calculated as Eq.(4.33)

$$\frac{\dot{u}_a}{a} = \frac{2}{3}\left\{\left[1 - \frac{B}{2}\left(\frac{3}{2n}\sigma_E\right)^n\right]^{-3} - 1\right\} \tag{4.33}$$

Eq(4.33) can be simplified and approximately expressed by Eq(4.34)

$$\frac{\dot{u}_a}{a} = B\left(\frac{3}{2n}\sigma_E\right)^n \tag{4.34}$$

The end-bearing load can therefore be calculated as in Eq.(4.35)

$$P_E = \pi a^2 \sigma_E = \left(\frac{1}{B}\frac{\dot{u}_a}{a}\right)^{\frac{1}{n}}\frac{2\pi a^2 n}{3} \qquad (4.35)$$

Similarly, equations above can be converted to fit the condition for ice-poor soils from the constitutive equation(3.5). The normalized pile tip displacement for ice-poor soil can be expressed as Eq.(4.36)

$$\frac{u_a}{at^b} = \left[\frac{3\sigma_E}{2c\omega(\theta + 1)^k}\right]^c \qquad (4.36)$$

The end-bearing load in ice-poor frozen soil can be calculated as in Eq.(4.37)

$$P_E = \left(\frac{u_a}{at^b}\right)^{\frac{1}{c}}\frac{2c\omega(\theta + 1)^k}{3}\pi a^2 \qquad (4.37)$$

4.1.3 Combination of End-bearing and friction piles

In order to simplify the approach of getting the calculated settlement, a new solution was being suggested. As shown in Figure 4-10, this approach assumes that the upper layer of soil will be deformed by the load transferred from the pile shaft and that the lower layer of soil will be deformed exclusively by the pile base load. This simplified approach is therefore only approximate, however, the acceptability of this model has been checked against numerical solutions and verified by Randolph and Wroth (1978).
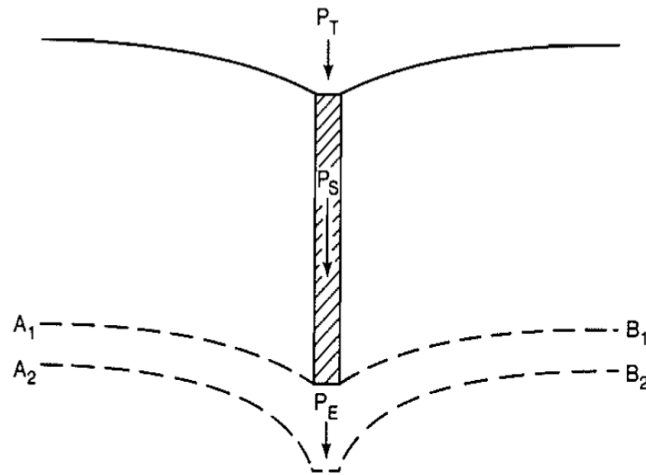
and

Figure 4-10Uncoupling of effects due to pile shaft and base(Randolph & Wroth, 1978)

Hence the total bearing capacity can be calculated by adding the shaft bearing capacity of equation(4.19) and end-bearing capacity of equation(4.35) together, then we can get the total pile bearing capacity P_T.

$$P_T = 2\pi a \left(\frac{1}{B}\frac{\dot{u}_a}{a}\right)^{\frac{1}{n}} \left[\left(\frac{n-1}{3^{\frac{n+1}{2}}}\right)^{\frac{1}{n}} L + \frac{na}{3}\right] \tag{4.38}$$

The percentage of load borne at the pile tip in isothermal ice-rich frozen soil may be determined from equation(4.35) and equation(4.38).

$$\frac{P_E}{P_T} = \frac{\dfrac{na}{3}}{\left[\left(\dfrac{n-1}{3^{\frac{n+1}{2}}}\right)^{\frac{1}{n}} L + \dfrac{na}{3}\right]} \tag{4.39}$$

Thus, for a 0.2 m diameter pile of length 25 m installed in an ice-rich saturated soil, i.e. $n = 3$, the fraction of load supported in end-bearing is 1.3%.

Similarly, the total pile load capacity in ice-poor frozen soil can be calculated from Eq.(4.24)and Eq.(4.37) and is given as shown in Eq.(4.40)

$$P_T = 2\pi a \left(\frac{u_a}{at^b}\right)^{\frac{1}{c}} \omega(\theta + 1)^k \left[\left(\frac{c-1}{3^{\frac{c+1}{2}}}\right)^{\frac{1}{c}} L + \frac{ca}{3}\right] \tag{4.40}$$

The percentage of load borne at the pile tip in isothermal ice-poor frozen soil is:

$$\frac{P_E}{P_T} = \frac{\frac{ca}{3}}{\left[\left(\frac{c-1}{3^{\frac{c+1}{2}}}\right)^{\frac{1}{c}} L + \frac{ca}{3}\right]} \tag{4.41}$$

Thus for a 0.2 m diameter pile of length 25 m installed in an ice-poor Ottawa sand experimented by Weaver and Morgenstern (1981), i.e. $c = 1.32$, the fraction of load supported in end-bearing is 2.1%.

It is found that the fraction of the pile load carried in end-bearing is only about 1-8% for most pile configurations. (Nixon & McRoberts, 1976)

From the preceeding review it follows that pile end-bearing is negligible in homogeneous frozen soils.

4.2 Shallow foundations

Shallow foundations are normally defined as footings having a width equal to or greater than their depth and are placed at a depth governed by the thickness of the active layer. In suitable soil conditions, they may be placed directly in contact with the frozen ground, but more often

the requirement to maintain thermal equilibrium in the frozen ground dictates that shallow foundations be placed on a gravel berm or a layer of suitable sandy soil with or without insulation. It is also general practice to excavate and construct shallow foundations in the fall, and to allow the cold winter temperatures to freeze back the disturbed subsoil area. (Andersland & Ladanyi, 2004)

A shallow foundation is a practical alternative to deeper, more costly foundations in cold regions. Although shallow foundation has advantages of saving materials, simple technology and low price, it still has been less used than piles because piles are prefabricated and can be mechanically installed, i.e., they do not need an open excavation and also the temperatures along the major part of a deeper pile foundation vary considerably less, and such foundations are likely to be less susceptible to seasonal thermal effects. Hence only light structures are preferred to be built on shallow foundations.

Unlike deep foundations like piles carrying the load in the relatively temperature homogeneous frozen soils under great depth. For shallow foundations, because the mechanical properties of frozen ground are temperature dependent, the ground temperature profile is one of the primary factors to be considered in the design of shallow foundations. The complete foundation design for cold regions is a complicated procedure involving a long-term prediction of the maximum temperature profile in the ground below the foundation, and the resulting temperature and time-dependent deformation and strength properties of the foundation soils. It is usual practice to use in the design the envelope of maximum temperature such as shown in Figure 4-11. Such a method is highly conservative and necessarily leads to an overprediction of settlement rates and total cumulative settlements of foundation in permafrost. In reality, because of a continuous temperature variation of permafrost, as well as the freezing and thawing phenomena in the active layer, the rate of settlement of a footing on permafrost will vary between wide limits

during the year. (Ladanyi B., 1983)
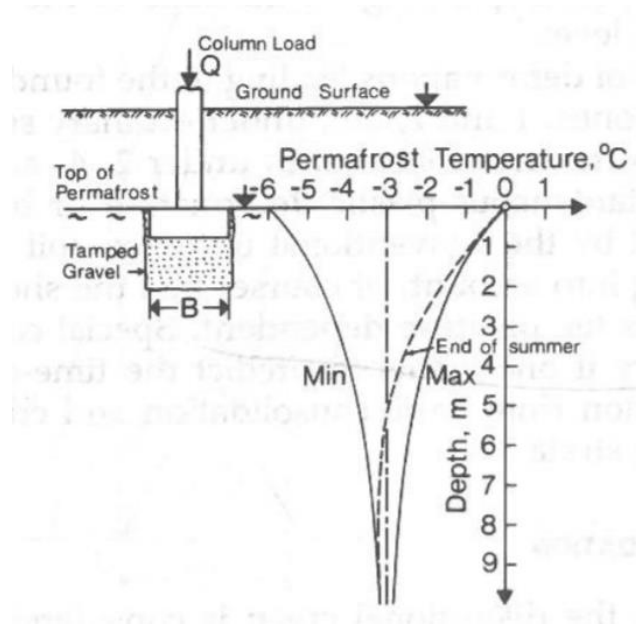
Figure 4-11 Typical shallow footing on permafrostwith maximum and minimum ground temperature envelopes

(Ladanyi B., 1983)

Spread footing is the most wide-used shallow foundation type. It may be used in permafrost areas in conjunction with an air space to transmit structural loads to a depth where the temperature of the frozen ground will not rise higher than a few degrees below freezing. (Nixon, 1978) In order to fulfill this criteria, floor and in-ground insulation must be used to dissipate heat losses from the structure in order to maintain the permafrost table at the desired level if required as shown in Figure 4-12.
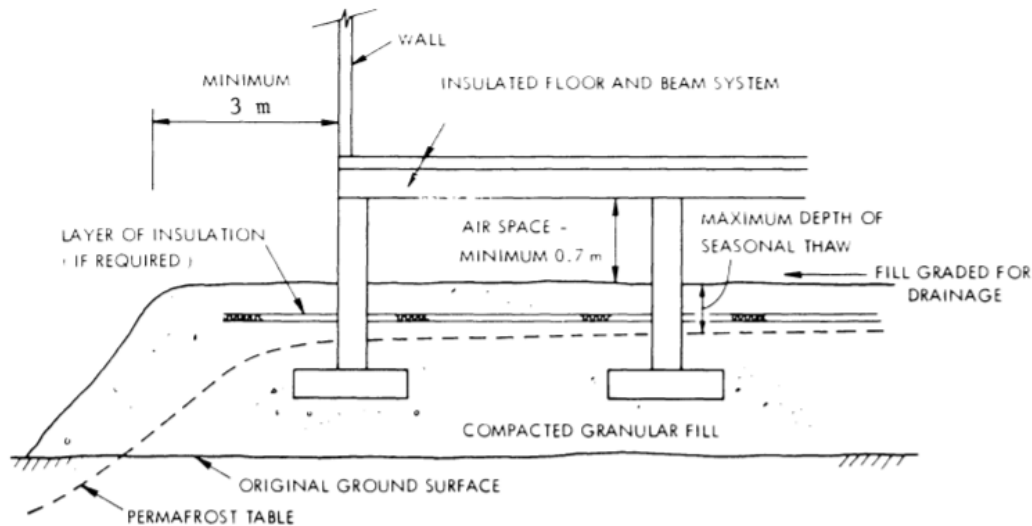
Figure 4-12 Typical footings in permafrost, embedded in a thick, insulated gravel padplaced on the ground surface

(Andersland & Ladanyi, 2004)

Assuming that the thermal aspects have been taken into account, the design of spread footings is concerned as before with preventing shear failure in the underlying frozen soil and limiting long-term creep settlements to tolerable levels. It will often be found, however, that allowable settlement governs the design of spread footings. (Nixon, 1978)

In general, present design practice is to avoid the problem of creep in frozen soil shallow foundations either by supporting footings on mats of well drained non-frost-susceptible gravel or other material which spread stresses sufficiently so that stresses on underlying confined frozen materials are conservatively low, or by placing foundations at a sufficient depth in the ground so that the overburden pressure effectively minimizes foundation-induced creep. (Linell & Lobacz, 1980)

It is found, however, for "cold" frozen soils, the main source of the settlements is from the creep. But in "warm" frozen soils, which have high percentage of unfrozen water, the consolidation may be quite substantial. The term "cold" and "warm" have been defined in section 3.3.3. Hence

it is important to determine the design bearing pressure for a foundation in frozen soil by predicting the settlements due to the combined effects of creep and consolidation. Preferably, it is ideal to consider the consolidation and the creep as two simultaneous but separate phenomena. However, very few investigations in frozen soils have been made to separate these two phenomena hence it's not able to analysis the settlement from different sources separately due to the lack of basic data. As a result, an approach to consider the frozen soil as a quasi-single-phase medium with mathematically well-defined creep properties, neglecting the fact that one portion of the observed creep is actually due to consolidations is widely being used and will be illustrated in the following paragraphs.

Creep settlements may be predicted by determining the stress state beneath the footings, using a creep law to obtain the strain rates in the permafrost and finally integrating the strain rates with depth to obtain the settlement rate of the footing.

The creep settlement and failure of a footing in frozen soil can be predicted by some approaches that have been proposed as introduced in the following.

The first approach assumes that the stresses beneath a footing founded on a linear elastic material can be determined from Boussinesq stress distribution theory. The Boussinesq stress distribution can be calculated as equation(4.42), and they can be visualized as in Figure 4-13

$$\sigma_z = \frac{3P}{2\pi}\frac{1}{z^2} \tag{4.42}$$

σ_z is the vertical stress at center line at depth z, z is the distance below base of footing, P is the load and is distributed uniformly over the end of a soil column with cross section equal to the base area of the footing with stress decreasing progressively in the column to the depth

where the stress is negligible.
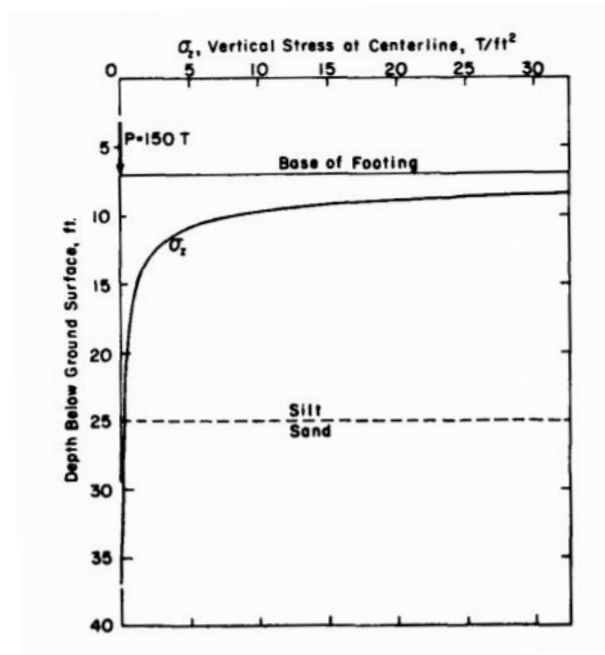
Figure 4-13 Vertical stress at centerline under Boussinesq's equation(Linell & Lobacz, 1980)

This approach was adopted by Linell and Lobacz (1980), they used this Boussinesq stress distribution assumption to separate the soil into different zones. Each zone has its constant temperature and constant stress as shown in Figure 4-14.
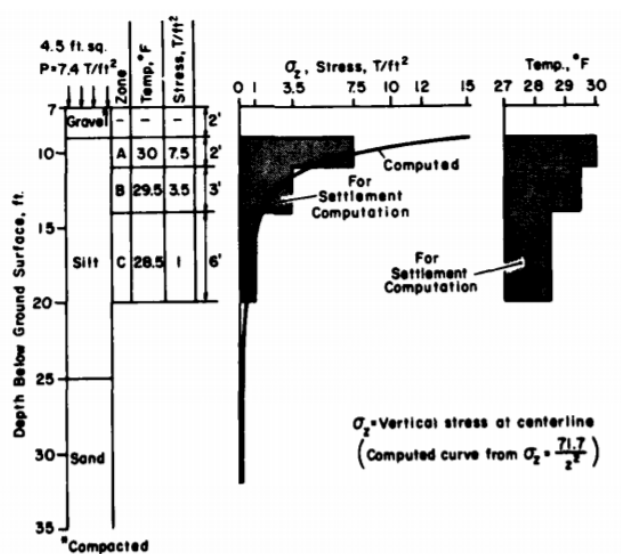
Figure 4-14 Conditions for creep analysis(Linell & Lobacz, 1980)

After determining the zones, the creep are calculated using the creep equations from Eq.(3.1) for ice-rich soils and Eq.(3.5) for ice-poor soils for each zones. Total creep movement is the sum of the creep of all the zones of soil in the soil column.

This approach is commonly adopted in conventional soil mechanics for unfrozen soils and has found reasonable acceptance. Clearly, however, as the material deviates more from linearity, this can be expected to yield less accurate results. (Nixon, 1978)

On the other hand, Ladanyi (1975) developed a theory in order to simulate closely the observed frozen soil behavior under load to furnish the basis for prediction the creep settlements of footings in frozen soils. The theory is based on the expanding cavity model as the same as the one for deep punching piles mentioned in the end-bearing pile paragraph by Ladanyi and Johnston (1974). Ladanyi and Johnston (1974) have used a constitutive equation in which the strain was related to stress by a power law, and to time by a linear relationship, for predicting the creep displacements of deep circular plate anchors, loaded beyond their long-term pulling capacity. A similar approach for predicting the creep displacement of shallow foundations will be addressed in the following.

Unlike the Boussinesq theory approach is based on the assumption that the material is linear elastic. The cavity expansion theory assumed that the frozen soil behaves as a nonlinear viscoelastic medium with time, temperature, and normal pressure dependent strength properties. It also assumes that the footing is underlain by a thick layer of relatively uniform and practically incompressible frozen soil.

Circular footing was considered to expand spherical cavity, this has been addressed in the section for end-bearing pile. On the other hand, the penetration in frozen soil of a strip footing

was considered to be similar to a cylindrical cavity with horizontal axis. Generally, for small values of settlement, the steady settlement rate $\dot{u}_a$ of shallow foundations in ice-rich soils can be calculated as equation(4.43)

$$\frac{\dot{u}_a}{a} = IB\sigma_s{}^n \tag{4.43}$$

Where a is the foundation radius or half of the width of the foundation, B and n are the creep parameters given by Eq.(3.1), σ_s is the applied vertical pressure for shallow foundations. I is the influence factor, which depends on the footing shape and can be calculated as Eq.(4.44) and Eq.(4.45)

For circular footings:

$$I_c = \left(\frac{3}{2n}\right)^n \tag{4.44}$$

From Eq.(4.43) and Eq.(4.44), it can be seen that for circular footings, the equation leads to the same form as for end-bearing pile in Eq.(4.34).

For strip footings:

$$I_{st} = \left(\frac{\pi\sqrt{3}}{4}\right)\left(\frac{\sqrt{3}}{n}\right)^n \tag{4.45}$$

For ice-poor soils, equation(4.43) can be converted to another form as shown in Eq.(4.46)

$$\frac{u_a}{at^b} = I\left[\frac{\sigma_s}{\omega(\theta+1)^k}\right]^c \tag{4.46}$$

The cavity expansion theory approach takes into the account the nonlinearity of the stress strain behavior of the frozen soil and is considered more appropriate. However, for nonhomogeneous soils, especially for shallow foundations that have considerable design temperatures variations, the approach based on Boussinesq stress distribution may be used.

Chapter 5 Experimental Investigations

5.1 Site Description

5.1.1 Location

In 2017, the Norwegian GeoTest Sites (NGTS) infrastructure project has established two field test sites in Svalbard, UNIS East and Adventdalen, shown in Figure 5-1. The NGTS projects are reference field sites for long-term geotechnical field testing. Hence the boreholes shown in Figure 5-2 are all recording the long series of ground temperatures. These observation data can be used for future research. For example, in this study, we have been used the ground temperature data from Borehole E1 as it is closest to the Nunataryuk project.

In April 2020, a Nunataryuk project launched a test site near the NGTS site in Longyearbyen, the location is marked by a yellow star in Figure 5-2. The soil that has been drilled out from this test site has been used for laboratory testing in this study.
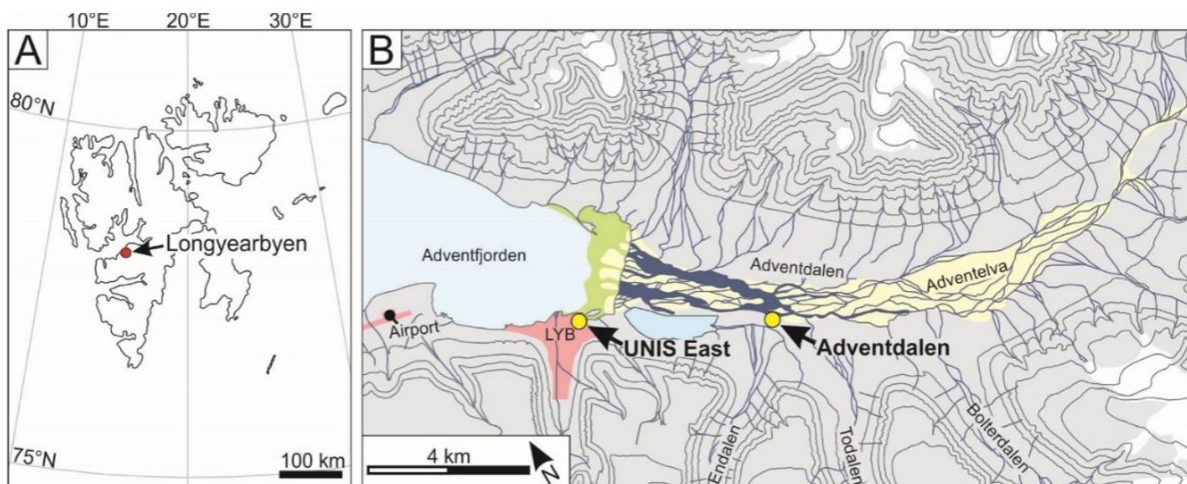
Figure 5-1 a) Location of Longyearbyen in Svalbard; b) Location of the NGTS siteUNIS East and the Adventdalen site (Adapted from (Gilbertt, Instanes, Sinitsyn, & Aalberg, 2019))

Figure 5-2 Detailed location of UNIS East site, red dots stands for boreholes, yellow star stands for the new

Nunataryuk project site (Adapted from (Gilbertt, Instanes, Sinitsyn, & Aalberg, 2019))

5.1.2 Geological conditions

The UNIS East site which the Nunataryuk project is located on is located within sediment filled former fjords. Fjords are incised bedrock valleys which are formed during glaciation and afterwards inundated by the sea. These depocenters are scoured by ice flow and accumulate subglacial deposits during glacial periods and are filled principally by fjord-head deltas during deglaciation and in post-glacial time. A typical fjord-valley fill succession consists of a veneer of till overlain by marine deposits, an upwards-coarsening sequence of deltaic sediments, and fluvial deposits. The bulk of the fjord-valley fill is deposited into a marine setting. (Gilbert G. L., 2018) This marine setting terrain leads to the soils in the site may be high in pore water salt content. A study carried for the UNIS campus site shows that the soil pore water salinities in permafrost increasing from 5 ppt at the surface to 25 ppt at 10 meters depth. (Instanes & Instanes, 1999)

The soil stratigraphy at UNIS East consists of a top layer of gravelly silty sand to approximately

77

3m depth underlain by fine grained material such as silty clay of more than 15 meters over diamicton to the bedrock of depth ranges from 21 m to over 30 m. (Gilbertt, Instanes, Sinitsyn, & Aalberg, 2019)

In Longyearbyen, the depth of the active layer during the summer time is between 1 and 2 m, and it is expected to increase in the order of tens of centimeters in the next decades due to warmer climate. (Jonsson, Nerland, Lande, Kanstad, & Hellum, 2018)

5.1.3 Climate conditions

As mentioned in Section 1.2, Svalbard has experienced devastating warming. This is shown in Figure 5-3. It can be observed from the figure that the 30-year mean has increased from a minimum of -6.7 °C to approximately -3.9 °C in 2018. It is important to inspect the impact of climate change in Longyearbyen. Longyearbyen is located within continuous permafrost zone. Scientists have been tracking the impact of a warming climate on permafrost because as it melts, permafrost releases its stores of frozen carbon into the atmosphere as methane and carbon dioxide, contributing to climate change. This climate change is a vicious cycle that is kind of inevitable in these decades.
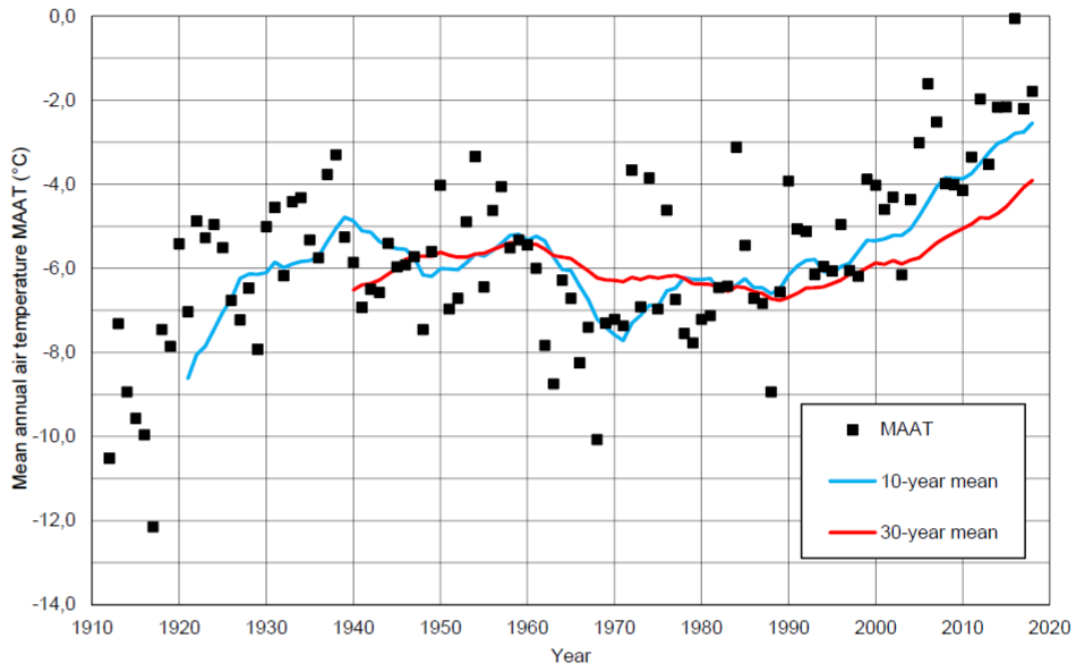
Figure 5-3 Mean annual air temperature Longyearbyen, Svalbard(Gilbertt, Instanes, Sinitsyn, & Aalberg, 2019)

Moreover, Longyearbyen is in one of the driest areas in Svalbard. The observed annual precipitation in the period from 1961-1990 was just about 300 mm, but in recent years the temperature has been increasing and less sea ice is observed which is thought to increase the moisture and precipitation. It is becoming more common to see the average day temperature to rise over 0° C midwinter with periods of rain instead of snow. (Jonsson, Nerland, Lande, Kanstad, & Hellum, 2018)

5.1.4 Ground temperature

Ground temperatures are determined by air temperatures, geothermal gradient, and soil thermal properties. Because the mechanical behavior of frozen soils is temperature sensitive, the foundation design for cold regions is therefore involving a long-term prediction of the maximum temperature profile in the ground below the foundation. The long-term recording of the ground temperature to obtain the trend of temperature change for predicting the future temperature is then necessary for the foundation design.

Thermistor strings are placed in plastic pipes installed in the boreholes. There are several sensors with varying spacing intervals on each thermistor string. For Borehole E1, the thermistors are closely spaced with 0.25m the first 1.5m depth, 0.5m from 1.5m depth to 5m depth, every meter from 5m depth to 12m depth and with 2m spacing down to the bottom. The temperature is logged every sixth hour.

A "FG2-Shell" software was used to obtain the ground temperature data.   Figure 5-4 shows the temperature curve resembles the curve in Figure 1-1. From the curve, it indicates the active layer in 2019 is from 1 to 1.25 thick. Figure 5-5 shows the curves as a result of average monthly ground temperature in 2019.
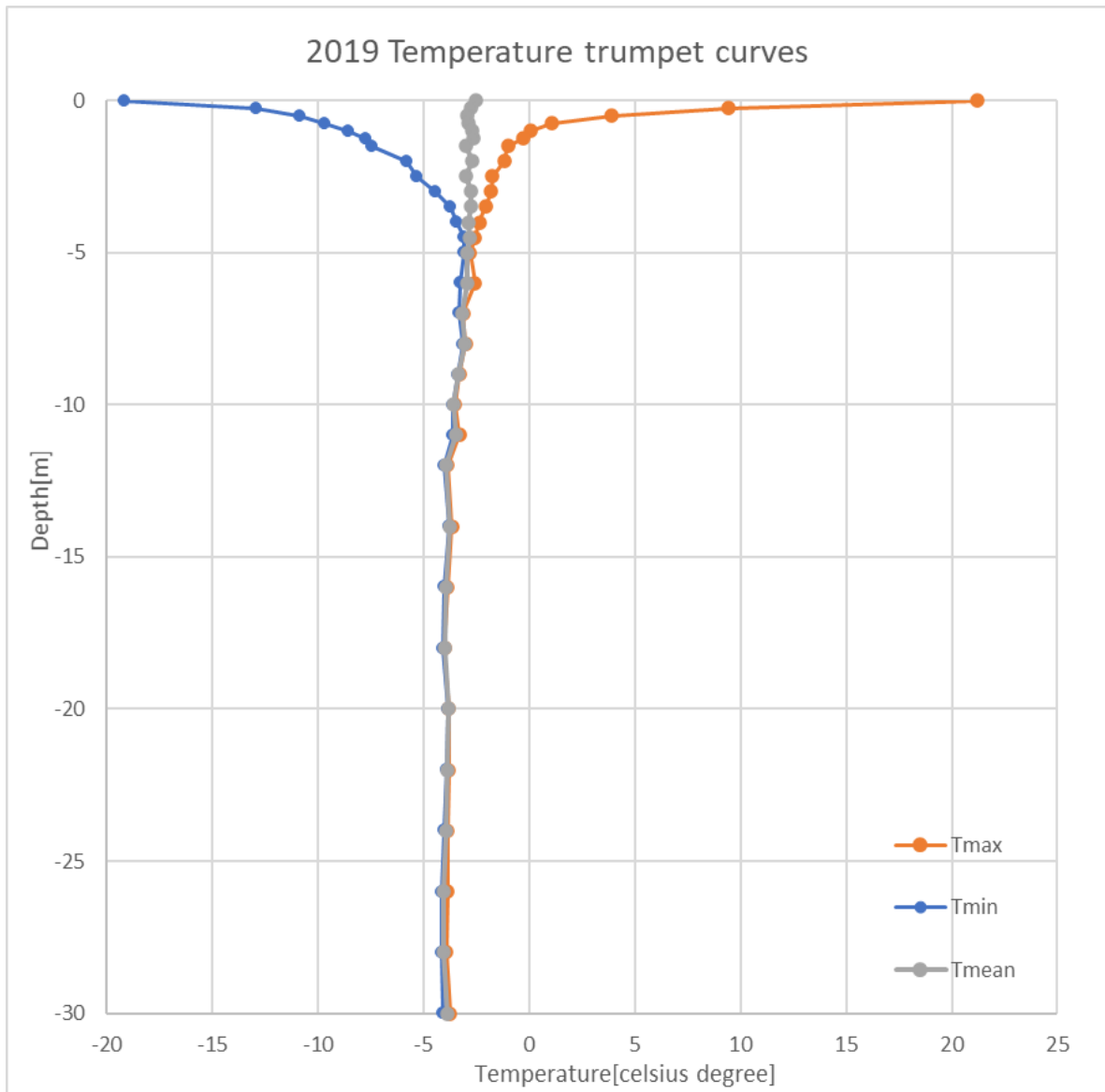
Figure 5-4 The Trumpet curve for ground temperature in 2019
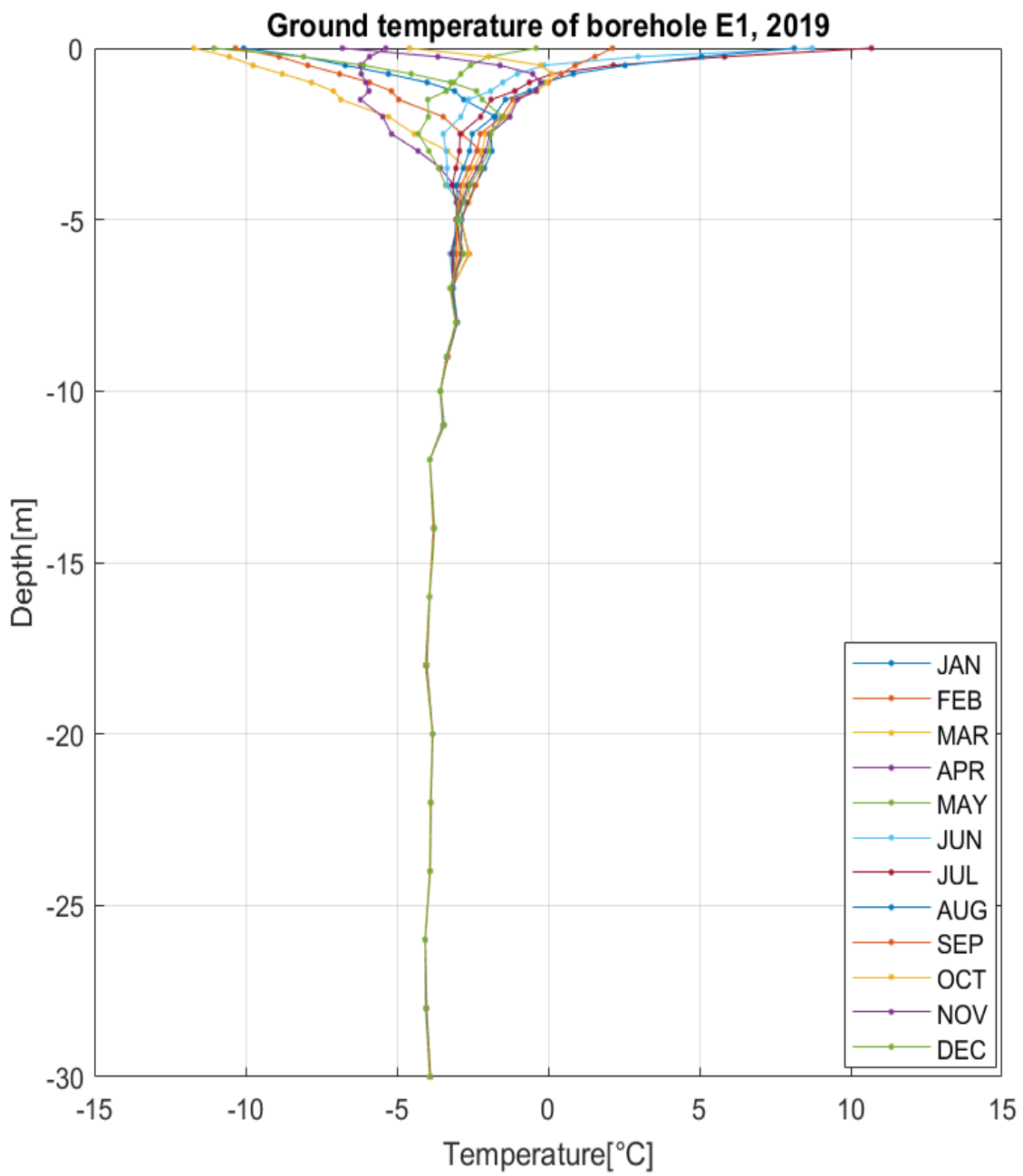
Figure 5-5 The temperature profile based on average monthly values in 2019for borehole E1 at the UNIS East

site.

5.2 Soil Classification results

Soil was obtained from a drilling process in the Nunataryuk project site. Soil was blasted out during the drilling and the soil this study used is the one getting from when the machine drilled to the end at approximately 4 to 4.5 depth.

5.2.1 Water content and densities

Water content

The soil used for determining the water content was taken from the sample after it has been tested for the 1% constant strain rate strength test. The sample was cut into two part, one for the water content the other for salinity. The empty box to let the sample put in was weighted first. Then the sample with box was then weighted immediately and put into the oven set at 110℃ for 24 hours. The sample with box then weighted after 24 hours of drying then the water content can be determined. To make sure the sample was completely dried, the sample was put back into the oven for 24 hours again and weighted again to confirm there was no more water left after the first day.

The result is: the empty box is 5.99 g, the natural sample with box is 281.15 g, the sample after dry with box is 223.90 g. With these data, the water content can be determined as from equation(A.1). The calculation is shown in equation(5.1)

$$w = \frac{M_w}{M_s} \times 100\% = \frac{281.15 - 223.9}{223.9 - 5.99} \times 100\% = 26.27\% \qquad (5.1)$$

Some errors might occur due to the water evaporation during the transportation of the soil and from some inaccuracy in weighting most likely.

Bulk density and dry density

Every cylindrical sample used for uniaxial compression tests was weighted and the diameter and height were also measured before the tests. Hence the bulk density can be easily known from the measurement. Take the measurements from sample one to calculate the bulk density. The diameter is 5.66 cm and the height is 12.32 cm. The weight is 572.36 g. From equation(5.2), we got the bulk density of our soil is 1.846 g/cm^3.

$$\rho_b = \frac{M}{V} = \frac{572.36}{\left(\frac{5.66}{2}\right)^2 \pi \cdot 12.32} = 1.846 \ g/cm^3 \tag{5.2}$$

From equation(A.3), the dry density can be calculated as the bulk density and the water content are known. The dry density is calculated in Eq.(5.3)

$$\rho_d = \frac{\rho_b}{1+w} = \frac{1.846}{1+0.2627} = 1.462 \ g/cm^3 \tag{5.3}$$

Particle density

Pycnometer was used to determine the particle density. The pycnometer is a flask with a close-fitting ground glass stopper with a fine hole through it, so that a given volume can be accurately obtained. Every pycnometer has its accurate volume value V_p engraved on the surface of the flask. The procedure in the following tells how to use pycnometer to determine the particle density.

(1) Make sure the pycnometer is completely dry before the initial weighting.

(2) Weight the empty pycnometer and record the weight as M_p. M_p is 44.74 g in this study.

(3) Add some soil to the pycnometer and weight it. We got $M_p + M_s = 50.89 \ g$

(4) Add distilled water such that pycnometer as well as capillary hole in the stopper is filled

with water. Dry the spare water that leaks through the capillary hole with a filter paper and measure total weight. $M_p + M_s + M_w = 148.01\ g$

(5) The volume of distilled water can be calculated as in equation(5.4), the density of the distilled water is assumed to be 0.997992 g/cm^3 at the laboratory temperature of 21°C. (Weast, 1972)

$$V_{H_2O} = \frac{(M_p + M_s + M_w) - (M_p + M_s)}{\rho_{H_2O}} = \frac{148.01 - 50.89}{0.997992} = 97.315\ cm^3 \qquad (5.4)$$

(6) The volume of the solids then can be determined as in Eq.(5.5)

$$V_s = V_p - V_{H_2O} = 99.540 - 97.315 = 2.225\ cm^3 \qquad (5.5)$$

(7) The particle density of the tested soil can finally be determined as in Eq.(5.6)

$$\rho_s = \frac{M_s}{V_s} = \frac{50.89 - 44.74}{2.225} = 2.764\ g/cm^3 \qquad (5.6)$$
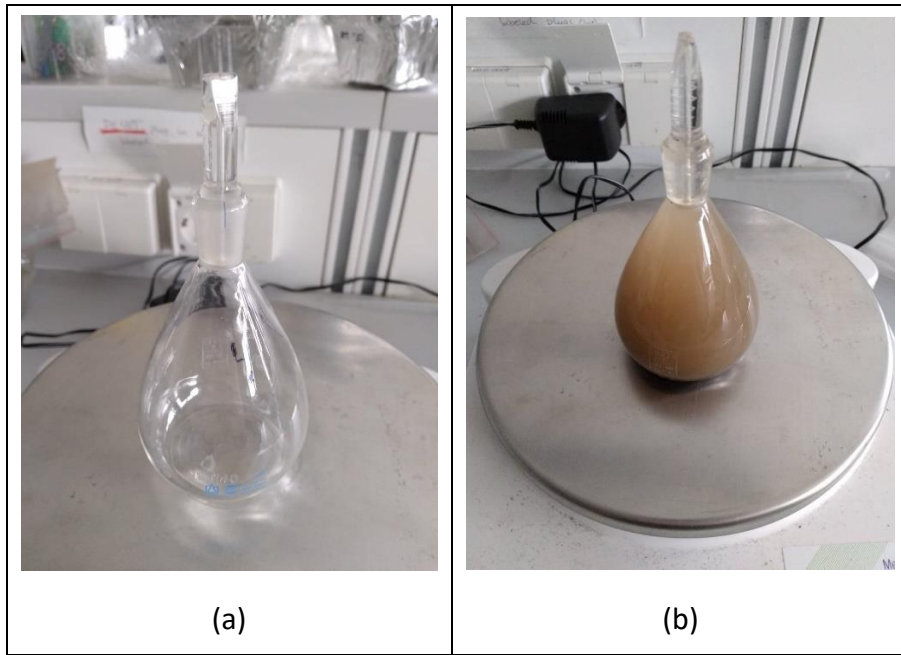
Figure 5-6 (a)empty pycnometer (b)pycnometer during measuring step with soil and water

It is in the acceptable range of the suggest particle density of soils. Though it is a little bit higher than the value suggested for clay (2.7 g/cm^3). Weighing inaccuracy is the most likely factor to cause errors.

With the known particle density and bulk density, the porosity, n, and the void ratio, e, can then be determined from Eq.(A.5) and Eq.(A.6) and be calculated as following.

$$n = 1 - \frac{\rho_b}{\rho_s} = 1 - \frac{1.846}{2.764} = 0.332 \tag{5.7}$$

$$e = \frac{n}{1-n} = 0.497 \tag{5.8}$$

5.2.2 Salinity

To measure the salinity of the soil, a handheld refractometer was used. The refractometer

measure how much the light bends when it enters the liquid. If the amount of salinity is high, the light will bend more. When looking into the refractometer, there is a scale where you read of the salinity. The scale is in percent.

To extract the liquid from the soil, the soil was put into a chamber and air pressure was applied on one side and the liquid with the solutes comes out on the other side. Then the liquid was collected and be dropped on the refractometer. As shown in Figure 5-8

The salinity of the soil is be determined as 2.3 %. With this salinity, we can use Eq.(2.1) to predict the freezing point depression.

$$\Delta T = T_k \left[\frac{S_n}{1000 + S_n} \right] = 57 \left(\frac{23}{1000 + 23} \right) = 1.28 \, °C \tag{5.9}$$

Figure 5-7 Device to extract liquid from the sample

Figure 5-8Refractometer with the liquid drop
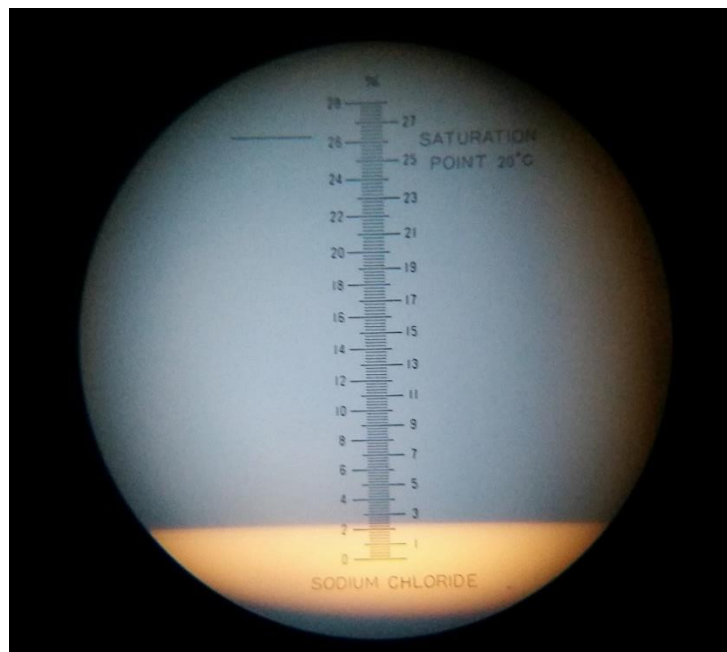
Figure 5-9 Reading from the refractometer

Freezing point depression

Temperature logger "testo 176T4" was used to measure the freezing point depression in the center of the samples. Samples were thawed and wrapped in plastic bags to prevent the loss of moisture content before and during the testing. The testing began when the soil is soft enough to let the probe insert in. There were two probes linked to the logger. One probe was carefully

inserted into the middle of the soil sample to measure the soil temperature. The other probe was placed in the air to measure the air temperature. Temperatures were measured and logged every 30 seconds. The sample and the temperature logger were placed in outdoor which the air temperature is around −15°C while logging. Figure 5-10 shows the experiment setting.

Figure 5-10 Experiment for determining freezing point

The measurements were continued until the temperatures decreasing rapidly again after the flat zone. The data from the temperature logger was transferred to a computer and treated with the Testo software. The temperature loggings plotted as function of time give curves showing rate of temperature change. The plotted curves resemble the curve shown in Figure 2-3. The flat parts of the plotted curves are used to identify the freezing point, T_f . The logged temperatures from the soil samples plotted against time are used to study the rate of temperature change which is the inclination of the curve. The temperature decreased rapidly until the freezing point (FP) was reached. The flat parts of the curves indicate the freezing points of the soil samples. The freezing point depression is the difference between freezing of bulk water and the freezing point for the soil.
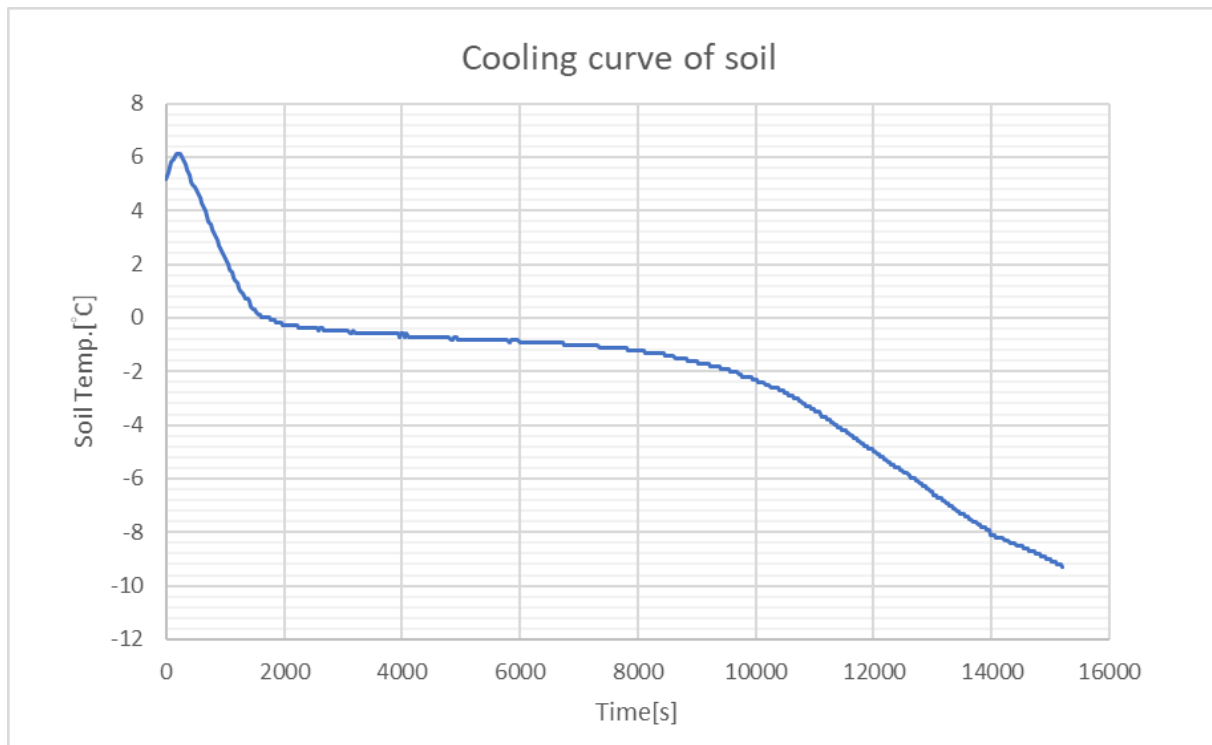
Figure 5-11 Experimental result of cooling curve

The experiment did not show perfect cooling curve and the freezing point can only be seen in a range with about -1.2℃ to -1.4℃. This is caused by the fact that the temperature was too low during the cooling and the soil was too small, hence the soil couldn't reach a long enough stable equilibrium state to let us determine the freezing point. It might be too short before it proceeded to the next stage of cooling. Although it would be precise to determine the freezing point directly from the experiment, but the empirical equation can help in this circumstance. Therefore, Eq.(5.9) has decided the freezing point depression value, we can assume the freezing point of the soil is -1.28 ℃.

5.2.3 Atterberg limits

Liquid limit

The Casagrande test uses the device shown in Figure 5-12. The liquid limit is determined as the

water content when pre-moistened soil put on the Casagrande apparatus flows together for a groove of 13 mm distance under the impact of 25 blows. When the groove closes after less than 25 drops, the soil is too wet, and some water must be allowed to evaporate. By waiting for some time, and perhaps mixing the clay some more, the water content will have decreased, and the test may be repeated, until the groove is closed after precisely 25 drops. Then the water content must immediately be determined, before any more water evaporates, of course.

Figure 5-12The Casagrande apparatus with soil sample and the groove

The result showed that the liquid limit of the soil is 23.79 %

Plastic limit

To determine the plastic limit, the way is to roll the soil into a thread and make sure the thread breaks when the diameter is exactly 3 mm. If it breaks when it's thicker then it means the water content is lower than the plastic limit. Contrarily, if it breaks when the diameter is smaller than 3mm, it means it needs to be dryer to attain the plastic limit.

The result of the plastic limit is 17.68%

With the results of liquid limit and plastic limit, the plasticity index can be known.

$$I_P = w_L - w_P = 23.79 - 17.68 = 6.11\ (\%) \tag{5.10}$$

With these data, the soil can be categorized from Figure 2-5 as CL-ML (Low plasticity silt or clay).

Some extra indices can also be determined from the consistency data. For example, the liquidity index (I_L) and the activity (A) can be calculated from Eq.(A.8) and Eq.(A.9). The determination of the percentage of the fraction of clay will be addressed in the later paragraph, we can now use the data to calculate the activity.

$$I_L = \frac{w - w_P}{I_P} = \frac{26.27 - 17.68}{6.11} = 1.41 \tag{5.11}$$

$$A = \frac{I_P}{\%\ of\ clay} = \frac{6.11}{16.67} = 0.37 \tag{5.12}$$

From the value of liquidity and activity indices, the soil can be viewed as the flowing and inactive soil.

However, the Atterberg experiments results may not be that accurate due to the inaccuracy during weighting and the evaporation of the water content right after the tests. Since the soil samples for the tests are really small and light, little inaccuracy can cause big error in the result. As the results, the Atterberg indices are still worth to be examined for the classification of the soil.

5.2.4 Particle size distribution

Sieving analysis

The first process used for determining the particle size distribution was called wet sieving. The first step was weighting all the empty sieves and a pan and then make a tower of sieves. The sieve with biggest openings was put on the top and continuously with smaller and smaller ones until the second last one with the smallest sieve and last one is a sealed pan. Secondly, putting soil samples on top of a tower of sieves. Distilled water was added to the top of the tower until all the particles smaller than the mesh went through to the next sieve, and the top sieve was removed and being put into the oven. This process repeated until all the soil particles have passed through all the sieves. Lastly, the sieves and pan were all put into oven for 24 hours to dry. After drying, weight the sieves and the pan with soil particles and subtract the mass of empty sieves and the pan, the mass of the soil at each particle size interval can be determined. The sieves this study used are listed in Table 5-1, since the soil was fairly fine, sieves were mainly for sand size analysis. Hence these sieves were chosen.

Sieve number	Opening size(mm)
4	4.75
30	0.6
50	0.3
100	0.15
200	0.075

Table 5-1 Sieves description

Hydrometer analysis

The second process used for further resolving the particle size distribution is the use of the hydrometer. Using Stoke's law, the particle size and percentage of the sediments can be determined from the hydrometer analysis.

With the results of the sieving analysis and hydrometer analysis, the particle size distribution can be known and plotted at Figure 5-13. The blue part represents the results from the sieving analysis, the orange part represents the results from the hydrometer analysis.
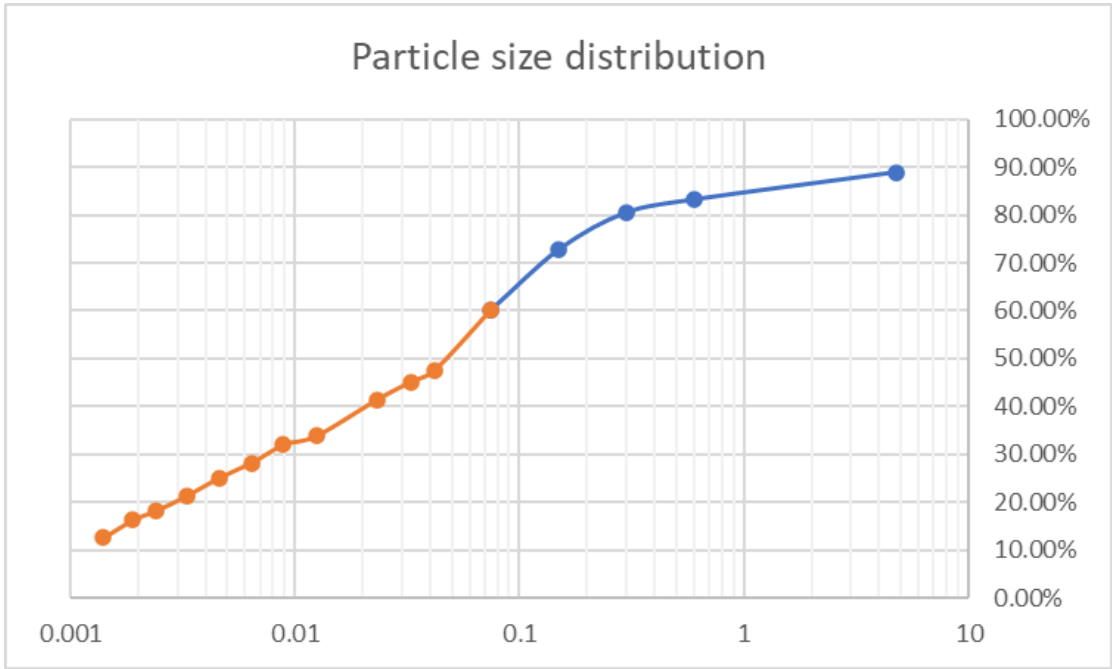
Figure 5-13 Particle size distribution of the tested soil, blue part is from sieving analysis, orange part is from hydrometer analysis

The percentage of each category of soil particles is listed in Table 5-2

Soil Category	Percentage
Gravel (4.75-75mm)	11.08 %
Sand (0.075-4.75mm)	28.76 %
Silt (0.002-0.075mm)	43.49 %
Clay (<0.002mm)	16.67 %

Table 5-2 Percentage of soil particles

5.3 Mechanical properties

A range of mechanical compression tests were conducted on frozen soil samples at temperatures close to the ground temperature at around 4 meters depth to determine both the creep and the strength properties under uniaxial stress conditions.

To test the soil strength, a machine called Knekkis in UNIS Cold laboratory was used. Knekkis is a rig used to test uniaxial compression strength. It is composed of two horizontal steel plates whose relative distance can be modified on command: the lower plate can move upwards and downwards while the upper one is fixed to the metal frame which forms the machine structure. The samples are loaded from below, yet the applied load is measured indirectly by a strain gauge situated above the upper plate. The load-displacement-time information is converted into ASCII format by a specific computer software. Before testing, on the control panel, the user has to select the type of test (constant load or constant strain) to be carried out and insert those parameters relevant to characterize the specimen geometry and the testing conditions (temperature) as well as the sampling frequency. (Nanetti, Marchenko, & Høyland, 2008)

In this study, both constant strain-rate test for evaluating the strength properties and constant

load test for measuring the creep properties are carried out. Data are presented for creep and strength characteristics acquired during testing of frozen clayey silt.

The specimens are remoulded into cylinders. Remoulded soil samples are of uniform quality and one may vary a single parameter like salinity, whilst keeping the others constant. (Furuberg & Berggren, 1988).

Laboratory test temperatures for frozen soils should be similar to those anticipated on the field site. On ground freezing projects, design temperatures are generally defined as the mean value for the volume of frozen soil characterized. (Andersland & Ladanyi, 2004) The temperature is hence be determined to set at -2.8℃ in the cold room to simulate the mean ground temperature at 4 meters depth in the field.

Each sample was weighted and height and diameters (top, middle, and bottom) were measured using a caliper. Therefore, these measurements can be used for calculating the strain and stress. The definition of strain and stress is needed for further investigation of the strength and creep tests. The true strain, ε, is defined as the deformation divided by the original specimen height as in Equation(5.13)

$$\varepsilon = \frac{\Delta h}{h_0} \qquad (5.13)$$

Δh is the change in height and h_0 is the original specimen height.

The stress, σ, can be calculated as Eq.(5.14)

$$\sigma = \frac{P}{\left(\frac{D}{2}\right)^2 \pi} \qquad (5.14)$$

P is the applied load; D is the diameter of the specimen.

The samples were wrapped by plastic wrap to prevent the loss of moisture as shown in Figure 5-14

Figure 5-14 Sample setting in the rig before test

5.3.1 Compressive strength tests

The strength was being tested under the constant strain rate(CSR) tests. Sayles et al. (1987) have recommended that applied constant strain rates of 0.1%/min and 1.0%/min be used to test frozen soil specimens in uniaxial compression. Generally, the highest value gotten during the test is defined to be the compressive strength of that material (maximum load). This is the strength the material has before failing.

The result of an unconfined compression test is a complete stress vs. strain curve for the soil sample under zero lateral confinement. The result of 1% strain per minute is shown in Figure 5-15 and the 0.1% strain per minute stress-strain curve is shown in Figure 5-16.
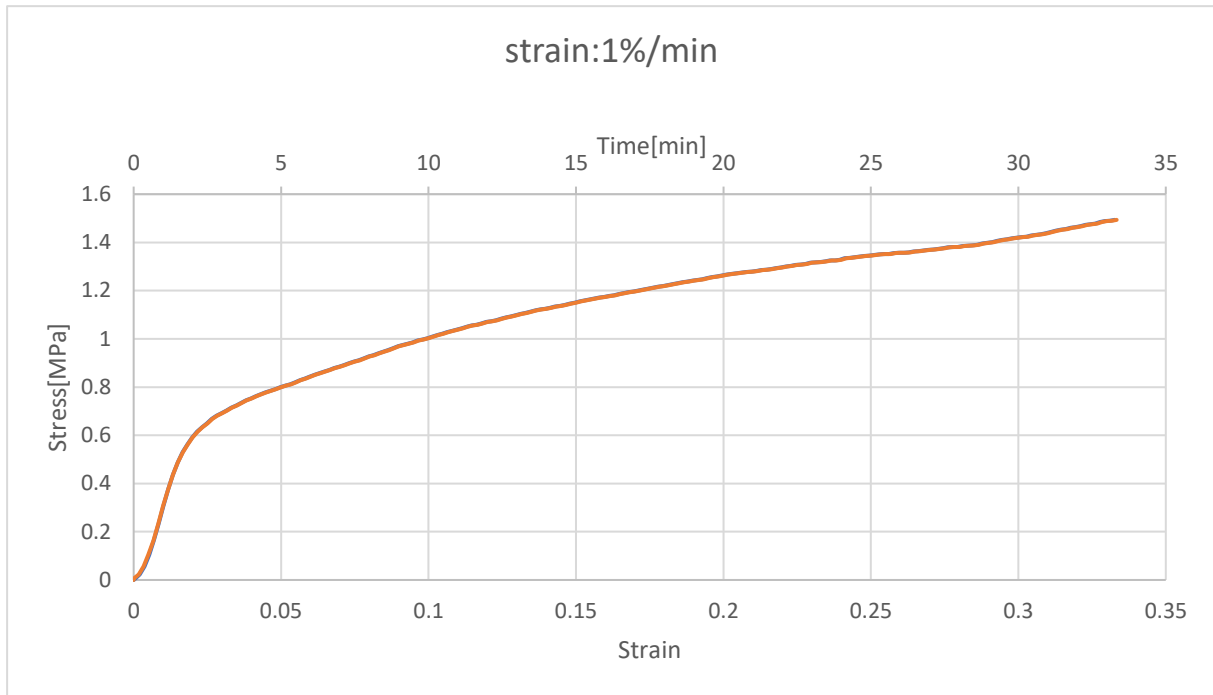
Figure 5-15 Stress-Strain curve of CSR:1%/min uniaxial compression test
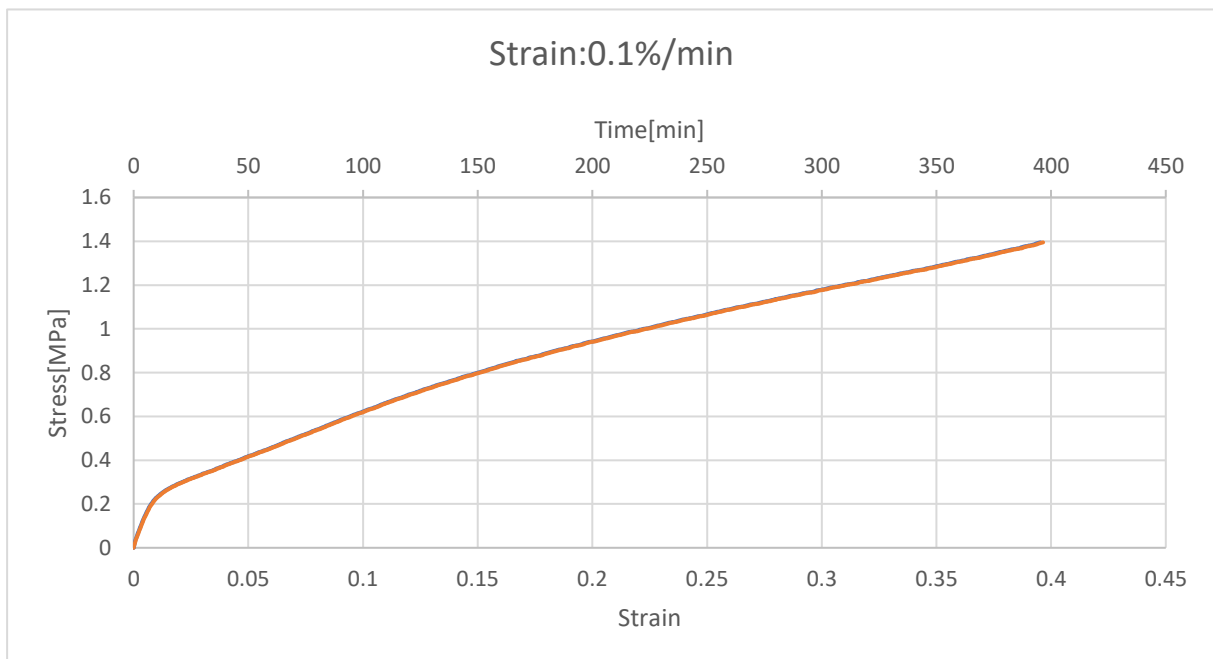
Figure 5-16 Stress-Strain curve of CSR:0.1%/min uniaxial compression test

In Frozen Ground Engineering book, Andersland and Ladanyi state that warm frozen fine-grained soils often show no distinct peak stress for strains as high as 20% or more. However, it does not indicate the definition of the term "warm" in the text. From our experiment, we can

refer our soil as one of the kinds that does not show the peak strength. This might cause by the reason that the existence of the unfrozen water, so the soil does not show much brittle behaviour.

Typically, for such soil with no peak strength, we can assume the compressive strength happens when the strain is at 20%. Hence for the soil in this study, the stress at the strain of 20% is 1.26 MPa at the condition of 1%/min constant strain rate compression test and 0.94 MPa at the condition of 0.1%/min constant strain rate test.

It is obvious the strain develops larger under the same compressive stress for the test of 0.1%/min CSR. In my opinion, this is due to the time dependent movement, namely the consolidation and creep. The consolidation and creep is not just influenced by strength but also the time. Hence the strain develops larger under the 0.1%/min CSR test at the same stress level because it takes longer time for the defined strain. Andersland and Ladanyi (2004) suggest that the 1%/min constant strain rate compression test is mainly used for mostly every frozen soil test. Hence the value obtained from the 1%/min constant strain rate compression test is favoured. As a result, we can conclude the unconfined compressive strength is 1.26MPa. From Mohr-Coulomb circle, the unconfined shear strength can be calculated as the half of the uniaxial compressive strength. Hence the shear strength of the soil in this study is 0.63 MPa.

5.3.2 Creep tests

Differential unconfined constant stress creep tests at low stresses have been carried out on frozen cylindrical soil samples to examine the influence of stress on creep rates. Samples have been measured the diameter and height with a caliper before the tests. The diameters were measured from the top, middle and bottom of the sample and then make the average of the three to determine the stress the sample being carried.

As introduced in Chapter 3, creep has different stages. As shown in Figure 3-2. Ice-rich silts and clays exhibit an abbreviated primary-creep period and a prolonged secondary-creep stage, while tertiary creep may never be attained. The strain versus time creep curves resemble to Figure 3-1(a) are plotted in Figure 5-17 and Figure 5-19. While the creep rate versus time curves resemble to Figure 3-1(b) are plotted in Figure 5-18 and Figure 5-20. The blue part of the curve represents the primary creep stage and the orange part of the curve stands for the secondary creep stage.
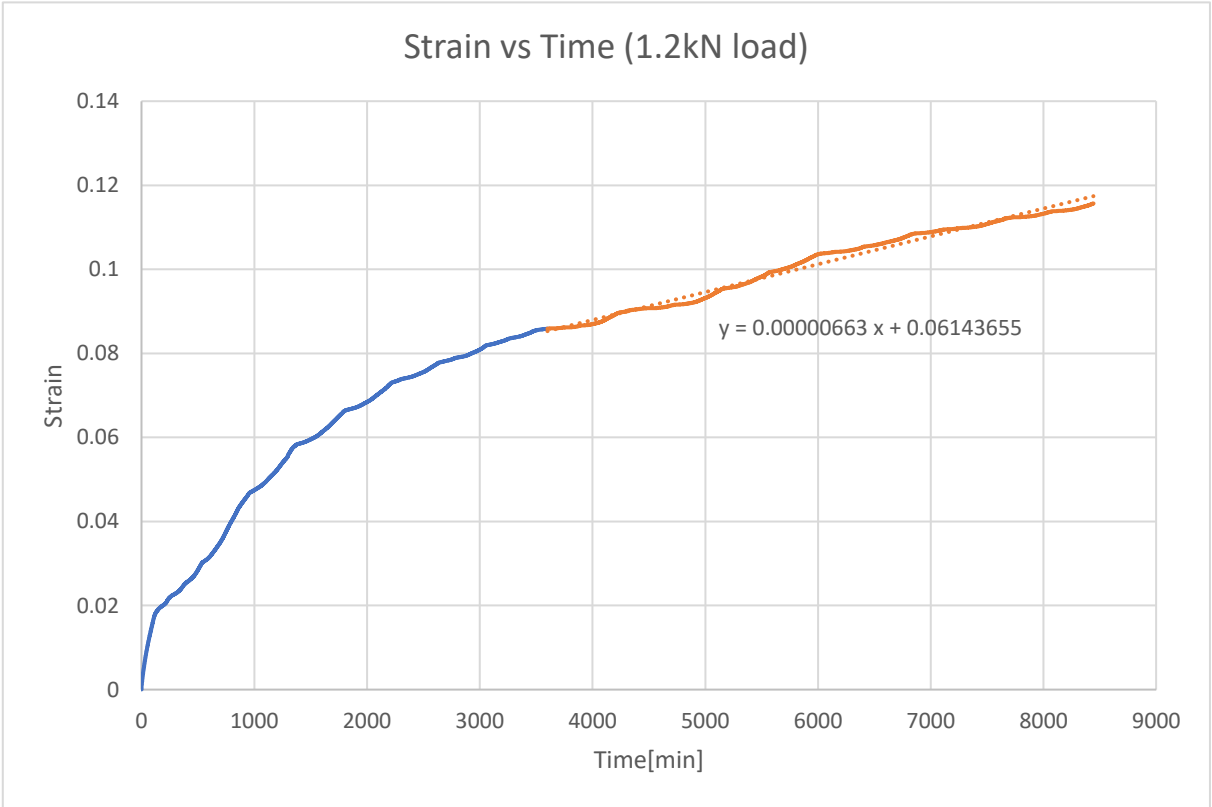
Figure 5-17 Strain vs Time curve under 1.2kN load
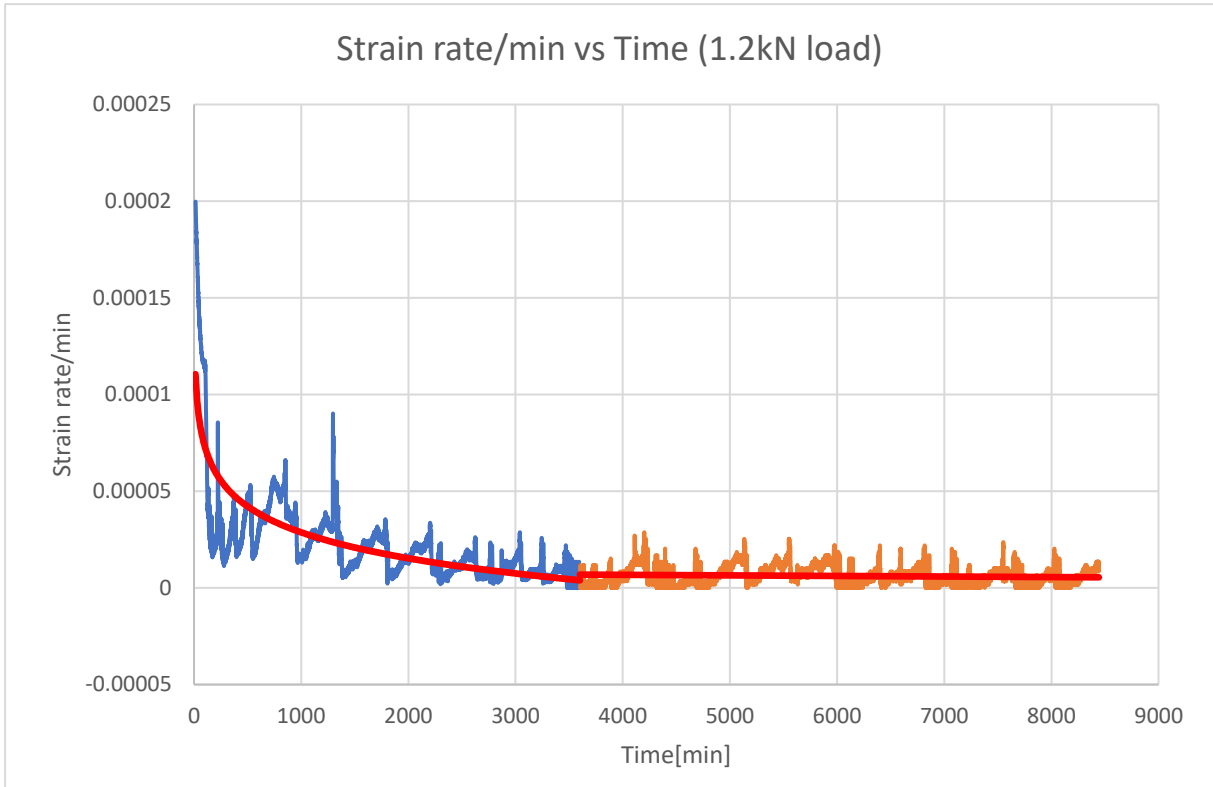
Figure 5-18 Strain rate vs Time curve under 1.2kN load
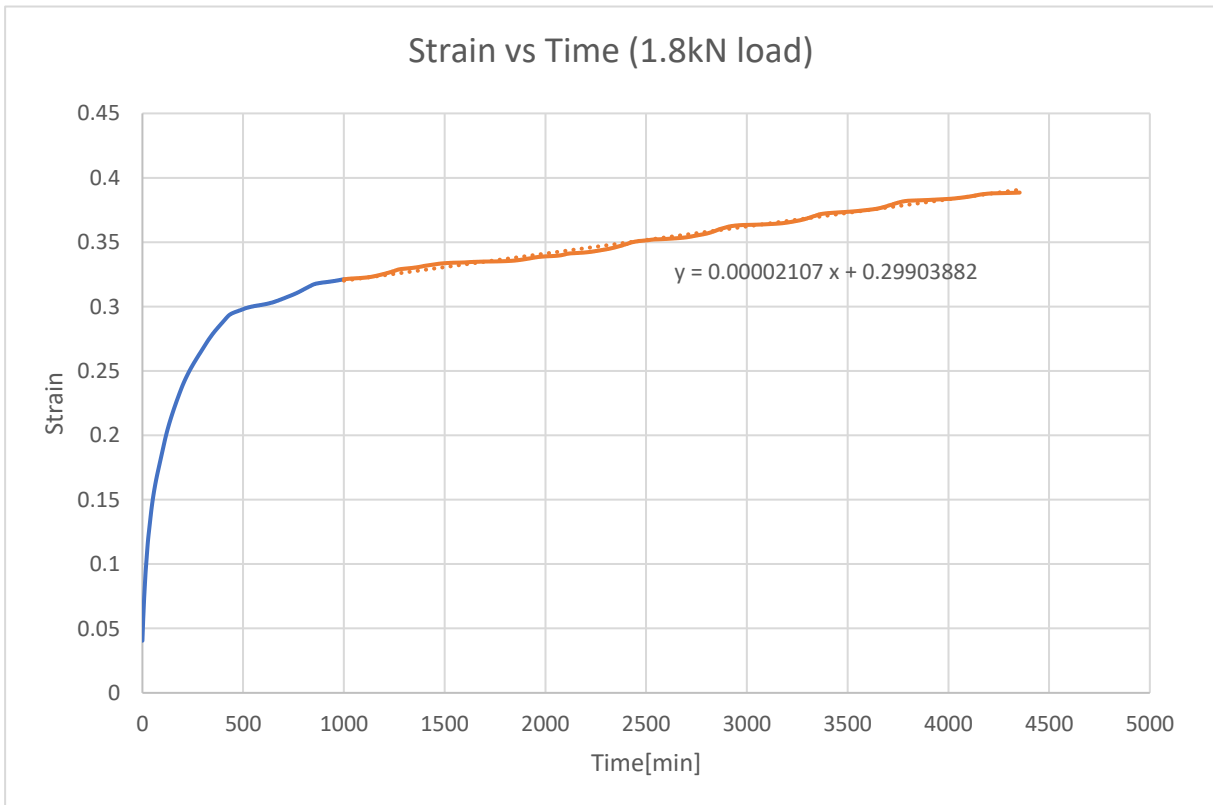
Figure 5-19 Strain vs Time curve under 1.8kN load
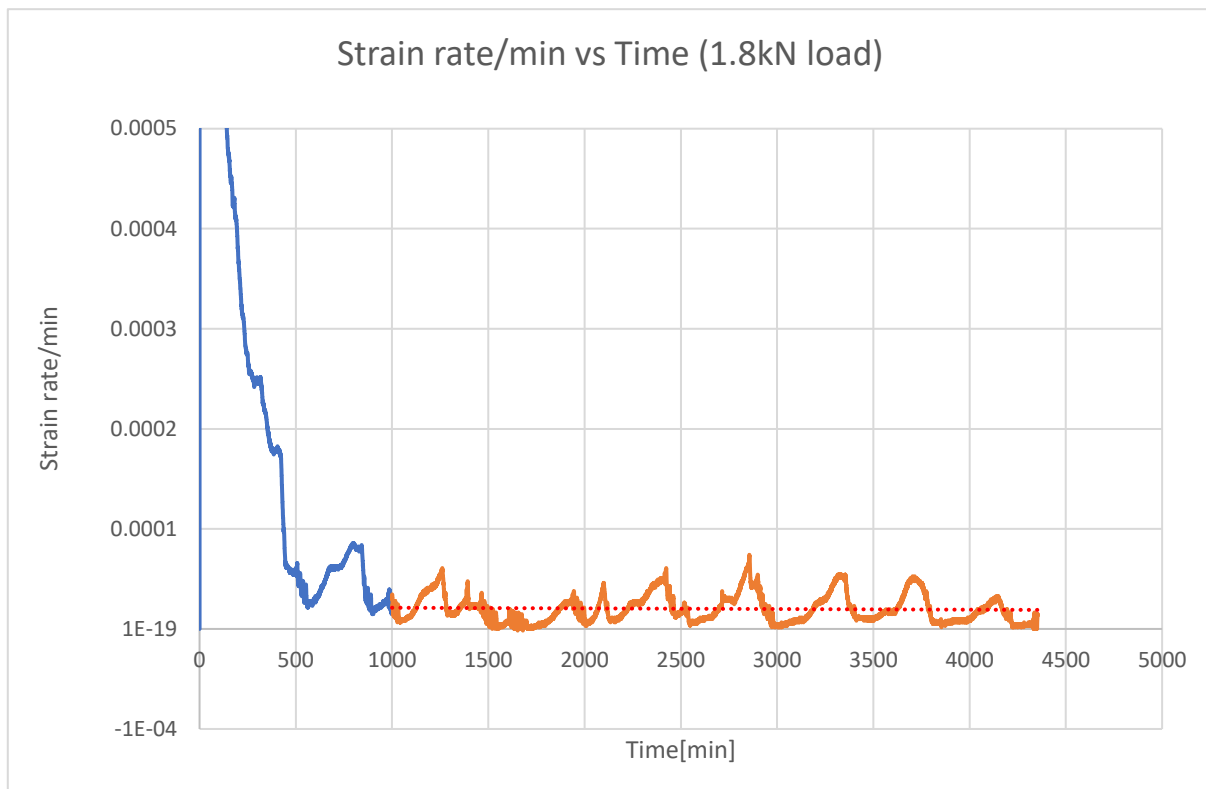
Figure 5-20 Strain rate vs Time curve under 1.8kN load

It is recommended that the creep test should run until the strain rate attain to zero. (Sayles, et al., 1987) However, because of the viscous nature of the ice in discrete layers and in the pore spaces, ice-rich ground will creep continuously at relatively low deviator stresses. (McRoberts, Law, & Murray, 1978) Hence in this study, the experiments were carried long until the fairly steady state creep rate has reached for a while as shown in Figure 5-18 and Figure 5-20.

In Figure 5-19 and Figure 5-20, it can be seen that the strain has reached over 30% in the primary creep stage. Even though in the Frozen Ground Engineering book states that some fine-grained soils can display primary-creep deformations up to strains exceeding 20%. (Andersland & Ladanyi, 2004). It is still a important property to take care for since most evaluation of creep settlement is based on the calculation of secondary creep parameters due to the fact that the

primary creep takes little portion in the settlement in long term.

One of the most significant reasons to carry these creep tests are to obtain the creep parameters. Fortunately, in this study, the tests have reached the steady state creep rate. They are shown as the slope in the trend line of the secondary creep stage in Figure 5-17 and Figure 5-19. The values are listed in Table 5-3. The n value is set to be 3 since it is widely used by former researches for ice-rich soils. (McRoberts, Law, & Murray, 1978) (Weaver & Morgenstern, 1981) (Nixon & Lem, 1984)

	$\sigma(kPa)$	$\dot{\varepsilon}$(per min)	n	$B(yr^{-1}kPa^{-3})$
Sample2(1.2kN)	475	0.00000663	3	3.2515×10^{-8}
Sample3(1.8kN)	689	0.00002107	3	3.3858×10^{-8}

Table 5-3 Creep parameters

B is dependent on the salinity and temperature. Ideally, the same soil with the same salinity and temperature will have the same B value. However, temperature cannot keep constant as the setting temperature during the testing. And the stress is also being influenced by the change of the sample area, hence it is not totally constant. Therefore, the B value is being calculated differently for two samples. But the two values are recognized as quite close compare to the tests for different salinity (Nixon & Lem, 1984) and temperature (Weaver & Morgenstern, 1981). Hence the result is reasonable and valuable.

With the data from Table 5-3, we can make the approximation of creep settlement based on the equations derived in Chapter 4 for different foundation design. The B value to be used can be the average number of the two test results.

5.3.3 Discussion

Soil behavior may change completely if the sample is thawed and then refrozen. (Andersland & Ladanyi, 2004) The study is based on remolded, which do not necessarily represent the field conditions. It is desired to evaluate quantitatively the mechanical properties of the frozen soil for foundations embedded in the soil based on undisturbed, naturally frozen soil specimens.

The creep test was carried out in a constant load setting condition and was assumed as a constant stress test. However, the contact area of the sample expanded while the sample being compressed. As a result, the stress could not be constant under a constant load. This factor influences the creep parameters. The properties of frozen soil change continuously with varying temperature and applied stress. Besides the fact that the stress changes a little due to the expansion in the sample diameter, the temperature change is the main source of error in this study.

Temperature control in the cold room could not hold the temperature at constant for the sample. Hence the temperature fluctuations led the creep rate could not stay constant at the secondary stage. This problem was noticed after analyzing the data from the test of sample 2. In the test of sample 3, the test was carried out with temperature recorded. This is shown in Figure 5-21. Sample temperatures were monitored directly by attaching a thermistor on the surface of the sample and wrapping both the sample and the thermistor by plastic wraps.
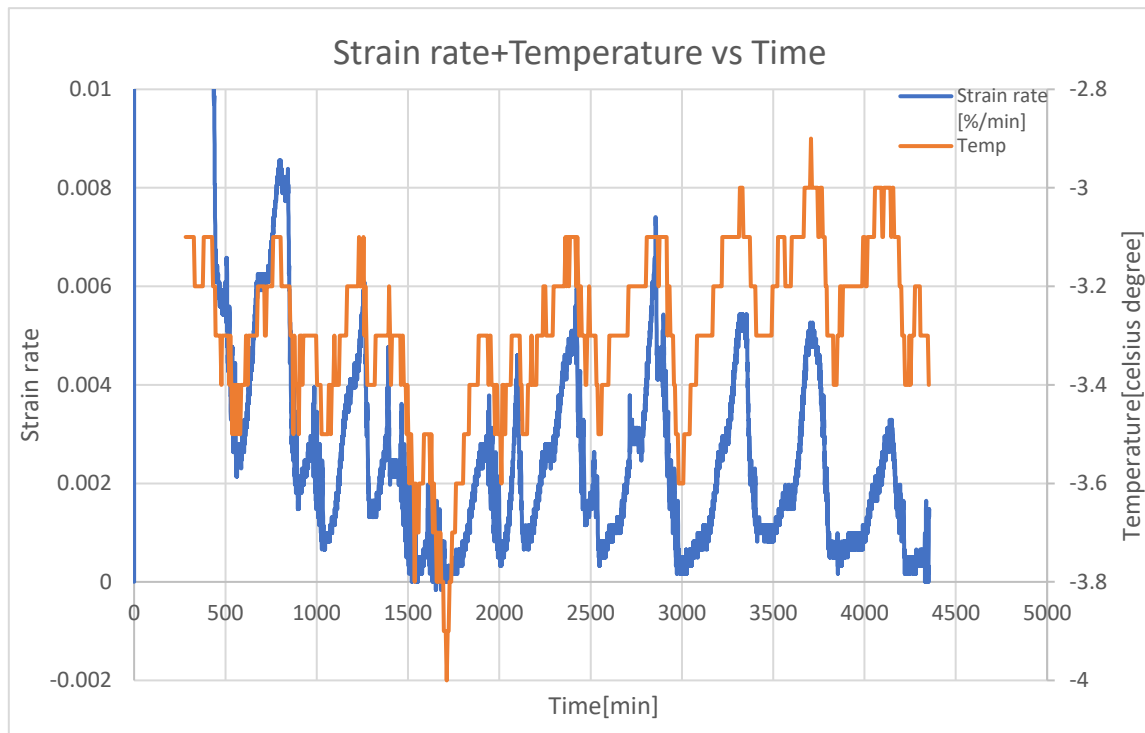
Figure 5-21 Temperature record of the creep test

It can be seen from Figure 5-21 that the creep rate fluctuates basically together with the temperature. This explains the fluctuation of the creep rate in Figure 5-18 and Figure 5-20. This problem could not be solved even by wrapping the whole Knekkis machine with thermal insulation materials. This defect was caused by the cold laboratory and was not easily to be solved.

Though in our study, we can basically assume the fluctuation was mainly caused by the change in temperature, it might still have some other reason. Zhu & Carbee (1987) also got the test result of the strain rate curves fluctuated frequently within the secondary creep stage. They called it "spikes", happened in the medium density samples tested at low stress. They found the spikes occurred over a time of a few days to more than one month even though the stresses and temperatures were constant. Not all of the tests they performed has shown this spike phenomenon, this indicates that the spikes are not artifacts of the test apparatus but are sample

responses. The exact reason of why this happening is still unknown.

B and n depend on the temperature, composition, and microstructure of the material and also to some extent on the applied stress level. Therefore these constants must be separately determined for almost every batch of material and each service temperature. These values were derived empirically by laboratory tests demanding quite precise measurements of the absolute values of strain and requiring several tests for evaluation of the constants. It is difficult to quantify the influence of pore water salinity on strength of frozen soils. The relative strength reduction caused by increasing salinity is different for different types of soils. (Furuberg & Berggren, 1988)

To apply the creep equation for predicting the settlements under foundations, the values for stress and temperature are assumed to be constant for the period of time under consideration. Although the stress condition can be pretty much the same in decades, the temperature is less possible to remain constant due to the challenge of global warming. Considering the service limit state that to have the limited settlement in a given service life, the current design must fulfill the criteria to meet the trend of global warming.

5.4 Case Study

The pile test campaign of the Nunataryuk project at the UNIS East test site has been launched in this spring in order to monitor the development of vertical displacements over time in this saline permafrost.

The piles are designed to resist the external loading only at the pile tip (footing) deep in the ground, to eliminate disturbance from frost jacking in the surface soil active layer. Therefore, the concept of end-bearing pile is used herein.

It was designed that a concrete slab with weight of 1400kg is loaded on the circular pile tip(footing) of diameter of 320mm. With this information, the predict creep settlement can be calculated from equation(4.34). The creep parameters are obtained from the creep tests described in section5.3.2. Table 5-4 listed the data for calculating the pile tip creep.

a (cm)	P_E (kg)	B $(yr^{-1}kPa^{-3})$	n
16	1400	3.3187×10^{-8}	3

Table 5-4 Pile test campaign creep calculation data

To start with, the end-bearing pressure should be calculated first:

$$\sigma_E = \frac{P_E}{\pi a^2} = \frac{1400}{16^2 \pi} = 1.7408 \left(\frac{kg}{cm^2}\right) = 170.8279 \ (kPa) \tag{5.15}$$

Then the normalized creep rate can be calculated from Eq.(4.34)

$$\frac{\dot{u}_a}{a} = B\left(\frac{3}{2n}\sigma_E\right)^n = 3.3187 \times 10^{-8} \times \left(\frac{3}{2 \times 3} \times 170.8279\right)^3 = 0.02068 \ (yr^{-1}) \tag{5.16}$$

The creep rate is finally can be determined by multiplying the footing radius of 16cm, the creep rate is then calculated as 0.33cm per year.

Figure 5-22 Nunataryuk pile tip test project site at UNIS East, Longyearbyen

Chapter 6 Conclusions & Recommendations for further work

6.1 Summary

The laboratory study investigated some of the geotechnical parameters of the soil. It unveiled that the soil composition is mainly ice-rich clayey silt and has high level of salinity. The strength of the soil was also tested and it showed a generally high compressive strength.

It is necessary to choose the most adapted creep model for the further consideration of creep design. Many different creep models have been developed over time. The strain or secondary steady strain rate can form relationships with stress from individual axis, unfrozen water content, secondary creep time, etc. However, most of the models demand either intensive and large amounts of tests or long time consuming up to months to determine the creep parameters. As a result, the simple Glen creep model is still most applicable for this study as the parameters from this model can be easily determined by a single uniaxial constant stress compression test for testing within a not so long time. Even though, it is still necessary that the selected constitutive equation properly represents the total delayed response of the frozen soil under the applied load. This requirement can be met if the time of testing is sufficiently long for an extrapolation of strains to become possible. Moreover, the design theories were primarily written based on the Glen creep model, using this model makes the analysis available. With the experimental data from two tests, the study obtained a satisfying enough result even with facing some limitations during the tests. This is a pleasant outcome.

The creep settlement analysis for foundation design was developed under two different methods. The pile adfreeze bearing capacity was being evaluate under the simple shear analytical model. The cavity expansion theory was used for the analysis of the creep settlement in the deep punching end-bearing pile and the shallow foundations. Boussinesq stress distribution theory was also mentioned for calculating the creep settlement in shallow foundations.

With the soil experimental creep data and the combination of the creep settlement analysis theory, especially the cavity expansion theory, the prediction was enabled to carry out to evaluate the soil creep settlement in the Nunataryuk pile campaign project. The result revealed that the creep settlement at the site will be 0.33 cm per year. This is the prediction under the condition that the total load is carried only by the pile tip. If a whole pile foundation will going to be build at the site, with the bearing capacity contributed by the friction pile, it can be assumed that the creep settlement will be less. Due to the rapid climate warming in the Svalbard region, it is necessary to assess the long-term consequences of observed climate change and future climate scenarios for existing and new buildings and structures. Since the mechanical behavior of frozen soil is also dependent on time and future ground temperature, the short-term creep tests discussed in this study could only be applied to investigate the general character of the ice-rich permafrost at the site, and the long-term field tests of the Nunataryuk project will be continued to measure the settlement of the soil at the site.

6.2 Recommendations for further work

Ice is the most important component of frozen soils. The mechanical properties of ice-rich frozen soil are dominated by the visco-plastic nature of ice. However, the existence of unfrozen water influences the mechanical properties and reduces the strength of frozen soils. Hence the measurement of the amount of unfrozen water is recommend to be done for further work.

It is recommended to take the uniaxial compression test under different temperatures especially at higher temperature than present as a method to predict the soil behavior under the influence of climate warming in the future.

In this thesis, the parameters are only be determined from two tests data. For more reliable results, additional tests should be carried. Hence it's recommended to carrying the experiments at a specific temperature with at least three tests at varying loads.

Considering the Nunataryuk project, as the pile campaign is built on three piles. This study only tested the soil from one pile hole. To make the analysis more reliable, it suggests that the test should be performed on soils from each hole to see if the differential settlement will be happened.

Lastly, it is better to find a cold room which can control the temperature more precisely to reduce the error caused by the fluctuation of temperature.

Bibliography

Andersland , O. B., Sayles, F. H., & Ladanyi, B. (1978). Mechanical properties of frozen ground. In O. B. Andersland, & D. M. Anderson, *Geotechnical Engineering for Cold Regions* (pp. 216-275). New York: McGraw-Hill.

Andersland, O. B., & Ladanyi, B. (2004). *Frozen Ground Engineering.* New Jersey: John Wiley & Sons.

Biggar, K. W., & Sego, D. C. (1992). *Field pile load tests in saline permafrost. I. Test procedures and results.*

Bragg, R. A., & Andersland, O. B. (1982). Strain rate, temperature, and sample size effects on compression and tensile properties of frozen sand. In P. E. Frivik, N. Janbu, R. Saetersdal, & L. I. Finborud, *Ground Freezing 1980: Developments in Geotechnical Engineering* (pp. 35-46). Amsterdam: Elsevier, vol. 28.

Bratlie, U. H. (2018). *An Experimental Study of Thermal Properties of Permafrost Soils.* Trondheim: Master thesis-Norwegian University of Science and Technology.

Briaud, J.-L. (2013). *Geotechnical Engineering (unsaturated and saturated soils).* New Jersey: John Wiley & Sons.

Das, B. M. (2011). *Geotechnical Engineering Handbook.* J. Ross Publishing.

Department of the Navy. (1982). Soil Mechanics. NAVFAC Design Manual 7.1. Alexandria. *Va.: Naval Facilities Engineering Command*.

Eiken, I. (2019). *An experimental study of thermal properties and the influence on the ground thermal regime in permafrost soil.* Trondheim: Master thesis-Norwegian University of Science and Technology.

Førland, E. J., Benestad, R., Hanssen-Bauer, I., Haugen, J. E., & Skaugen, T. E. (2011). Temperature and Precipitation Development at Svalbard 1900–2100. *Advances in*

Meteorology, doi: 10.1155/2011/893790.

Furuberg, T., & Berggren, A. -L. (1988). Mechanical properties of frozen saline clays. *International Conference on Permafrost* (pp. 1078-1084). Trondheim: Tapir Publishers.

Gilbert, G. L. (2018). *Cryostratigraphy and sedimentology of high-Arctic fjord-valleys.* Dissertation for the degree of Ph.D. of University of Bergen and UNIS.

Gilbert, G. L., O'Neill, H. B., Nemec, W., Thiel, C., Christiansen, H. H., & Buylaert, J.-P. (2018). Late Quaternary sedimentation and permafrost development in a Svalbard fjord-valley, Norwegian high Arctic. *Sedimentology-Volume 65 Issue 7*, 2531-2558.

Gilbertt, G. L., Instanes, A., Sinitsyn, A. O., & Aalberg, A. (2019). *Characterization of two sites for geotechnical testing in permafrost: Longyearbyen, Svalbard.* Longyearbyen: AIMS Geoscience.

Glen, J. W. (1955). The creep of polycrystalline ice. *Proceedings of the Royal Society of London, Series A, 228(1175)*, 519-538.

Groenendyk, D. G., Ferré, T. P., Thorp, K. R., & Rice, A. K. (2015). Hydrologic-Process-Based Soil Texture Classifications for Improved Visualization of Landscape Function. *PLoS One*.

Head, K. H. (2006). *Manual of Soil Laboratory Testing Volume 1: Soil Classification and Compaction Tests.* Caithness, Scotland, UK: Whittles Publishing.

Hooke, R. L., Dahlin, B. B., & Kauper, M. T. (1972). Creep of ice containing fine dispersed sand. *Journal of Glaciology*, 327-336.

Humlum, O., Instanes, A., & Sollid, J. L. (2003). Permafrost in Svalbard: a review of research history, climatic background and engineering challenges. *Polar Research*, 191-215.

Instanes , A., & Instanes, D. (1999). Pile design in saline permafrsot at Longyearbyen.

Instanes, A. (2016). Incorporating climate warming scenarios in coastal engineering design-Case studies from Svalbard and Northwest Russia . *Cold Region Science Technology 131*, 76-87.

Instanes, A., & Rongved, J. L. (2019). Climate change and geotechnical design in permafrost

and frozen ground. *Proceedings of the XVII European Conference on Soil Mechanics and Geotechnical Engineering(ECSMGE).*

Johnston, G. H., & Ladanyi, B. (1972). Field Tests of Grouted Rod Anchors in Permafrost. *Canadian Geotechnical Journal* .

Jonsson, A., Nerland, Ø., Lande, E. J., Kanstad, S. B., & Hellum, Ø. S. (2018). *The Challenges of Mitigation Measures in Longyearbyen Svalbard.*

Ladanyi, B. (1972). An Engineering Theory of Creep of Frozen Soils. *Canadian Geotechnical Journal*.

Ladanyi, B. (1975). Bearing Capacity of Strip Footings in Frozen Soils. *Canadian Geotechnical Journal*, 393-407.

Ladanyi, B. (1983). Shallow Foundations on Frozen Soil: Creep Settlement. *Journal of Geotechnical Engineering-asce*, 1434-1448.

Ladanyi, B., & Johnston, G. H. (1974). Behavior of Circular Footings and Plate Anchors Embedded in Permafrost . *Can. Geotech*.

Linell, K. A., & Lobacz, E. F. (1980). *Design and Construction of Foundations in Areas of Deep Seasonal Frost and Permafrost .* Hanover, N.H.: U.S. Army C.R.R.E.L., Special Report 80-34 .

Lunardini, V. J. (1981). *Heat Transfer in Cold Climates.* New York: Van Nostrand Reinhold.

McRoberts, E. C., Law, T. C., & Murray, T. K. (1978). Creep tests on undisturbed ice-rich silt. *Proceedings, 3rd International Permafrost Conference*.

Mellor, M. (1972). Normalization of specific energy values. *Int. J. Rock Mech. Min. Sci.*

Morgenstern , N. R., Roggensack, W. D., & Weaver , J. S. (1979). Pile creep in ice-rich soils.

Nanetti, M., Marchenko, A., & Høyland, K. V. (2008). Experimental study on friction between saline ice and steel. *IAHR International Symposium on Ice*.

Nixon, J. F. (1978). Foundation design approaches in permafrost areas. *Canadian Geotechnical Journal*, 96-112.

Nixon, J. F., & Lem, G. (1984). Creep and strength testing of frozen saline fine-grained soils. *Canadian geotechnical journal*, 518-529.

Nixon, J. F., & Lem, G. (1984). Creep and strength testing of frozen saline fine-grained soils. *Canadian Geotechnical Journal*, 518-529.

Nixon, J. F., & McRoberts, E. C. (1976). A design approach for pile foundations in permafrost. *Canadian Geotechnical Journal*, 40-57.

Nordli, Ø., Wyszyński, P., Gjelten, M. H., Isaksen, K., Łupikasza, E., Niedzwiedz, T., & Przybylak, R. (2020). Revisiting the extended Svalbard Airport monthly temperature series, and the compiled corresponding daily series 1898–2018. *Polar Research*.

Norwegian Meteorological Institute. (2019). *Climate Data from the Norwegian Meteorological Institute.* Oslo, Norway.

Nybo, M. S. (2017). *An Experimental Study of Unfrozen Water Content in Fine Grained Permafrost Soils.* Trondheim: Master thesis-Norwegian University of Science and Technology.

Patterson, D. E., & Smith, M. W. (1985). Unfrozen water content in saline soils: Results using time-domain reflectometry. *Canadian Geotech*.

Pounder , E. R. (1965). The Physics of Ice. *Pergamon Press.* London.

Randolph, M. F., & Wroth, P. C. (1978). Analysis of deformations of vertically loaded piles. *ASCE Journal of the geotechnical engineering division* , 1465-1488.

Sayles , F. H., & Carbee, D. L. (1981). Strength of frozen silt as a function of ice content and dry unit weight . *Engineering Geology*, 55-66.

Sayles , F. H., & Haynes, D. (1974). *Creep of frozensilt and clay.* Hanover: U.S. Army Corps of Engineers, Cold Region Research and Engineering Laboratory Technical Report 190.

Sayles, F. H. (1973). Triaxial constant strain-rate and triaxial creep tests on frozen Ottawa sand. *Proc. 2nd Int. Conf. Permafrost*, 384-391.

Sayles, F. H., Baker, T. W., Gallavresi, F., Jessberger, H. L., Kinosita, S., Sadovskiy, A. V., . . . Vyalov,

S. S. (1987). Classification and laboratory testing of artificially frozen ground. *Cold Reg. Eng. ASCE 1(1)*, 22-48.

Shusherina, E. P., & Bobkov, Y. P. (1969). Effect of moisture content on frozen ground strength. *Natl. Res. Coun. Can. Tech*, 122-137.

U.S.S.R.-GOSSTROI. (1976). *Handbook for the design of bases and foundations of buildings and other structures in permafrost .* Moscow: National Research Council Canada.

Velli, Y. Y., & Grishin, P. A. (1983). On the Functional Dependence of the Freezing Point of Soils on the Composition of Water-Soluble Salts in the Interstitial Solution (Transl. from Russian. *Natl. Res. Counc. Can. Tech. Transl*.

Vialov, S. S. (1959). Rheological properties and bearing capacity of frozen soils. *Transl. U.S. Army*.

Vialov, S. S., Gmoshinskii, V. G., Gorodetskii, S. E., Grigorieva, V. G., Zaretskii, L. K., Pekarskala, N. K., & Shusherina, E. P. (1962). *Strength and creep of frozen soils and calculations for ice-soil retaining structures.* US Army Corps of Engineers.

Weast, R. C. (1972). *Handbook of Chemistry and Physics 53rd Edition.* Chemical Rubber Pub.

Weaver, J. S. (1979). *Pile foundations in permafrost.* University of Alberta, Doctoral thesis.

Weaver, J. S., & Morgenstern, N. R. (1981). Pile design in permafrost. *Can. Geotech*, 357-370.

Wijeweera, H., & Joshi, R. C. (1991). Creep behavior of fine-grained frozen soils. *Canadian Geotechnical Journal*, 489-502.

Zhu, Y., & Carbee, D. L. (1987). *Creep and strength behavior of frozen silt in uniaxial compression.* Hanover, New Hampshire: U.S. Army Cold Regions Research and Engineering Laboratory.

Notation

a	Pile or foundation radius
A	Activity
A_s	Surface temperature amplitude
A_z	The amplitude of the attenuation with depth
α_u	Thermal diffusivity
b	Parameter in Vialov creep model
B	(1) Creep parameter (2) Foundation width
c	Parameter in Vialov creep model
C_c	Coefficient of curvature
C_u	Coefficient of uniformity
D	Soil particle diameter
ΔT	Freezing point depression
e	Void ratio
$E(T)$	Fictitious Young's modulus
ε	Creep strain=$\Delta h/h_0$
$\dot{\varepsilon}$	Secondary (or minimum) axial creep rate=$d\varepsilon/dt$
$\dot{\varepsilon}_c$	Reference strain rate,
$\dot{\varepsilon}_{cr}$	Critical creep rate
$\dot{\varepsilon}_e$	Equivalent strain rate
ε_k	Reference strain
$\dot{\varepsilon}_m$	Minimum creep rate
$\dot{\varepsilon}_r$	Reference creep rate
ε_0	Instantaneous deformation

$\varepsilon^{(c)}$	Creep strain
$\varepsilon^{(i)}$	Pseudo-instantaneous strain
$\varepsilon^{(ie)}$	Elastic portion in pseudo-instantaneous strain
$\varepsilon^{(ip)}$	Plastic portion in pseudo-instantaneous strain
γ	Shear distortion or shear strain
$\dot{\gamma}$	Shear strain rate
γ_f	Unit weight of the fluid
γ_s	Unit weight of the soil particle
h	Specimen height
h_0	Initial specimen height
I	Influence factor depends on footing shape
I_L	Liquidity index
I_P	Plasticity index
k	Parameter in Vialov creep model
$k(T)$	Exponent in stress-strain equation
K	Creep parameter as a function of time
L	Length
M	Mass
M_i	Mass of ice
M_s	Mass of soil particles
M_{uw}	Mass of unfrozen water
M_w	Mass of water
μ	Viscosity of the liquid
n	(1) Porosity (2) The exponent of the base of stress in the creep equations
$n(T)$	Exponent in creep equation

v	Fall velocity of the soil particle sphere
ω	Parameter in Vialov creep model
P	(1) Period (2) Load
P_i	Cavity expansion pressure
P_E	End-bearing capacity
P_S	Load carrying capacity of a friction pile
P_T	Total pile bearing capacity
ϕ	Angle of internal friction
ϕ_c	Slope angle of a Coulomb envelop
r	Radius
r_i	Corresponding radius to u_i
ρ_b	Bulk density
ρ_d	Dry density
ρ_s	Particle density
S_n	Salinity in ppt
σ	Stress
σ_{cr}	Critical creep strength
$\sigma_c(T)$	Temperature dependent creep modulus, corresponding to $\dot{\varepsilon}_c$
σ_e	Equivalent stress
σ_E	Applied end-bearing pressure
$\sigma_k(T)$	Temperature dependent deformation modulus, corresponding to ε_k
σ_m	Mean stress value
σ_r	Reference stress
σ_s	Applied vertical pressure for shallow foundations
σ_z	Vertical stress at depth z

t	Time
t_m	Time to creep failure
T_f	Freezing point
T_k	Refrence temperature
T_m	Mean annual surface temperature
$T_{s,t}$	Ground surface temperature
T_{sc}	Supercooling temperature
T_z	Range in tempertures
$T_{z,t}$	Temperature at a given depth and time
τ	Shear stress/ pile shaft stress
τ_a	Applied shaft stress
θ	(1) Number of degrees Celsius below $0°C$ (2)Temperature in $°C$
θ_0	Reference temperature taken as $-1°C$.
u	Displacement
$\dot{u}$	Displacement rate
u_a	Axial displacement
$\dot{u}_a$	Axial displacement rate
u_i	Radial displacement of the cavity wall
V	Volume
V_i	Current cavity volume
V_{io}	Original cavity volume
V_s	(1) Particle volume (2) Volume displacement
V_v	Void volume
w	Water content
w_L	Liquid limit

D

w_P Plastic limit

z Depth

Appendix A

A.1 Basic soil properties definition

Water content

Water content is critical in the geotechnical investigation for soil properties. In frozen soil, the soil behaves totally different between dry and wet soil.

The soil will expand upon freezing and settle when thawing where the rates of movement are highly depended on moisture content of soil.

Ice crystals that form in soil pores expand the pore diameter and cause a decrease in the bulk density of the soil. The effect of freezing is more pronounced in soil that contains moisture than it is in dry soil.

The water content can be calculated as Equation(A.1)(A.1)

$$w = \frac{M_w}{M_s} \times 100\%$$
(A.1)

Bulk density

Ascertaining the bulk density is the first step when it comes to soil testing as it stands for the density of the soil in natural state. The bulk density, ρ_b, is calculated as follows.

$$\rho_b = \frac{M}{V} = \frac{M_s + M_w}{V}$$
(A.2)

Dry density

Dry density represents the condition when the water is gone and the pores are all occupied by air. Dry density serves as a basis for describing the degree of soil compaction. An equation of the dry density in relation with the water content and bulk density is established.

$$\rho_d = \frac{M_s}{V} = \frac{\rho_b}{1+w} \tag{A.3}$$

Particle density

Particle density is defined as the weight of solid particle in its unit volume as listed in equation(A.4). Unlike bulk density or dry density, it is not dependent on the degree of compaction of the solid. It is therefore well defined in a range. Typical values of particle density for most soil solids range from 2500 to 2800 kg/m^3. It is common to use particle density equal to 2650 kg/m^3 for sand and 2700 kg/m^3 for clay.

Knowing the bulk density and particle density, the porosity, n can be known. The porosity, n indicates the voids in the soil that are available for water and/or air, can be calculated as equation(A.5)

Void ratio, e, is another volumetric ratio relating volume of voids to volume of solids. It has a positive relationship with the porosity. Both low porosity and low void ratio indicate the better compaction of the soil. It can be calculated as Equation(A.6)

$$\rho_s = \frac{M_s}{V_s} \tag{A.4}$$

$$n = \frac{V_v}{V} = 1 - \frac{\rho_b}{\rho_s} \tag{A.5}$$

$$e = \frac{V_v}{V_s} = \frac{n}{1-n} \qquad (A.6)$$

Liquid limit

The liquid limit (w_L) is the water content of a fine-grained soil when it passes from a liquid state to a plastic state. The liquid limit states the point when the soil no longer flows like a liquid.

Plastic limit

Plastic limit (w_P) is the water content of a fine-grained soil at the boundary between the plastic and semi-solid states. It is the point at which a soil will just begin to crumble and the soil can no longer be remolded without cracking.

Plasticity Index

The plasticity index (I_P) is the numerical difference between the liquid limit and the plastic limit.

$$I_P = w_L - w_P \qquad (A.7)$$

It is the range of water content over which a soil behaves plastically, indicating the degree of plasticity of the soil. The greater the difference, the greater the plasticity of the soil. Soils with a high I_P tend to be predominantly clay, while those with a lower I_P tend to be predominantly silt. Soils with high plasticity index are highly compressible. Plasticity index is also a measure of cohesiveness with high value of I_P indicating high degree of cohesion.

Liquidity Index

Liquidity index (I_L) is a parameter used to define the consistency of a fine-grained soil with respect to liquid limit and plastic limit. It is defined as Eq.(A.8)

$$I_L = \frac{w - w_P}{I_P}$$

(A.8)

It takes a value of 0 at plastic limit and 1 at liquid limit. Table A-1 shows the ranges of liquidity index and the soil behavior under the index.

I_L	Classification
0	Stiff
0-0.25	Semi-stiff
0.25-0.50	Stiff-plastic
0.50-0.75	Soft-plastic
0.75-1.0	Flow-plastic
>1	Flowing

Table A-1 Liquidity index ranges

Activity

Activity (A) is a term used to quantify the plasticity of the clay fraction in a fine-grained soil and is defined as Equation(A.9)

$$A = \frac{I_P}{\% \ of \ clay}$$

(A.9)

Fine-grained soils contain clays and silts, where the clays are plastic and silts are nonplastic. The plasticity of fine-grained soil is derived mainly from the clay fraction. Activity is a good indicator of potential shrink-swell problems associated with expansive clays. Clays with $A >$ 1.25 are generally expansive and those where $A < 0.75$ are inactive. Clays with $A = 0.75\text{-}1.25$

are known as normal clays. (Das, 2011)

Shrinkage limit

Shrinkage limit is the water content of a soil when it's at the boundary between the semi-solid and solid states. Right after the shrinkage limit, a reduction in water content will not cause a decrease in volume of the soil mass. It is the lowest water content at which soil can still be saturated, further than this limit, any loss of moisture is compensated by the entry of air into the pores. This limit is less being tested as it is not needed to classify the soil.